Dynamic control of spindle motors for milling applications

By

Qinwei Pan

A thesis submitted for the degree of PhD. in the

Department of Electronic and Electrical Engineering

The University of Sheffield

October 2017

Abstract

This programme of research is concerned with investigating novel methods for enhancing the machining of metals in terms of increasing material removal rates while maintaining surface finish and dimensional tolerance. This thesis provides a detailed investigation of the interaction between the drive control system, the power converter and the cutting process. Especially the coupling between the controller and power converter behaviour and the dynamic cutting conditions is the key novelty in this research.

Specifically, the research explores the merits of high speed and precise torque modulation of the drive and its influence on the cutting tool to suppress chatter in milling operations. The study focuses on the following areas:

1. **The open-loop torque matching to achieve precise speed control.** A high frequency component of the machine load is generated due to the milling process, resulting in speed fluctuation. This research demonstrates a method for precise speed control using a low bandwidth PI controller by applying a torque correction signal to the control loop.
2. **Rapid torque modulation for chatter suppression in milling operations.** The past research of variable speed milling on chatter suppression is limited by industrial milling machines. The industrial speed controller limits the frequency of speed variation that can be applied around the operating condition. This thesis increases the speed variation frequency capability for high speed milling process.
3. **Investigating the complex interactions between speed control settings and cutting performance.** By applying torque match and rapid torque modulation the speed variation frequency capability is significantly increased. A detailed investigation of the dynamic behaviour with a high frequency speed variation and the effect of chatter suppression on high frequency variable speed milling (HFVSM) is presented.
4. **Detecting the onset of chatter using speed measurements.** The cutting torque fluctuation is reflected as a disturbance of the motor speed. Chatter can then be identified by monitoring the motor speed. The application of this technique benefits the milling industry by providing a more robust chatter detection compared with conventional techniques.
5. **Combined dynamic operation.** The combined operation of torque match, rapid torque modulation and chatter detection is demonstrated and has potential application to a milling machine capable of detecting and auto suppressing chatter during milling.

By combining auto chatter detection identification technique and high frequency variable speed milling, this research provides a detailed study with significant potential for industrial application. The key enabling methods demonstrated increase the operating speed capability for milling activities and hence reduce the time taken to manufacture a part and consequently increase the productivity of a milling machine.

ACKNOWLEDGEMENTS

This thesis became a reality with the kind support and help of many individuals. I would like to extend my sincere thanks to all of them.

Foremost, I want to offer this endeavour to my supervisor Professor Geraint W Jewell for his continuous encouragement, guidance and insightful support during my research. I have been benefited from his regular critical reviews and inspiration throughout my work.

I would also like to thank my colleagues Dr. Alex Duke, Dr. Keir Wilkie and Dr. Maurice Shortte for their constant encouragement, suggestions and moral support throughout the duration of my project.

I must express my gratitude to Fan, my dearest wife, for her continued support and encouragement. I also would like to thank my little daughter Xining, who tried very hard not being naughtier during my thesis writing up.

I would like to thank all the people in the Electrical Machines and Drives Group for all the support during my PhD study.

Last but not least, I would like to thank my parents and parents in law, who have supported me physically and spiritually throughout my life.

Table of Contents

List of Figures

Nomenclature and abbreviations

Symbol	Description	Units
B	Viscous friction coefficient	---
b_a	Axial depth of cut	meters
C	System viscous damping coefficient	---
c	Cutting force ratio	---
d	Radial depth of cut	meters
dz	Width of cut	meters
f	Variation frequency	Hz
f_t	Feed rate	mm/tooth/rev
F_c	Shear cutting force and is the also rubbing force.	N
F_{pd}	Process damping force also the rubbing force	N
F_r	Radial cutting force	N
F_{rix}	Radial cutting force for ith tooth in x axis	N
F_{riy}	Radial cutting force for ith tooth in y axis	N
F_t	Tangential cutting force	N
F_{tix}	Tangential cutting force for ith tooth in x axis	N
F_{tiy}	Tangential cutting force for ith tooth in y axis	N
F_y	Total force acting	N
h	Dynamic chip thickness	meters
$i_{sd} i_{sq}$	d-q axis stator current	A
J	Moment of inertia	$kg.m^2$
J_1	the inertia of bar 1	$kg.m^2$
J_2	inertia of bar 2	$kg.m^2$
k	system stiffness	---
$k_s{}'$	Tangential cutting force coefficient	---
K_e	Back-emf constant	Nm/A
K_s	Unknown cutting force coefficient	---
K_t	Torque constant of a machine	$(kg.m^2)/(A.s^3)$
k_p	Proportional coefficient	---
k_i	Integral coefficient	---
k_d	Derivative coefficient	---
L_d, L_q	d-q axis inductances	H
m	Total flute number of the cutter	---
M	System equivalent mass	kg
$M_{dq} M_{qd}$	Mutual inductance between the d-q axis	H
N_0	Mean spindle speed	rpm
N	Spindle speed	rpm

N_A	Spindle speed variation amplitude	rpm
Pn	Pole pair numbers	---
r_t	Machine tool radius	meters
R_s	Stator resistance	ohms
R	Cutting tool radius	meters
RVA	ratio of variation amplitude	---
RVF	ratio of variation frequency	---
(S_{sx0}, S_{sy0})	Previous wave surface segment geometry point 0	---
(S_{sx1}, S_{sy1})	Previous wave surface segment geometry point 1	---
S_{ctx}, S_{cty}	Tooth tip position	---
S_{otx}, S_{oty}	Machine tool centre position	---
T	Periodic variation period	s
$t(\varphi)$	Under formed chip thickness of the tooth element at the helix lag angle position φ	meters
t_0	Initial under formed chip thickness	meters
t_1, t_2	Start and exit time	s
T_1, T_2	Acting time	s
T_{1-2}	transmitted torque from bar 1 to bar 2.	Nm
T_L	Load torque	Nm
T_S	Sampling time	s
T_e	Electromagnetic torque	Nm
U_α	Voltage in α axis in $\alpha\beta$ reference system	V
U_β	Voltage in β axis in $\alpha\beta$ reference system	V
u_0	Initial total cutting energy per unit volume	J/mm^3
v_{sd}, v_{sq}	d-q axis stator voltage	V
W_c	Work done to the system	J
W_{pd}	Process damping work.	J
W_s	Work of structural damping forces	J
y	Relative displacement	M
$\ddot{y}$	Acceleration,	m/s^2
$\dot{y}$	Relative velocity	m/s
α_e	Effective rake angle	degree
α_{e0}	Initial effective rake angle	degree
θ_1	Position of bar 1	radian
θ_2	Position of bar 2	radian
θ_{re}	Rotor electrical angle	radian

τ_0	Time delay between two flutes of cutter	sec (second)
φ_m	Permanent magnet flux	Wb
$\varphi_{sq}\varphi_{sd}$	d-q axis stator flux linkage	Wb
ω_e	Electric speed	radian/s
ω_m	Mechanical speed	radian/s
Ω	Cutter radial immersion angle within the radial depth of cut	degree
β	Helix angle of the cutter	degree
θ	Spindle rotation angle	degree
φ	Helix lag angle position	degree
φ_i	Angular position of current tooth/layer	radian
ψ	Helix lag angle	degree
ω	Spindle rotation speed	radian/s
$\varepsilon_s\varepsilon_e$	Start and end cutting angle	degree

Chapter 1 - Introduction

1.1. Background

1.1.1. Introduction to milling

Milling is a widely-used technique for the removal of metal in manufacturing. In all the industrial sectors in which milling is used, there is a continuing drive towards increasing material removal rates and enhancing surface finish while also minimising tool-wear and energy consumption.

Milling provides a precise and reasonably high through-put means of machining a component to its final, or very near final, dimensions. The essence of the milling process is shown in Figure 1. A milling cutter, which is usually a cylindrical tool equipped with a series of cutting teeth, is rotated about the axis shown. By progressive traversal of the work-piece, material is removed to a prescribed depth along a well-defined path. Many modern milling machines are computer controlled (so-called Computer Numerically Controlled or CNC). These machines are able to take Computer Aided Design (CAD) drawings and directly convert these into a series of traversal paths to produce the final component geometry. Many larger and more advanced machines are equipped with the ability to automatically change the cutting tools, often with many tens or even hundreds of tools in a carousel.

In recent decades, technologies applied in milling operations have advanced greatly, with the addition of computer control and increased use of sensors. These have provided many opportunities to increase productivity and accuracy. Although production capabilities have increased significantly as a result of the development of new concepts, devices, tool materials, new tool shapes, coatings, etc. [QUI 11] there remains significant potential to increase the accuracy, flexibility and productivity of milling machines. One of the major problems is the

build-up of vibrations during milling and hence understanding milling fundamentals and machine vibration mechanism has become a topic of significant research.

This programme of research is focussed on establishing methods for realising dynamic control of the cutting process. The ability to dynamically control torque and/or speed (recognising that the latter is limited by the effective moment of inertia) may provide a means of enhancing cutting rate, through avoiding the onset of chatter more effectively than simple set-point control.

Milling cutters

Within the general term 'milling' there are many different type of operation, which can broadly be divided into two categories: face milling and peripheral milling. A schematic of each of these is shown in Figure 1 (a) and (b).

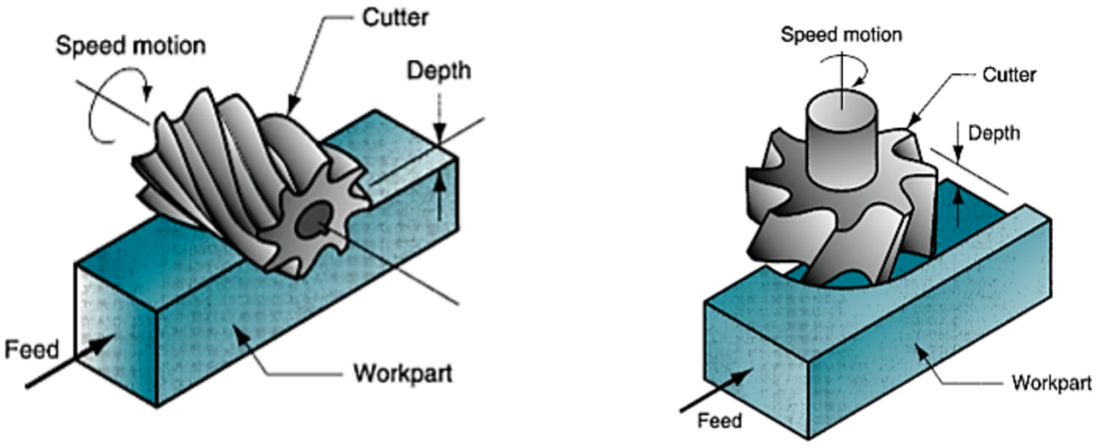

(a) Peripheral milling (b) Face milling

Figure 1 Schematic representations of common milling processes (Source: [ALT 00])

The cutting tools which perform the milling come in a wide variety of shapes and sizes. The most widely used cutters are so-called end-mills which can be applied in various operations, including face milling, slotting, channel cutting, plunging and even drilling. Within the broad category of end-mills, there are a number of different geometries as shown in Figure 2

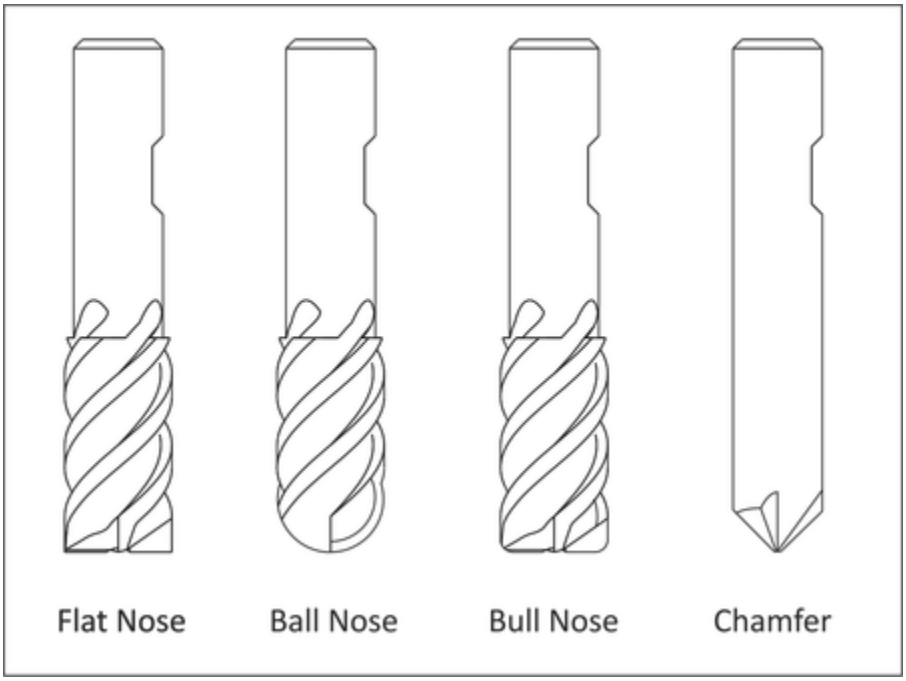

Figure 2 Different geometries of the end-mills (Source: [ALT 00])

Flat nose end-mills, which are also often referred to as square end mills are usually preferred for square corner milling. This leaves a square shape bottom in the work piece. Ball nose end mills are hemispherical at their ends and are usually used for milling complex 3D shapes. Bull nose end-mill is also referred to as rounded edge end-mill. These types of the cutter usually have longer tool life, because of the rounded edges on the cutter tips. The research reported in this thesis is focussed on a straight flute end milling. Figure 3 shows a HTC 780-4625 straight end mill tool which is representative of the milling tool simulated in this thesis.

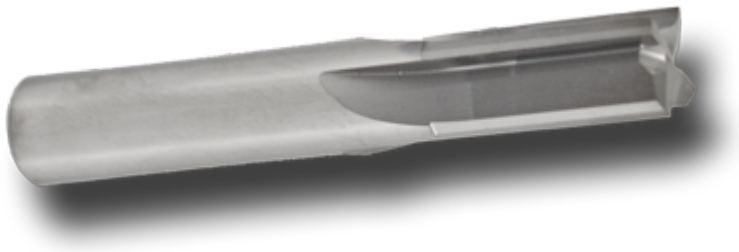

Figure 3 Typical straight end mill tool (Source: [HTC 17])

1.1.2. Control of milling machines

Almost all modern high-performance milling machines are driven by electrical machines controlled by power electronic converters. The combination of machine and power converter is often referred as a spindle drive. They are capable of providing precise speed control, although it is important to recognise the outer speed control loop is often built around an inner torque control loop.

Standard spindle drives tend control speed to a prescribed set-point, although this set-point can be varied during operation [SS 08], e.g. ramped up during starting, adjusted as different depths or wall thicknesses are encountered. This speed control is usually achieved with a relatively standard PI control structure, although additional features such as current limits are often included [SS 08].

The extent to which the speed controller responds to very short-term events, e.g. periodic fluctuations in cutter torque with individual passing of teeth, depends on the gains selected. The standard factory default gains for commercial PI controllers are often low with an emphasis on stability and reducing longer-term deviations from the set-point [SS 08]. A key feature of these controller is that speed and/or torque is not usually being controlled dynamically within one revolution.

During the milling process, the load torque applied on the shaft of machine varies dramatically as individual cutting teeth enter and leave the work-piece, although the exact form of the torque pulsations depends whether the curter is straight edged or helical [ALT 00]. Speed controllers tends to control average speed and average power of the motor. For the remainder of this thesis, this mode of control will be referred to as set-point speed control.

Modern electrical machines and power converters can exercise very precise control over the instantaneous torque, the limiting factor being the electrical time constant, i.e. the rate at which

current can be changed. It is possible to achieve very high dynamic rates of change of current by oversizing the converter in terms of its VA rating as compared to the VA rating required to provide the average power. This ability to dynamically control current, and hence torque, in principle provides a means to realise complex torque waveforms during one revolution, or even during an individual cutter tooth passing interval. Detailed control systems which aim to exploit this dynamic capability will be discussed and presented in the later chapters

1.1.3. Vibrations in machining processes

One of the limiting factors on the metal removal rate is the need to avoid excessive vibration of the cutter. Other limitation includes excessive temperature rise of the cutter and work-piece [ABU 06]. In addition to limiting material removal rates, vibration of the cutter will also inevitably affect the quality of surface finish. There are three main types of the vibrations encountered in milling machines, viz. free vibrations, forced vibrations, self-excited vibrations [ALT 00]. Free vibrations occur in a mechanical system when it is displaced from its equilibrium position and is allowed to vibrate freely. In milling, free vibrations are usually the result of erroneous operations such as an incorrect tool paths leading to cutting tool and work-piece collisions. Forced vibrations occur when an external source of excitation excites the system harmonically [KHA 13]. In milling, this predominantly occurs when the cutting edges of the tool successively enter and exit the work-piece. Both free vibration and forced vibration can be mitigated to some degree by various methods when the source of the vibration is identified.

Self-excited vibrations are the main causes of chatter, also referred to as regenerative chatter. Self-excited vibrations, from the energy perspective, start with excess energy and then grow at a rate which depends on the damping of the system [ALT 00]. During the milling process, a mismatch between the surface remaining from the last cut and the surface being generated from current tooth path, leads to the progressive growth of chatter.

Figure 4 shows the effect of related phase difference and dynamic under-formed chip thickness. If the phase difference is zero, the chip thickness will only relate to the feed rate and cutting speed. However, if the relative phase difference is at π, the variation of the dynamic chip thickness is at its maximum value which leads to cutting force varies dramatically, resulting in tool vibrations. The vibration left new waves on the work surface. This process is called the regenerative effect and eventually leads to the regenerative chatter.

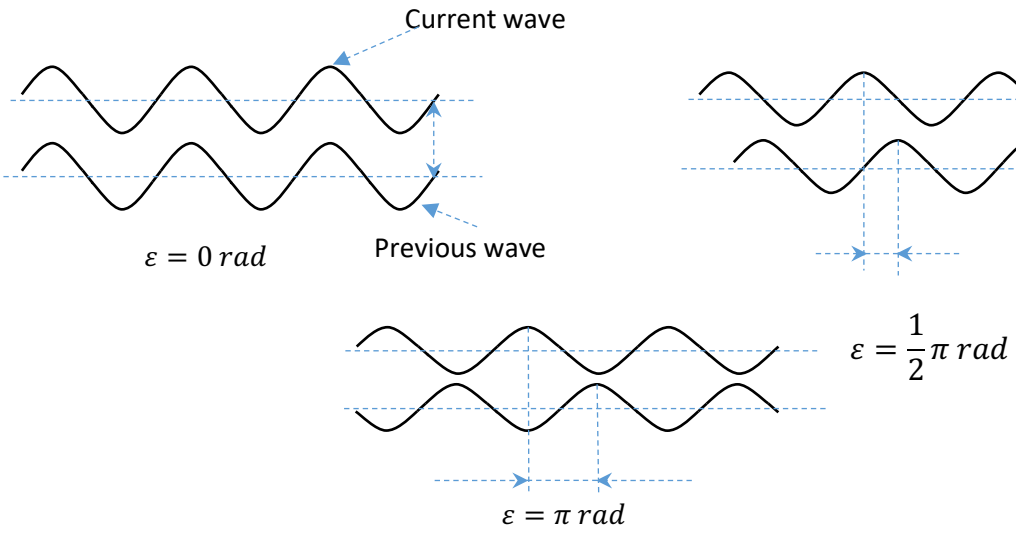

Figure 4 The effect of related phase difference and dynamic chip thickness [ALT 00].

The topics of online chatter monitoring, measurement and control have received significant academic and industrial attention in recent years as this is arguably the main obstacle to achieving increased through-put in many milling applications.

Rahman and Ito [RAH 86] proposed a method to detect the chatter by measuring the horizontal deflection of the work piece using microphone and dynamometer. This showed some promise in terms of being able to detect chatter, but did not propose any novel methods to deal with the chatter once detected. Liao and Young [LIA 96] proposed an online chatter detection and avoidance method. The method proposed was based on reading a dynamic cutting force signal

from a dynamometer and analysing the signal with the Fast Fourier Transform (FFTs). Once a characteristic chatter signal was detected, a real-time control system calculates a new spindle speed to disturb the regeneration behaviour which is causing the chatter. However, this method requires additional dynamometer equipment.

Skilled machining operators can readily identify the onset of chatter from a distinct change in acoustic noise. There are several papers which have successfully employed microphones to detect and identify the characteristic signature of chatter [DEL 92] [SCH 01] [SCH 02] [SCH 03] [WEI 06]. However, such techniques are very sensitive to the local acoustic environment, as the micro-phone can be easily influenced by the other sources of acoustic noise.

High speed milling has developed a great deal in recent years. It offers scope for greater material removal rates and fine surface finish through a combination of very high spindle speed and feed rate. [MEB 16] The typical milling speed for high speed milling is above 7000 rpm on spindle speed and 0.05 mm/tooth on the feed rate. However, with high-speed milling, the spindle drive will need to run at high speeds and accommodate high frequency variation in the load on the cutter.

1.1.4. Existing chatter suppressing strategies

Machine tools experience two major vibrations during the machining process, forced vibration and self-excited vibration. In the milling process, cutting forces applied on the machine tool are normally periodic at four or five times the tooth passing frequency. Forced vibration occurs when any of these harmonics resonate with machine system and/or work piece natural frequency. However, this category of vibration can be readily solved while self-excited vibration is a more problematic issue.

Self-excited vibration, which is also referred as chatter, is a major cause of poor surface finish, and often limits the material removal rate that can be achieved. During the milling process, the

machine tool leaves a wave like surface due to relative displacement between the tool and the work-piece, i.e. vibrations. Since previous cutter passes also left a wave surface, the phase shift between the two waves cause the chip thickness to vary, which can lead to the cutting force growing if it is oscillating at the chatter frequency. This increasing force produces further vibrations, and eventually enters full chatter which can leave a poor surface finish. Self-excited chatter either caused by mode-coupling or regeneration effects. Due to the nature of mode-coupling, regenerative chatter often occurs earlier than mode-coupling in milling process. This research mainly focuses on regenerative chatter.

Starting from the principles of regenerative theory, many methods to suppress the chatter have been developed. In general, industrial milling processes use straightforward set-point control of speed especially in high speed milling processes. To suppress the onset of chatter, several methods have been proposed and employed. [YUS 10A] [DUN 05]:

- Increase the effective stiffness of the mechanical components
- Introduce additional damping by adding dampers or reducing cutting speed (low speed milling),
- Use of cutting tools with variable pitches or with variable helix angles in order to disrupt the regenerative effect.

However, these established approaches have their short comings. Magnetorheological fluid is a popular way of changing the mechanical stiffness by varying the magnetic field applied to it. However, this method is only valid for boring operations [SAT 08] [MEI 09] [MEI 10] [BRE 10]. Most added dampers would have limited application, for particular operations such as a resonator [OLG 98] [DOH 04] and variable pitch and helix angle method [SHI 96] [BUD 03A] [BUD 03B] [SIM 08] [TUR 06] [TUR 07] [FAZ 09] [YUS 10B] or risk been contaminated by the coolant fluid, like piezoelectric actuator [PRA 01] [BRO 97] [ZHA 05].

Many studies have focused on variable speed milling as a potential solution. Variable speed milling first appeared in the 1970's, having been proposed by Takemura et al. [TAK 74] It has been demonstrated by many papers [ALT 92] [JAY 00] [SAS 02] [REG 03] [YAN 03] [ZAT 08] that with low-speed milling, spindle speed variation around a set-point can be very effective in suppressing chatter.

In 1979, Stoferle and Grab [STO 72] introduced sinusoidal spindle speed variation (S^3V), a technique which is straightforward to implement on a CNC machine. It has been demonstrated that regenerative chatter can be suppressed in the milling process with an appropriate combination of amplitude and frequency of speed variation [ALT 92] [STO 72] [LEE 91]. However, despite these advances, variable speed milling still poses challenges in terms of acceptance in industry, especially for sinusoidal spindle speed variation. The main problem is the absence of a systematic means to determine the combination of speed variation amplitude and frequency for a given milling task.

Variable speed operation in high-speed milling can have opposite effect and cause chatter in what would otherwise be stable operation. [LIN 90] [TSA 93] To overcome this problem, research has also focussed on energy balance theory. Al-Regib, et al [REG 03] in 2003 proposed a new method based on varying the spindle speed for minimum energy input to work piece. This method considered sinusoidal spindle speed variation using a systematic procedure to select the effective amplitude and frequency for designing a stabilizing spindle speed profile.

In 2009, S. Seguy et al. [SEG 10] recognised that speed variation not only benefits low speed milling processes but also assists in high-speed milling processes. More specifically, with variable speed technique, the stability properties such as critical depth of cut can always be improved. Furthermore, the authors also demonstrated that that amplitude of speed variation has a greater effect on system stability than frequency.

1.1.5. Variable speed milling

The underlying principle of variable speed milling for avoiding chatter is to cycle the spindle speed, such that the regenerative delay is progressively varied in duration. In this way, the regenerative reinforcement is disturbed, resulting in reduced the self-excited vibrations. During milling, the spindle speed is modulated around a mean speed [SEG 09] [SEG 10]. In the case reported in [SEG 09], a triangular modulation was employed with the general form shown in Figure 5. There are two different approached to modulation, viz. by amplitude and by frequency. In both cases, performance is limited by the spindle dynamic response abilities [SEG 09].

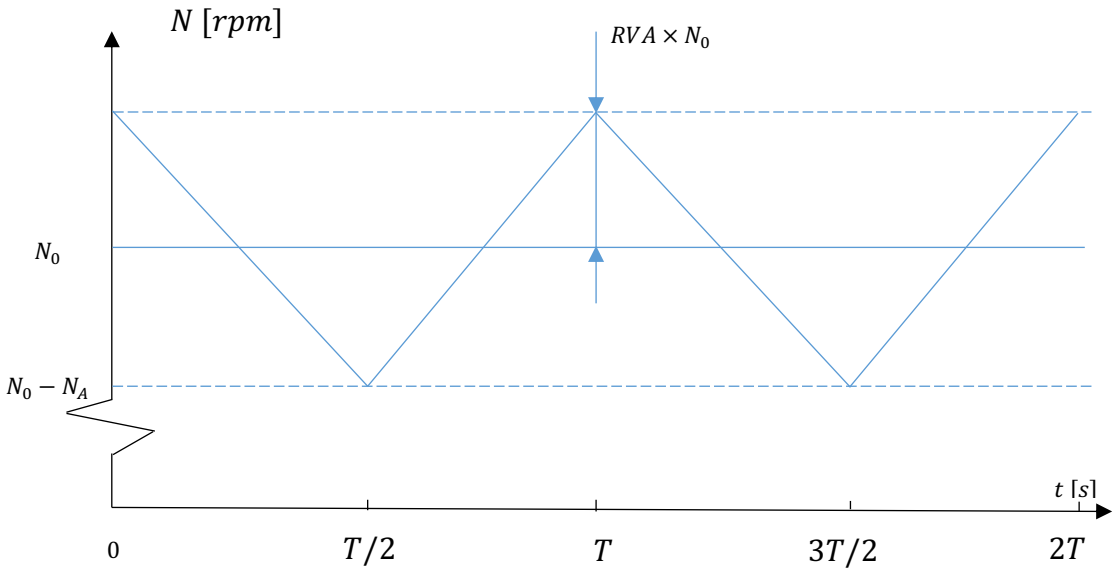

Figure 5 Typical triangular speed modulation [SEG 09]

For each periodic variation period, T, the spindle has mean value,N_0, with amplitude variation, N_A. The shape function of the triangular variation in speed is:

$$S(t) = S(t + T) \qquad (1\text{-}1)$$

Where:

$$S(t) = \begin{cases} 1 - \frac{4\ mod\ (t,T)}{T} & if \quad 0 < mod\ (t,T) \leq T/2 \\ -3 + 4\ mod \frac{t,T}{T} & if \quad T/2 < mod\ (t,T) \leq T \end{cases} \qquad (1\text{-}2)$$

where mod (t, T) is the modulo function, i.e. the integer remainder of t/T.

By defining $RVA = N_A/N_0$, the triangular modulation can be expressed as: [SEG 09]

$$N(t) = \begin{cases} N_0(1 + RVA) - \frac{4\ N_0 RVA}{T} mod\ (t,T) & if \quad 0 < mod\ (t,T) \leq T/2 \\ N_0(1 - 3RVA) + \frac{4\ N_0 RVA}{T} mod\ (t,T) & if \quad T/2 < mod\ (t,T) \leq T \end{cases} \qquad (1\text{-}3)$$

In the regenerative theory, the time delay between two blades of the cutter is critical in determining the behaviour.

For a constant spindle speed N_0, the time delay is constant:

$$\tau_0 = \frac{60}{mN_0} \qquad (1\text{-}4)$$

For variable speed milling, the time delay for regenerative vibration is:

$$\int_{t-\tau(t)}^{t} \frac{N(s)}{60} ds = \frac{1}{m} \qquad (1\text{-}5)$$

Thus, for triangular modulated variable speed milling, the regenerative delay is:

$$\tau(t) = \begin{cases} \tau_0(1 - RVA) + \frac{4\ \tau_0 RVA}{T} mod\ (t,T) & if \quad 0 < mod\ (t,T) \leq T/2 \\ \tau_0(1 + 3RVA) - \frac{4\ \tau_0 RVA}{T} mod\ (t,T) & if \quad T/2 < mod\ (t,T) \leq T \end{cases} \qquad (1\text{-}6)$$

$$\text{Define } RVF = \frac{60}{N_0 T} = \frac{60f}{N_0} \text{ and } T = \frac{1}{f}. \qquad (1\text{-}7)$$

In conventional variable speed milling, the frequency of the modulation is only 1-2 Hz. The resulting time delays which are achieved with this method, can be adjusted more readily at low

speed then at high speeds. This limitation of variable speed milling leads to poor performance in high speed milling.

1.1.6. Energy balance theory for chatter identification

The basic dynamics of machining process are well established and documented [KHA 13]. In steady state, a single degree of freedom can represent the key dynamic using the following equation of motion:

$$M\ddot{y} = F_y - C\dot{y} - ky \qquad (1\text{-}8)$$

During the milling process, the force equation is:

$$F_y = F_c - F_{pd} \qquad (1\text{-}9)$$

which in turn leads to :

$$M\ddot{y} + C\dot{y} + ky = F_c - F_{pd} \qquad (1\text{-}10)$$

The energy balance equation can be established by straightforward integration:

$$\int_{t_1}^{t_2} M\ddot{y}\ \dot{y}dt + \int_{t_1}^{t_2} C\dot{y}\ \dot{y}dt + \int_{t_1}^{t_2} ky\ \dot{y}dt = \int_{t_1}^{t_2} F_c\ \dot{y}dt - \int_{t_1}^{t_2} F_{pd}\ \dot{y}dt \quad (1\text{-}11)$$

Since kinetic energy and potential energy are conservative, they can be neglected during the calculation of net changes in energy.

Hence:

$$\int_{t_1}^{t_2} F_c\ \dot{y}dt = \int_{t_1}^{t_2} c\dot{y}\ \dot{y}dt + \int_{t_1}^{t_2} F_{pd}\ \dot{y}dt \qquad (1\text{-}12)$$

$$W_c = W_s + W_{pd} \qquad (1\text{-}13)$$

From this energy based theory, it is possible to suppress the chatter from being initiated either by reducing the excess energy with better balancing of the force acting on the material and the shear cutting force or through increasing the system damping though ancillary devices.

In this thesis, unstable operation is defined both in terms of the energy balance and self-excitation damping ratio [SIM 05]. Figure 6 shows a comparison between stable operation and unstable operation at 3,000 rpm, conditions which are achieved with depths of cut of 10 mm and 14 mm respectively. The details of the cutting parameters and milling model will be presented in the later chapters. The chip thickness under stable cutting follows a well-defined profile which is governed by the tool geometry and the feed rate. When the cutting is unstable, the chip thickness profile includes significant disturbances which is caused by vibration of the tool in the feed direction.

For stable cuts, the tool centre is vibrating asynchronously with the tooth passing frequency and provides a tight tool centre distribution. While for chatter occurs, the tool vibrations are not synchronous with the spindle rotation and oscillate around the system natural frequency. This chatter frequency can be detected from the tool centre vibrations using short time Fourier transfer once per revolution. More factor which determines whether the operation is deemed stable or unstable is the accumulated work done by the contact loss. Specifically, whether the work done by the contact loss is non-zero and increasing the system is deemed to be unstable. This definition is consistent with the definitions used in [KHA 13] and [SIM 05]. In the case shown in Figure 6, when the cutting is stable, the accumulated work done by loss of contact remains to zero, while for unstable cutting, it is clear that this component of work is growing and hence this point is considered to be unstable. It is important to note that the work associated with contact loss is much smaller than the other components of work and is plotted on a greatly expanded scale.

Stable operation **Unstable operation**

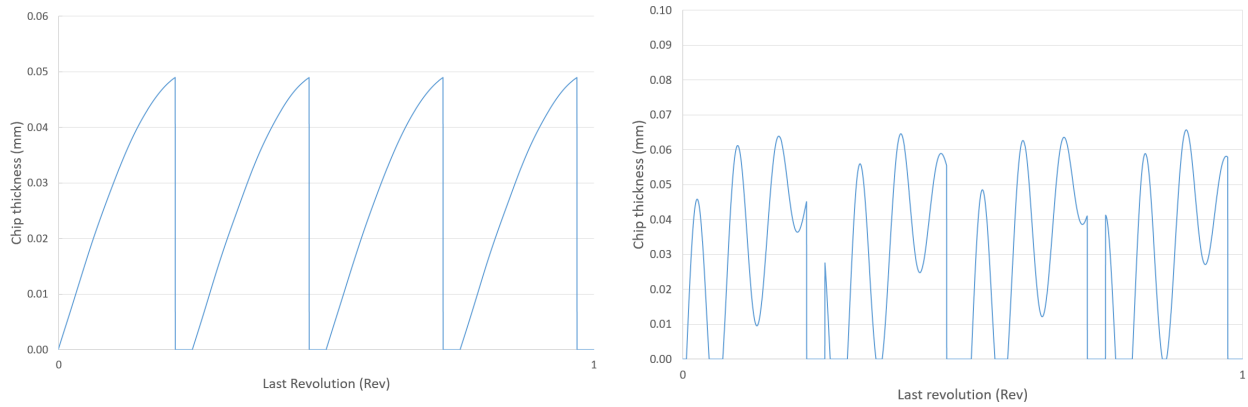

Displacement in the direction of feed

Figure 6 Comparison between stable and unstable operation at 3,000 rpm

1.2. Thesis layout

The research reported in this thesis is an investigation into the scope for exploiting the full dynamic response of modern spindle drives to improve milling performance. The research encompasses machine controls, machine modelling, chatter identification and chatter suppression strategies.

Chapter 2 describes the development of a system model that encompasses the drive system model and detailed cutting models. The system model is validated through comparisons with published simulation results and experimental measurements.

Chapter 3 investigates dynamic performance under three modes of control: standard speed control, open-loop torque matching and rapid torque modulation. A series of simulations are discussed which demonstrate the potential to overcome chatter.

Chapter 4 investigates, through a series of simulations, the potential to identify in real-time the onset of chatter using rotational speed. Studies are performed on both an ideal speed signal and from a detailed model of incremental encoders.

Chapter 5 draws the various control and monitoring methods together to model the performance of a system following a complex schedule of operating conditions, including responding to the detection of chatter.

Chapter 6 summarises key conclusions from the research and describes potential avenues for future research which build on the findings reported in this thesis.

Chapter 2 - System level model

2.1.Drive system model

Published models of the milling process such as [LEE 91] [OLG 98] [SAS 02] [SIM 08] [MEI 10] [MEB 16] are based on a simplified model of the system which drives the cutting tool. In all the published cases [ALT 92] [LEE 91] [BUD 03A] [SIM 08] [MEI 10] [BRE 10] [MEB 16], the drive is modelled as an ideal constant speed drive which is speed-stiff, i.e. the speed does not fluctuate in response to changes in the load torque applied to the cutter. This is a reasonable approximation for many aspects of analysis given the good speed regulation achieved by modern speed controlled drives and the moment of inertia of typical higher power spindles. However, the research described in this thesis is concerned with interactions in the milli-second range and hence a higher fidelity model of the drive system is required. This chapter describes a complete system model, the key elements of which are shown in the top-level block diagram of Figure 7. The block diagram in Figure 7 is the basic version with a standard closed-loop speed controller, to which various additional control elements will be added in later chapters.

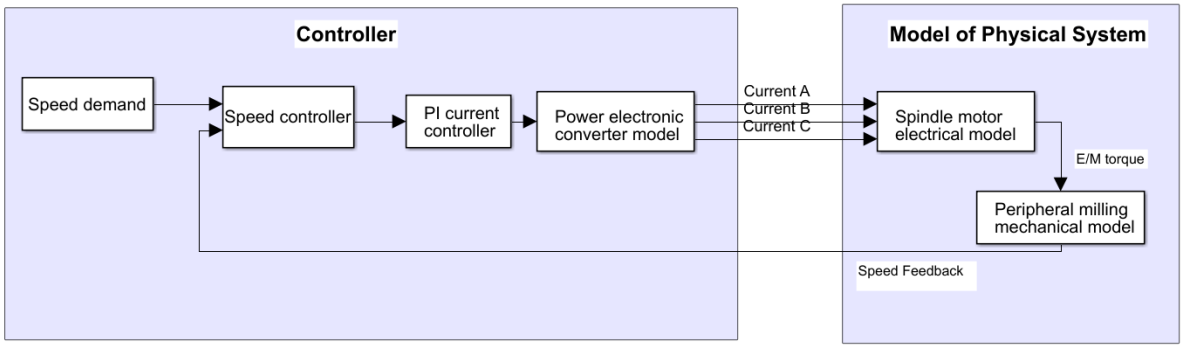

Figure 7 Block diagram of basic system model

2.1.1. Permanent magnet synchronous motor (PMSM)

Although AC induction motors are used in some CNC machining centres, the highest levels of performance in terms of efficiency and dynamic control are achieved with permanent magnet synchronous machines (PMSMs). In this thesis, a Siemens1FE series PMSM was selected as the reference machine design. This is a 11.5 kW machine with a maximum speed rating of 10,000 rpm. A detailed specification of this machine is contained in Appendix A

The instantaneous electromagnetic torque T_e produced by a star-connected three phase permanent-magnet synchronous machine in d-q reference frame is given by well-established torque equation [LIU 05]:

$$T_e = \frac{3}{2} Pn \left[\left(\frac{dL_d}{d\theta_{re}} i_{sd} + \frac{dM_{dq}}{d\theta_{re}} i_{sq} + \frac{d\varphi_{rd}}{d\theta_{re}} - \varphi_{sq} \right) i_{sd} + \left(\frac{dL_q}{d\theta_{re}} i_{sq} + \frac{dM_{qd}}{d\theta_{re}} i_{sd} + \frac{d\varphi_{rq}}{d\theta_{re}} + \varphi_{sd} \right) i_{sq} \right] \quad (2\text{-}1)$$

To maximise the torque produced for a given magnitude of current (and hence loss) it is usual to control the three-phase stator currents which orients the stator field. Maximum torque is achieved by aligning that the current with the so-called quadrature or 'q' axis while the current in the direct or 'd' axis is regulated to zero. Since the flux linkage due to the permanent magnets in an idealised PMSM varies sinusoidally with time, then $\varphi_{rq} = 0$ and $\varphi_{rd} = \varphi_m =$ constant.

In a well-designed PMSM, this sinusoidal flux distribution can be realised to a high degree of conformity and in such cases the expression for the electromagnetic torque when the maximum torque condition is satisfied by appropriate field control can be simplified to:

$$T_e = \frac{3}{2} Pn \varphi_m i_{sq} \qquad (2\text{-}2)$$

The corresponding d- and q-axis voltage equations are given by:

$$\begin{cases} v_{sd} = R_s i_{sd} + L_d \frac{di_{sd}}{dt} - \omega_e L_q i_{sq} \\ v_{sq} = R_s i_{sq} + L_d \frac{di_{sq}}{dt} + \omega_e L_d i_{sd} + K_e \omega_m \end{cases} \quad (2\text{-}3)$$

Where:

$\omega_e = \omega_m \times P_n$

$K_e = \varphi_m \times P_n$

The rotational motion expression which gives transient response of the machine is given by:

$$\frac{d\omega_m}{dt} = \frac{1}{J}(T_e - T_L - B\omega_m) \quad (2\text{-}4)$$

2.1.2. Servo control system

For applications such as spindle drives for milling machines, servo control is by far the most widely implemented control method. Three-term PID control is one of the most widely implemented control structures, although for most industrial machinery, PI controllers are often sufficient.

In a PI controller, the measured quantity being controlled is compared with the demand to generate an error signal. The control action is taken by combining contributions which are proportional to the error and the integral of the error over a prescribed interval. Different control actions have different effects. The proportional term produces control action which is proportional to the error:

$$u(t) = k_p e(\tau) \quad if\ e_{min} \leq e \leq e_{max} \quad (2\text{-}5)$$

Where the term $e_{min} e_{max}$ are the control band, the controller is only valid within the control band. However, since a proportional controller needs an error to produce any control action,

which leads to a so called steady-state error. This shortcoming can be overcome by introducing integral control action:

$$u(t) = k_i \int_0^t e(\tau)d\tau \qquad (2\text{-}6)$$

Most machine dynamics problems can be solved by PI controllers. Derivative control action can be used to refine the control effect by providing an anticipative ability for the control system. The principal of the derivative controller is to calculate the slope of the error over an interval and apply a gain k_d. The equation (2-8) shows the control law:

$$u(t) = k_d \frac{de(t)}{dt} \qquad (2\text{-}7)$$

A representative block-diagram for a PI speed controller is shown in Figure 8.

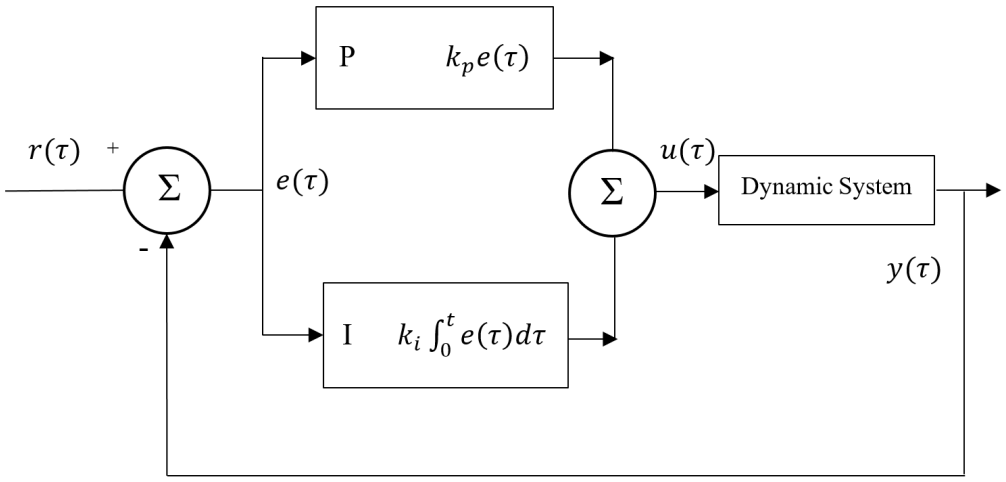

Figure 8 Block diagram of a typical PI speed controller

For a typical brushless AC motors in d-q reference frame, the de-coupled current control schemes for the d- and q-axes are shown in Figure 9. For the q-axis controller, improved performance is achieved by accounting for the back-emf from the permanent magnet flux.

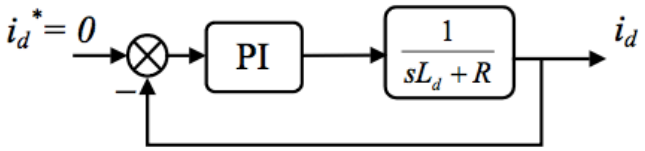

(a) d-axis current control loop

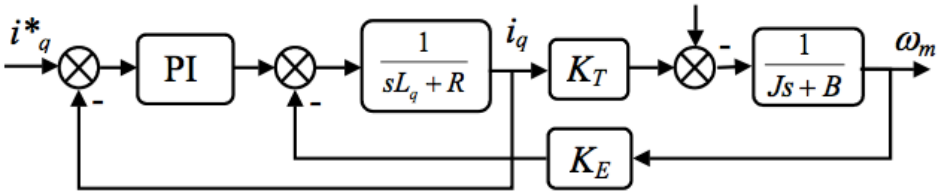

(b) q-axis current control loop

Figure 9 d- and q-axis current control block diagrams - d-axis demand of zero is for maximum torque conditions and non-field weakening. (Source [WAN 2011])

For detailed PI controller turning, please see **Appendix B.**

2.1.3. Pulse width modulation (PWM)

The control over the voltage applied to the PMSM is a key requirement for precise servo control. Except for some very low power drives, the control of output voltage in modern power converters is achieved almost universally by controlled switching of a DC voltage link rather than through linear amplifier control. The most widely used method for producing a given voltage waveform at the converter output are based on so-called pulse width modulation (PWM) techniques. Several variations of PWM strategies have been developed to achieve different aims [ZHO 02].

The basic principles of pulse width modulation to modulate a reference signal are illustrated by Figure 10. In the case shown a high frequency triangular waveform modulated a sinusoidal reference waveform signal to produce a pulse train.

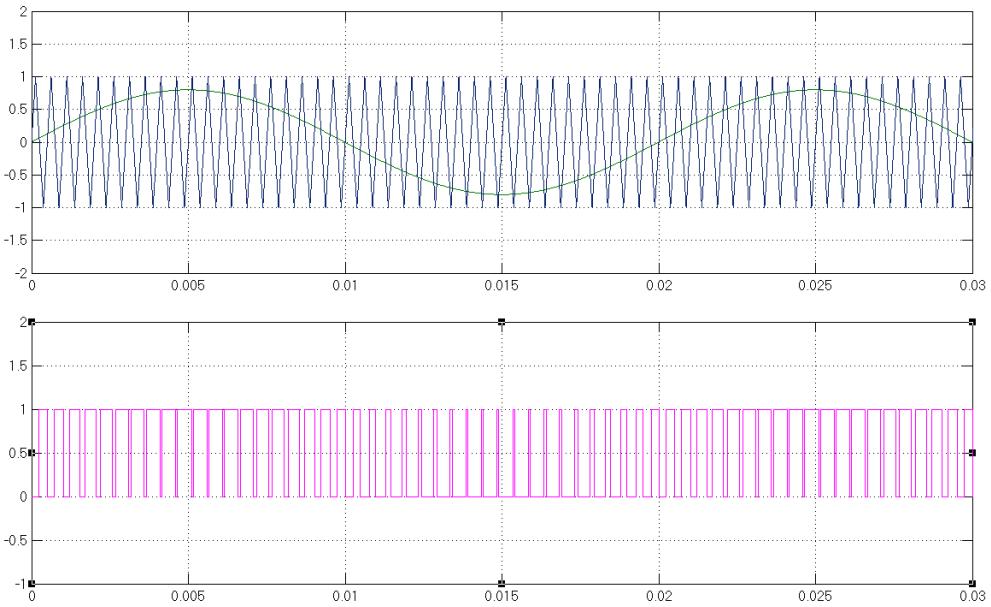

Figure 10 Pulse width modulation of sinusoidal reference signal with triangular carrier

The frequency of the modulation signal, also called PWM frequency, must be much greater than the fundamental of the reference signal in order to avoid excessive distortion in the output. It is a convenient rule of thumb the PWM frequency should be at least an order of magnitude higher than the reference signal. For a 10,000 rpm speed spindle, the PWM frequency is often at least 5000 Hz [SS 08]. Whereas this will lead to some distortion of the current waveform, it is likely to be adequate for set-point speed control which is reliant on average power delivery. However, for a highly dynamic control technique, such a low PWM frequency could be problematic. If the cutter has four flutes and torque needs to be modulated twice for each flute, the PWM frequency will need to increase up to 30kHz, a value towards the top-end or even beyond the capability of many industrial drives.

Space-vector PWM (SVPWM)

Space-vector PWM, has become a favoured PWM method in many three-phase converters. It is well suited to implementation in microprocessors to compute the duty cycle of the switches [HOL 92]. A classical Space-vector PWM technique from textbook is presented in [ZHO 02].

Space-vector PWM has eight different switching states. These eight switching states $S_0, \dots, S_7$ are defined by eight voltage vector combinations between $\overrightarrow{U_0} = [000], \dots, \overrightarrow{U_7} = [111]$ as shown in Figure 11. Voltage vectors $\overrightarrow{U_0}, \overrightarrow{U_7}$ are zero vectors while the remaining vectors, $\overrightarrow{U_1}, \dots, \overrightarrow{U_6}$ are switching state vectors and all vectors are displayed in Figure 12 shows the corresponding states of switches in the inverter. For detailed calculation see **Appendix C**

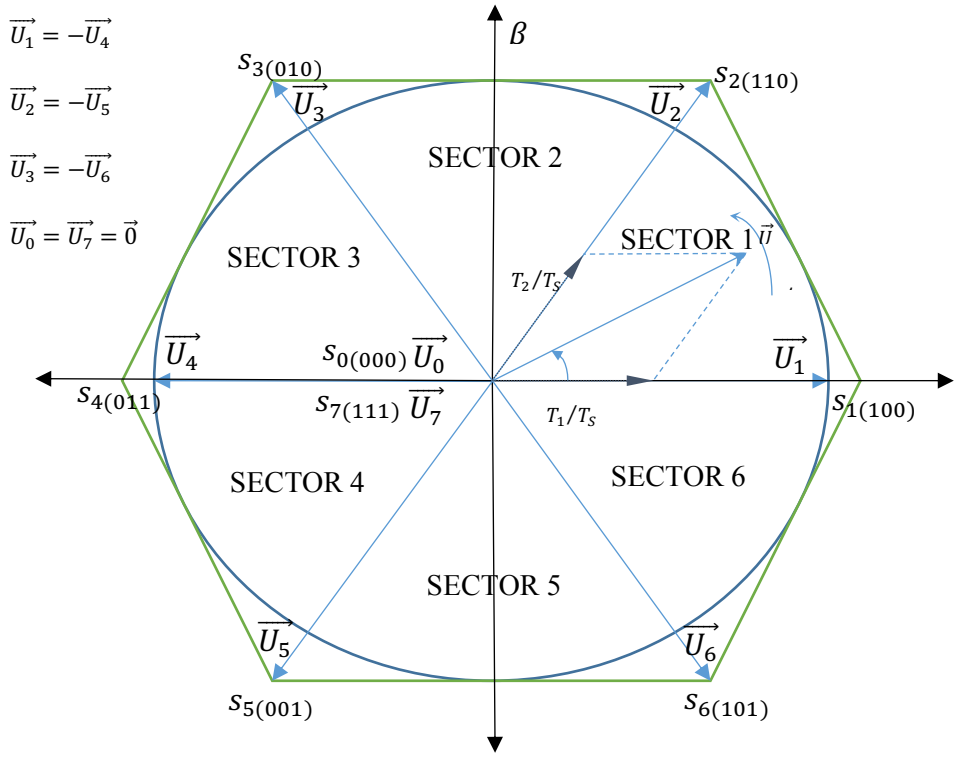

Figure 11 The corresponding states of switches in the inverter [ZHO 02]

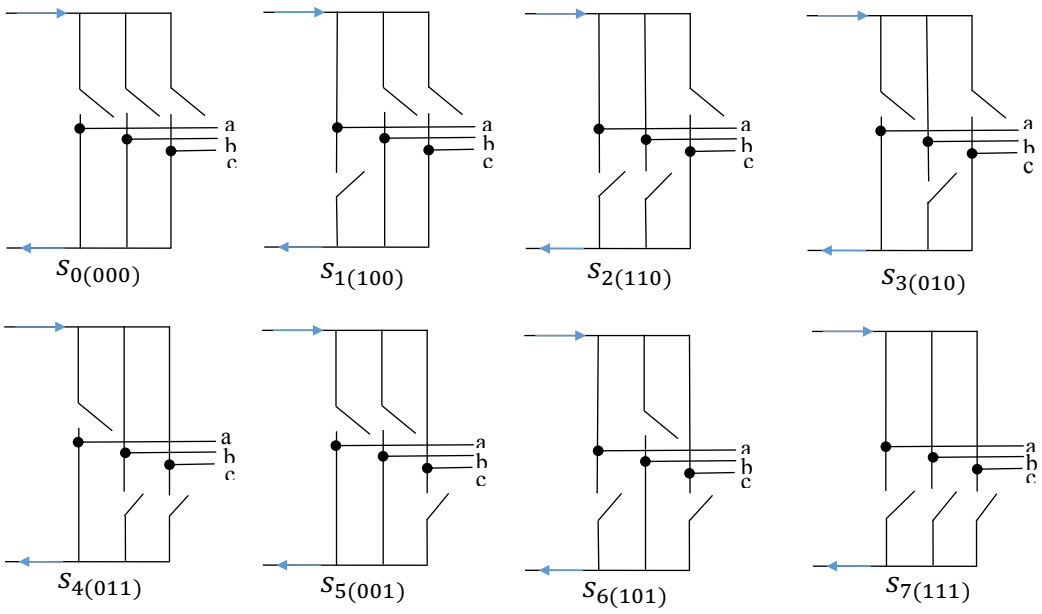

Figure 12 Voltage vector space [ZHO 02]

2.2. Time-domain milling model

2.2.1. Average cutting force model

The most straightforward representation of the cutting process is a simple constant load torque applied to the spindle drive. Although this is a very simple representation, it may well be adequate for modelling some aspects of behaviour, e.g. steady-state speed set-points, tuning of slow response speed controllers, calculation of machine efficiency and/or power consumption, rating of machines. It is important to recognise that even though the representation of the cutting load is very simple, the calculation of its magnitude may well be far from straightforward.

2.2.2. Dynamic modelling of cutting force

In order to investigate the relationship between cutting performance and the spindle control system it is necessary to establish a high-fidelity model of the cutting process including instantaneous predictions of dynamic forces on the cutting tool. The overall force exerted on the

cutting tool can be categorised into cutting forces and process damping forces. For a fixed depth of cut, the cutting force is proportional to the under-formed chip thickness. The process damping forces are caused by deformation of the work piece by the cutter [WU 88]. During milling, the cutter leaves a waved surface finish due to vibrations, process damping force occurs when the cutter interacts with the waved surface.

In high speed milling, the cutting forces dominate the process damping force and the latter can often be neglected [KHA 13] [SIM 08] [SIM 05]. Consequently, this research mainly focusses on the cutting forces in high speed milling process.

2.2.3. Vibration-free model of the cutting process

The most straightforward cutting models of the peripheral milling process do not account for vibration of the cutter. This approach assumes that there is no relative displacement between the cutter and the work-piece and hence the chip formation between successive passes of the cutter blades remains consistent and defined by the geometry of the cutter and the feed rate. The vibration free model employed in this thesis is formulated from orthogonal cutting theory, building on the model presented by Tlusty [TLU 00]. The overall cutting force is formed through a combination of differential, tangential and radial cutting force components:

$$dF_t = K_s t(\varphi) dz \qquad (2\text{-}8)$$

$$dF_r = c dF_t \qquad (2\text{-}9)$$

The key factor in establishing the magnitude of the cutting force is the tangential cutting force coefficient, K_s. This is established using the method proposed in [LIU 02] [WU 88] Figure 13 shows a schematic representation of the helical flute edge geometry of a peripheral end milling cutter. The cutting force is dependent on the under formed chip thickness

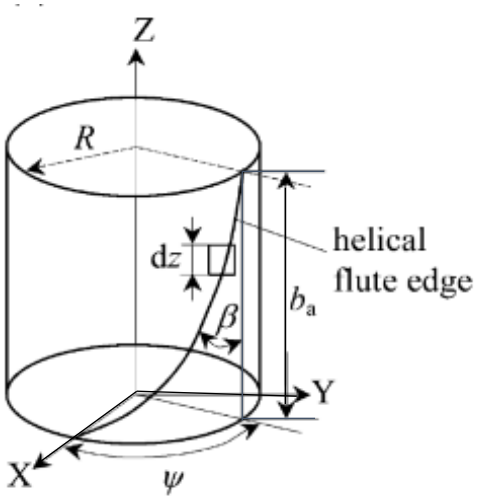

Figure 13 Helical flute edge geometry (Source: [SHA 05])

$$K_s = k_s{}' R cot\beta \qquad (2\text{-}10)$$

The calculation of tangential cutting force coefficient is based on the size effect of under formed chip thickness and the influence of effective rake angle as presented in [SHA 05].

$$\text{For } k_s{}' = u_0\left(1 - \frac{\alpha_e - \alpha_{e0}}{100}\right)\left(\frac{t_0}{t_i(\varphi_i)}\right)^{0.2} \qquad (2\text{-}11)$$

Calculation of $t(\varphi)$

In the up-milling process, for i[th] helical tooth of ideal non-vibration model the under formed chip thickness at position φ_i can be calculated as [SHA 05]:

$$t_i(\varphi_i) = \begin{cases} f_t \sin\varphi_i & if\ 0 \le \varphi_i \le \Omega \\ 0 & else \end{cases} \qquad (2\text{-}12)$$

Where f_t is feed per tooth per revolution, Ω is the cutter radial immersion angle within the radial depth of cut, and $\Omega = \arccos\left(1 - \frac{d}{R}\right)$, where d is radial depth of cut in peripheral milling and the position angle is:

$$\varphi_i = \varphi + \theta + (i-1)\frac{2\pi}{m} \qquad (1 \le i \le m,\ 0 \le \varphi \le \psi) \qquad (2\text{-}13)$$

ψ is the helix lag angle is determined by:

$$\psi = \frac{b_a \tan\beta}{R} \qquad (2\text{-}14)$$

Substituting (2-14) and (2-15) back into (2-13) and (2-12) yields:

$$dF_{ti} = u_0\left(1 - \frac{\alpha_e - \alpha_{e0}}{100}\right)\left(\frac{t_0}{t_i(\varphi_i)}\right)^{0.2} Rt(\varphi_i) cot\beta d\varphi_i \qquad (2\text{-}15)$$

$$dF_{ri} = c dF_{ti} \qquad (2\text{-}16)$$

The cutting forces can be resolve into a Cartesian x-y system

For the tangential component of cutting force:

$$\begin{cases} dF_{tix} = -k_s{}'t(\varphi_i)Rcot\beta \sin\varphi_i \, d\varphi_i \\ dF_{tiy} = k_s{}'t(\varphi_i)Rcot\beta \cos\varphi_i \, d\varphi_i \end{cases} \qquad (2\text{-}17)$$

and similarly, for the radial component cutting force:

$$\begin{cases} dF_{rix} = -ck_s{}'t(\varphi_i)Rcot\beta \cos\varphi_i \, d\varphi_i \\ dF_{riy} = -ck_s{}'t(\varphi_i)Rcot\beta \sin\varphi_i \, d\varphi_i \end{cases} \qquad (2\text{-}18)$$

Summing these two sets of equations together yields:

$$\begin{cases} dF_{ix} = -k_s{}'t(\varphi_i)Rcot\beta(\sin\varphi_i + c\cos\varphi_i)d\varphi_i \\ dF_{iy} = k_s{}'t(\varphi_i)Rcot\beta\,(\cos\varphi_i - c\sin\varphi_i)\,d\varphi_i \end{cases} \qquad (2\text{-}19)$$

The cutting force applied on entire cutter for i^{th} flute is:

$$\begin{cases} F_{ix} = \int_{\varepsilon_s}^{\varepsilon_e} dF_{ix} d\varphi_i \\ F_{iy} = \int_{\varepsilon_s}^{\varepsilon_e} dF_{iy} d\varphi_i \end{cases} \qquad (2\text{-}20)$$

Where ε_s and ε_e are the start and end points angular locations of cutting edge.

For the whole cutting tool with m flutes, the summation of the cutting forces gives:

$$\begin{cases} F_x = \sum_{i=1}^{m} F_{ix} \\ F_y = \sum_{i=1}^{m} F_{iy} \end{cases} \qquad (2\text{-}21)$$

2.2.4. Mathematical model of Peripheral Milling with vibrations

The main difference between this model and idealised vibration free model is the continuous calculation of a dynamic chip thickness. In the vibration free model in section 2.2.3, the under formed chip thickness in up-milling is assumed to be constant and hence does not reflect any displacements during vibration. In order to incorporate vibration into the model, the dynamic chip thickness calculated from a combination of the current tooth is tip position and the waved surface of the work piece. The model adopted in this thesis draws on the analysis method developed in [SIM 05] but has been implemented in a custom SIMULINK function and included several additional features, i.e. vibration free, errors on the frequency and amplitude. The detailed calculation is shown in the following sections. (Note: all coordinates are defined in the global coordinate system)

Calculation of current tooth tip position:

For any instantaneous time-step, the tooth tip position (S_{ctx}, S_{cty}) in i_{th} layer can be calculated from machine tool centre (S_{otx}, S_{oty}), the angular position φ_i and machine tool radius r_t as:

$$\begin{cases} S_{ctx} = S_{otx} + r_t \cos(\varphi_i) \\ S_{cty} = S_{oty} + r_t \cos(\varphi_i) \end{cases} \qquad (2\text{-}22)$$

Calculation of current work piece wave surface points:

At each time step, the work piece wave surface can be discretised into number of points using semi-discretized theory. For the current tooth tip position, the two nearest surface points along

the previous wave surface segment geometry are (S_{sx0}, S_{sy0}) and (S_{sx1}, S_{sy1}). As the surface wave is left by the tool tooth tip from previous passes, the points on the surface is determined by the tooth tip position from a previous pass of a tooth. However, is it not necessarily from the most recent passing tooth pass, e.g. excessive vibration can cause the tooth to jump out of the work piece and in such a case the wave pattern will be determined from a previous pass of a cutting tooth. The angular position from previous wave surface points to current tooth centre are:

$$\begin{cases} \varphi_{p0} = \tan^{-1}\left(\frac{S_{oty}-S_{sy0}}{S_{otx}-S_{sx0}}\right) \\ \varphi_{p1} = \tan^{-1}\left(\frac{S_{oty}-S_{sy1}}{S_{otx}-S_{sx1}}\right) \end{cases} \quad (2\text{-}23)$$

Calculation of the dynamic chip thickness:

As the chip thickness is distance between current tooth tip position and wave surface segment, the distance from tool centre to two points on the wave surface r_0, r_1 needs to be calculated. The geometry representation of Figure 14 can be used as the basis for the calculation of dynamic chip thickness.

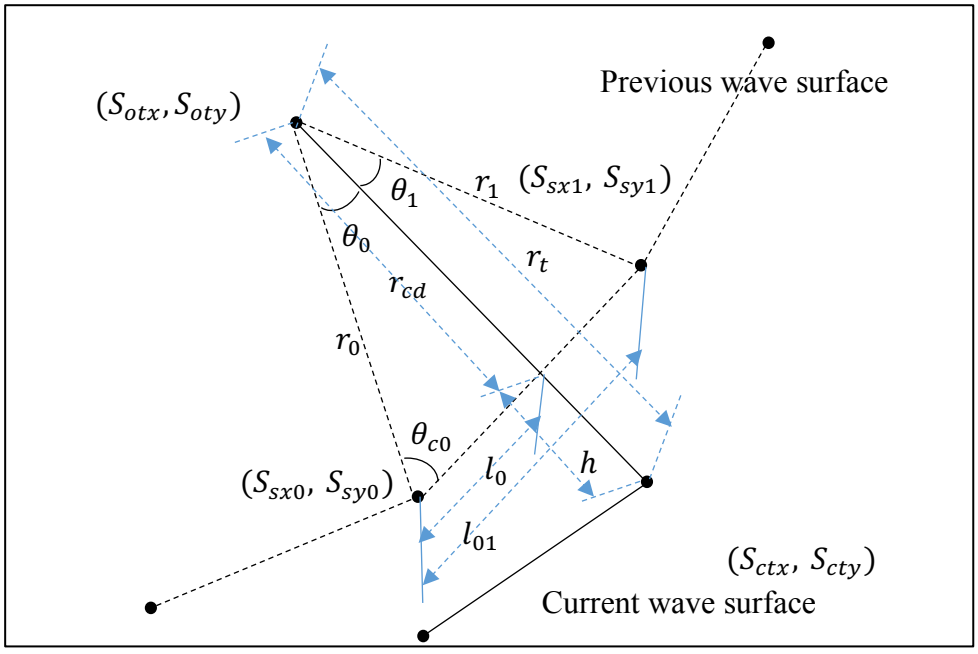

Figure 14 Geometry for chip thickness calculation

The expressions for r_0 and r_1 are:

$$\begin{cases} r_0 = \sqrt{(S_{otx} - S_{sx0})^2 + (S_{oty} - S_{sy0})^2} \\ r_1 = \sqrt{(S_{otx} - S_{sx1})^2 + (S_{oty} - S_{sy1})^2} \end{cases} \quad (2\text{-}24)$$

$$\begin{cases} \theta_0 = |\varphi_i - \varphi_{p0}| \\ \theta_1 = |\varphi_i - \varphi_{p2}| \end{cases} \quad (2\text{-}25)$$

The length of the segment is given by:

$$l_{01} = \sqrt{r_0^2 + r_1^2 - 2r_0 r_1 \cos(\theta_0 + \theta_1)} \quad (2\text{-}26)$$

$$\theta_{c0} = \cos^{-1}\left(\frac{r_0^2 + l_{01}^2 - r_1^2}{2r_0 l_{01}}\right) \quad (2\text{-}27)$$

Since

$$\begin{cases} r_0 = r_{cd}\cos\theta_0 + l_0 cos\theta_{c0} \\ r_{cd} sin\theta_0 = l_0 sin\theta_{c0} \end{cases} \quad (2\text{-}28)$$

Thus

$$r_{cd} = r_0 \frac{sin\theta_{c0}}{sin\theta_0 cos\theta_{c0} + cos\theta_0 sin\theta_{c0}} \quad (2\text{-}29)$$

For calculation of dynamic chip thickness h,

$$h = r_t - r_{cd} \quad (2\text{-}30)$$

Dynamic cutting force depends on the instantaneous chip thickness formation, since the thickness is directly related to the current tooth tip position and the waved surface left by the last cut. The cutting force applied on the cutter then excites vibration in the cutting system, which yields a small shift in the cutting tool centre. This results in a change in the coordinates of tooth tip position. As the tooth tip shifts away from its original nominal trajectory, it leaves a fine-scale wave like surface in the material. When the second cutter engages the material, the

wave like surface and the oscillating cutter generates an uneven cutting force, giving rise to further vibration. Due to phase shifts in the tool position with successive passes, the vibration can either be reinforced or diminish with time.

The term ‘chatter’ refers to the case when the vibration builds up in magnitude with successive tooth passes resulting in a growing and unstable vibrations. The transition between stable and unstable cutting is influenced by a number of complex interactions and not simply with increasing rotational speed or material removal rates.

A second order representation is usually deemed adequate to describe the dynamics of the milling cutter [SIM 05]. Figure 15 shows a block diagram representation of the model mechanism.

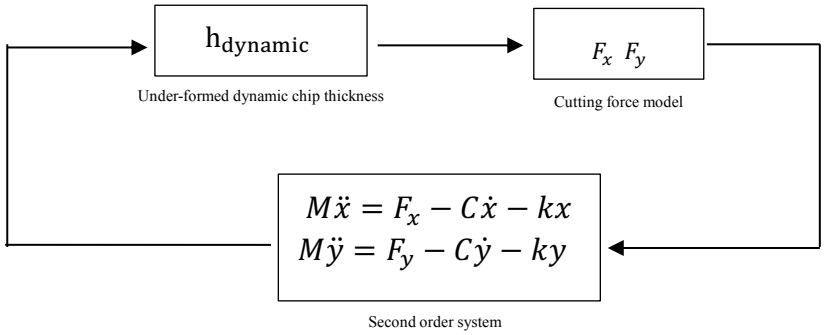

Figure 15 Dynamic model of vibration

2.3. Validation by comparison with published simulations

In the absence of access to an instrumented milling machine in direct support of this research, the validation of the system model, in particular the cutting model, was initially performed by comparison with published simulation and experimental results [KHA 13] and [SIM 05]. The simulations presented in [KHA 13] which form the basis of the comparison are for an up-milling operation using tool parameters and machine settings listed in Table 1.

Table 1 Tool parameters and machine settings from [KHA 13] for validation

Parameter	**Value**
Cutting tools radius	10 mm
Radial depth of cut	10 mm
Maximum axial depth of cut	20 mm (10 12 14 16 &18 mm)
Number of teeth	4
Feed rate	0.05 mm/tooth
Natural frequency	700 Hz
Stiffness	8×10^7 N/m
Damping Ratio	0.3%
Tangential cutting coefficient	796.1 N/mm^2
Radial cutting coefficient	168.8 N/mm^2
Helix angle	0°
Spindle speed	3000 rpm
Iteration per revolution	256 (iters)

This is a tool with straight sided teeth (i.e. no helical twist) and hence there will be intervals during which there is no tool engagement and hence zero load torque. It is also likely that impact effects associated with the tool will be more pronounced that is the case for a helical tool.

The model described and deployed in [KHA 13] is based on an idealised speed-stiff drive system. The authors in [KHA 13] and [SIM 05] employed a fixed-time step of 7.8×10^{-5} sec in their simulations. The rationale for selecting this time step duration was not discussed in any meaningful sense in both papers.

A series of simulations were performed with the model described previously in sections 2.1 and 2.2, for a cutting depth of 10 mm and a nominal rotational speed of 3,000 rpm. These conditions were used as they provide stable cutting conditions. In the first instance, all simulations were performed with a fixed time-step of 4×10^{-6} s. Two different models were considered:

- A simple speed-stiff input to the cutting model block in order to provide a like-for-like comparison with the results presented in [KHA 13]
- A model in which the full spindle drive model was used. Parameters of the motor applied in this research are given in **Appendix A**. The speed controller bandwidth was set to 314 rad/s (~50 Hz), settings which led to a typical speed fluctuation of ±95 rpm during milling for a set-point of 3,000 rpm. These conditions are near constant speed and hence provide a reasonable comparison with the speed-stiff results presented in [KHA 13] but are likely to include additional features introduced by the speed controller.

2.3.1. Simulations for a 10 mm depth of cut at 3000 rpm

Figure 16, Figure 17 and Figure 18 show comparison of cutting forces predicted in [KHA 13] and those predicted by the two simulation models. There is good agreement in terms of cutting force peak magnitude torque (3.64 Nm, 3.64 Nm and 3.65 Nm respectively), the corresponding time variations in chip thickness and the work done to the system. (Note: all the figures are based on first 20 revolutions)

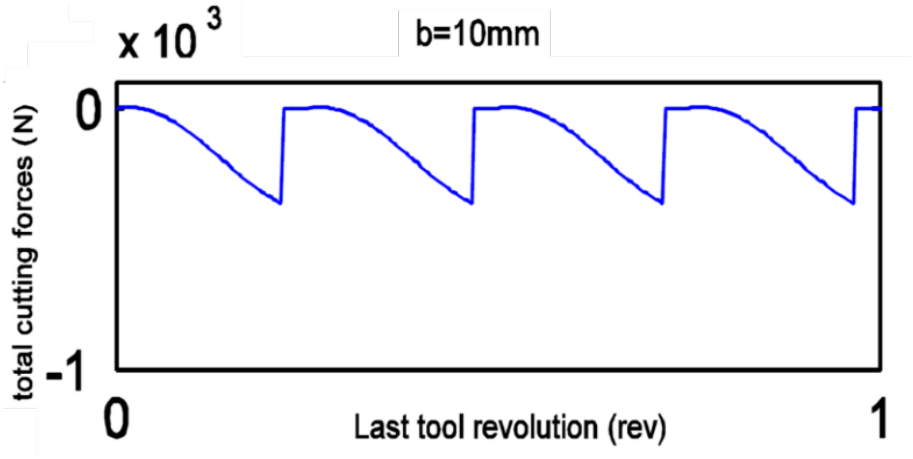

(a) Predicted force variation from (Source [KHA 13])

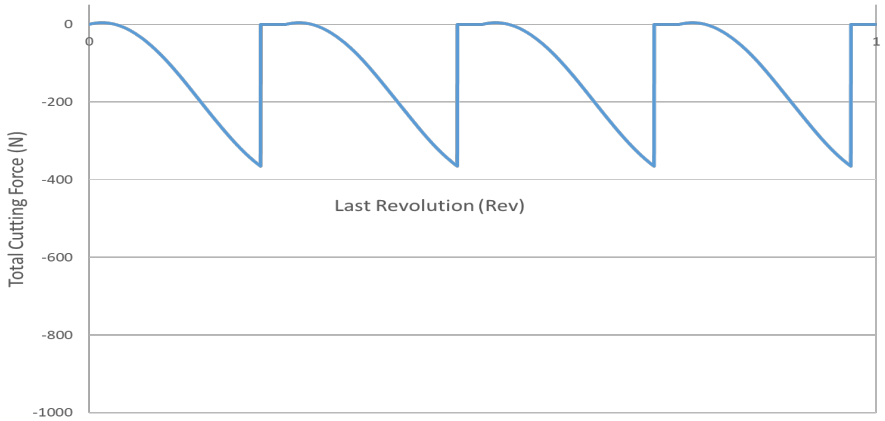

(b) Predicted force variation with speed stiff input to cutting model

(c) Predicted cutter force with 314 rad/s bandwidth speed controller in a full spindle drive model

Figure 16 Comparison of cutting forces predicted by three models for a nominal rotational speed of 3000 rpm and a cutting depth of 10 mm (all other parameters as specified in Table 1)

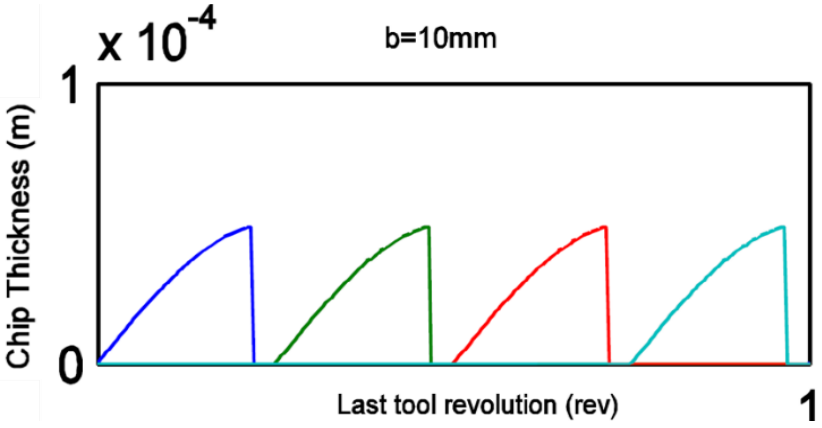

(a) Predicted chip thickness variation from (Source [KHA 13])

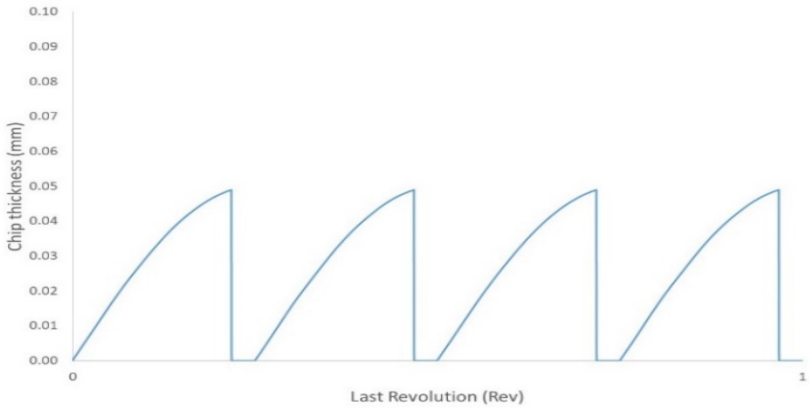

(b) Predicted chip thickness variation with speed stiff input to cutting model

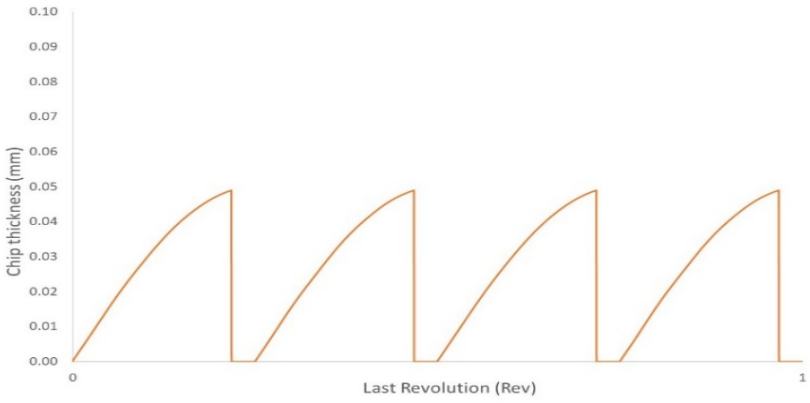

(c) Predicted chip thickness with 314 rad/s bandwidth speed controller in a full spindle drive model

Figure 17 Comparison of chip thickness predicted by three models for a nominal rotational speed of 3000 rpm and a cutting depth of 10 mm (all other parameters as specified in Table 1)

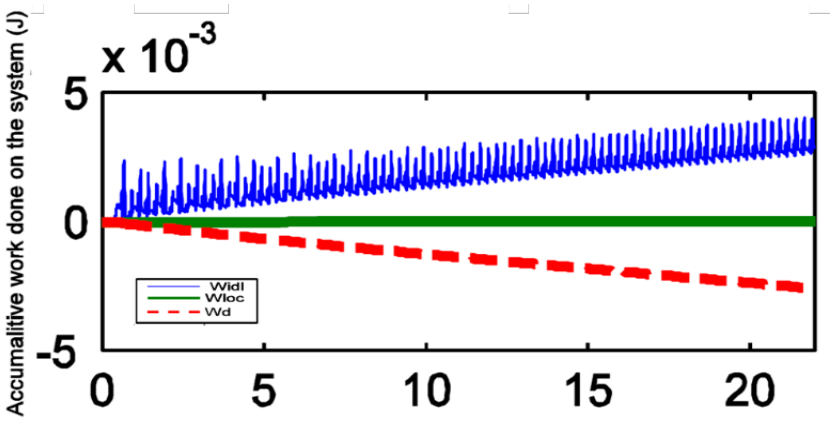

(a) Predicted work done to the system variation from (Source [KHA 13])

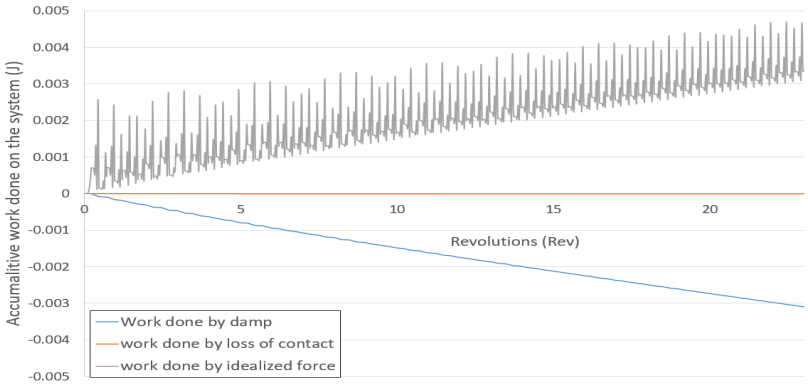

(b) Predicted work done to the system variation with speed stiff input to cutting model

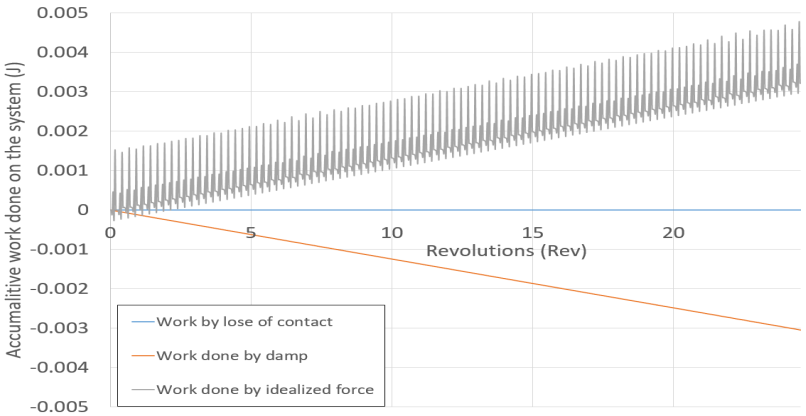

(c) Predicted work done to the system with 314 rad/s bandwidth speed controller in a full spindle drive model (interval shown is for steady-state conditions)

Figure 18 Comparison of work done to the system predicted by three models for a nominal rotational speed of 3000 rpm and a cutting depth of 10 mm (all other parameters as specified in Table 1)

2.3.2. Simulations for a 14 mm depth of cut at 3000 rpm

The comparisons in section 2.3.1 are at stable cutting operation with a combination of speed at 3000 rpm and depth of cut at 10 mm. If the cutting depth is increased to 14 mm at the same speed of 3,000 rpm, then the results in [KHA 13] indicate cutting is unstable. It is stable in that the vibration predicted in [KHA 13] does not keep increasing to become unstable, but it does involve some significant vibration. This is evident in the form of the various cutting waveforms. Figure 19 shows the variation in cutting force for the two speed-stiff models at this new operating point (the corresponding speed controller waveform is separated out on this occasion). As will be apparent, the cutting force predicted in [KHA 13] is no longer periodic with successive blade passes as there are vibration induced effects which are not synchronous with the blade passing. The cutting force predicted by model described in section 2.2.4, and which is shown in Figure 19 (b), is good agreement in both form and magnitude with the force variation from [KHA 13]. It is worth noting that due to absence of periodicity, it was necessary to scan through the full waveform if cutting force with the speed stiff model to identify the corresponding interval with that published in [KHA 13].

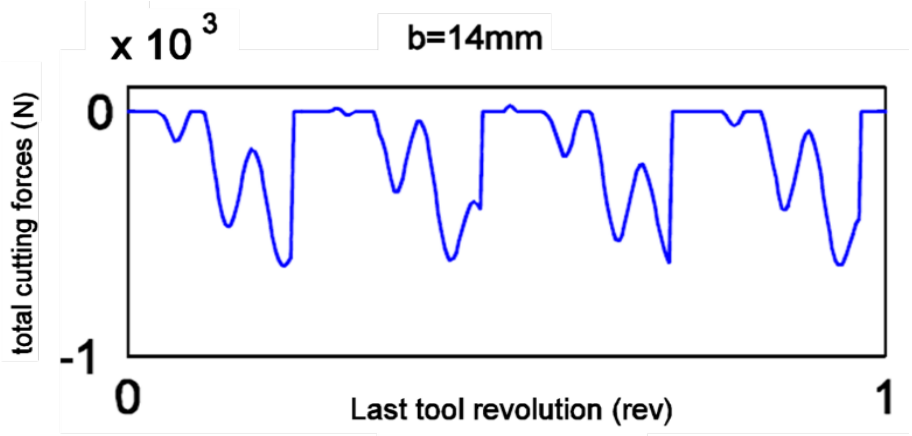

(a) Predicted force variation from (Source [KHA 13])

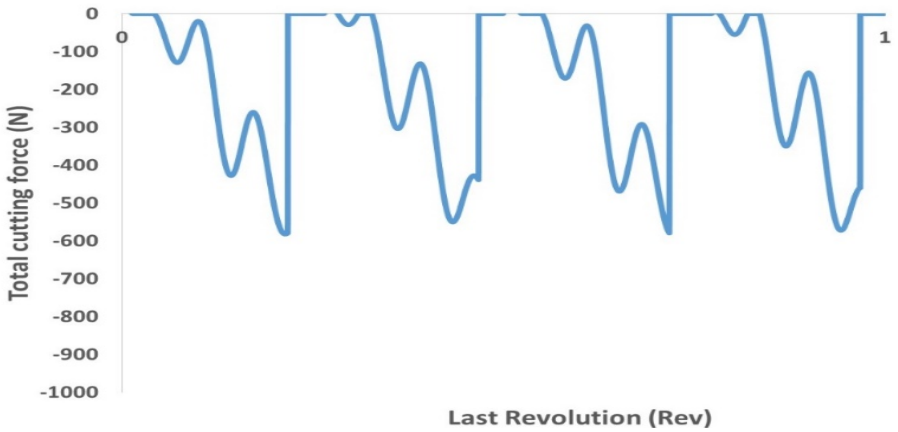

(b) Predicted force variation with speed stiff input to cutting model

Figure 19 Comparison of cutting forces predicted for the two speed stiff models for a nominal rotational speed of 3000 rpm and a cutting depth of 14 mm (all other parameters as specified in Table 1)

With a cutting depth of 14 mm, the speed controller with a bandwidth of 314 rad/s eventually leads to unstable cutting. The evolution of this instability is shown in Figure 20. The first 0.5 sec involves the spindle machine accelerating up to the reference speed of 3000 rpm with no cutting action. At 0.5 sec, the cutter begins to engage with the work-pieces. Three zoomed-in waveforms for intervals A, B and C of Figure 20 are shown in Figure 21. As will be evident from Figure 21 , the variations of total cutting force at time 0.58 sec, 1.4 sec and 2.602 sec predicted by the model described in this chapter shows good agreement with those from [KHA

13] in the case of the speed stiff model and reasonable agreement with the speed controller model. The effect of the speed controller on the chatter building up is neglectable.

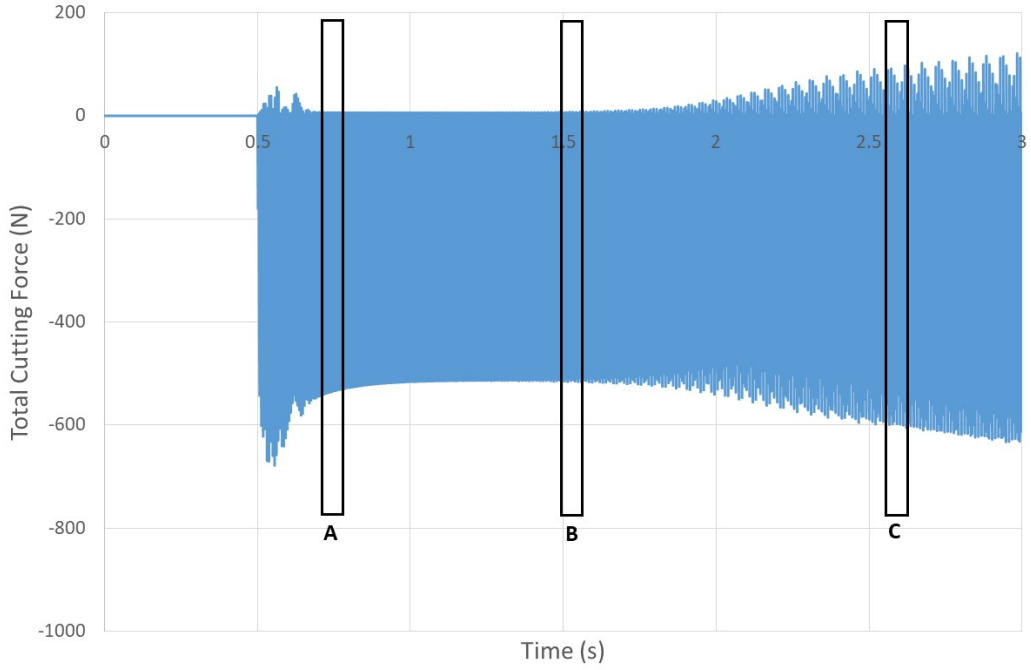

Figure 20 Predicted cutting force for a speed controlled drive (bandwidth of 314 rad/s) for a nominal rotational speed of 3000 rpm and a cutting depth of 14 mm (all other parameters as specified in Table 1)

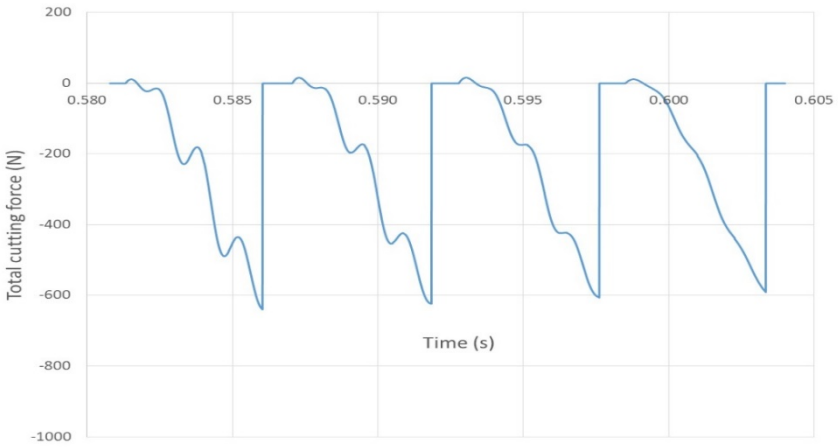

(a) Zoom-in of region (A) in Figure 20

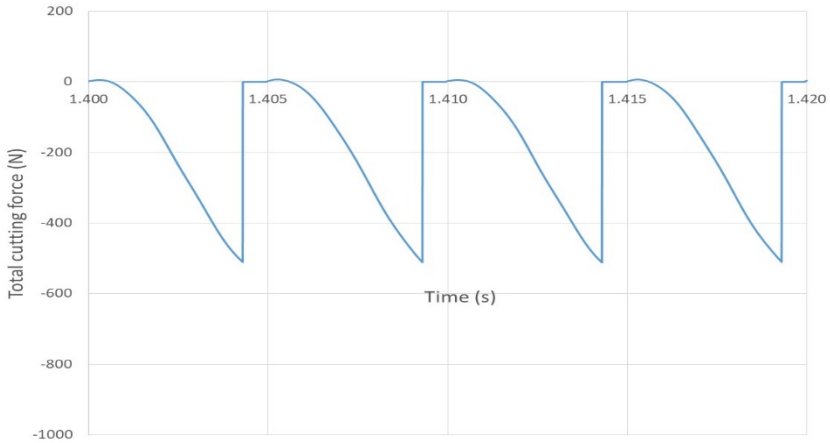

(b) Zoom-in of region B in Figure 20

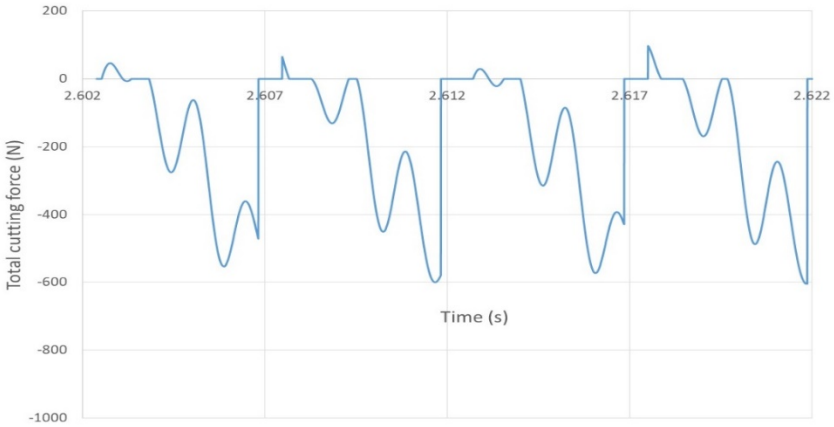

(c) Zoom-in of region C in Figure 20

Figure 21 Close-up of key regions in Figure 20 Predicted cutting force for a speed controlled drive (bandwidth of 314 rad/s) for a nominal rotational speed of 3000 rpm and a cutting depth of 14 mm (all other parameters as specified in Table 1)

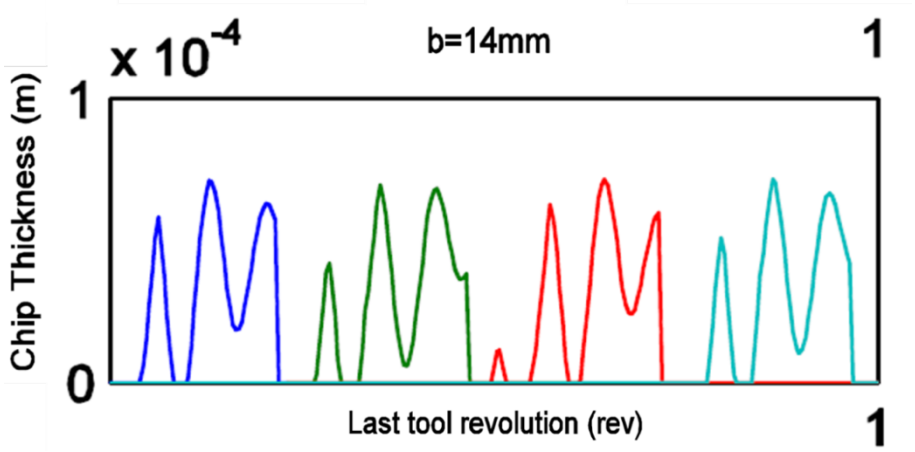

(a) Predicted chip thickness variation from (Source [KHA 13])

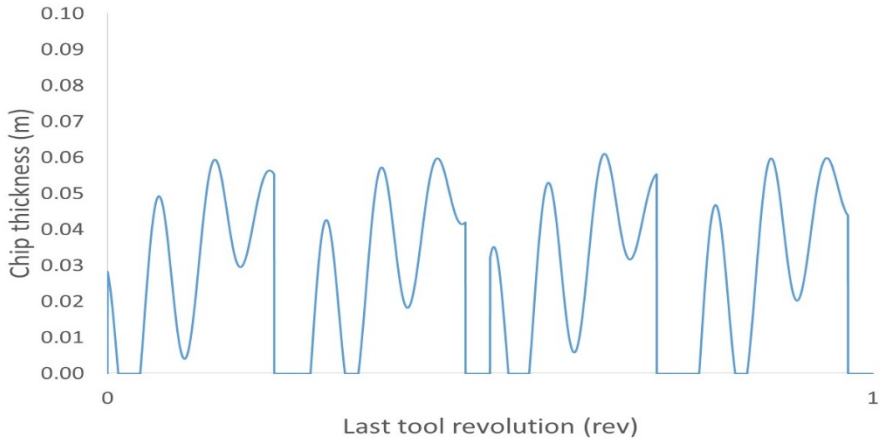

(b) Predicted chip thickness with 314 rad/s bandwidth speed controller in a full spindle drive model

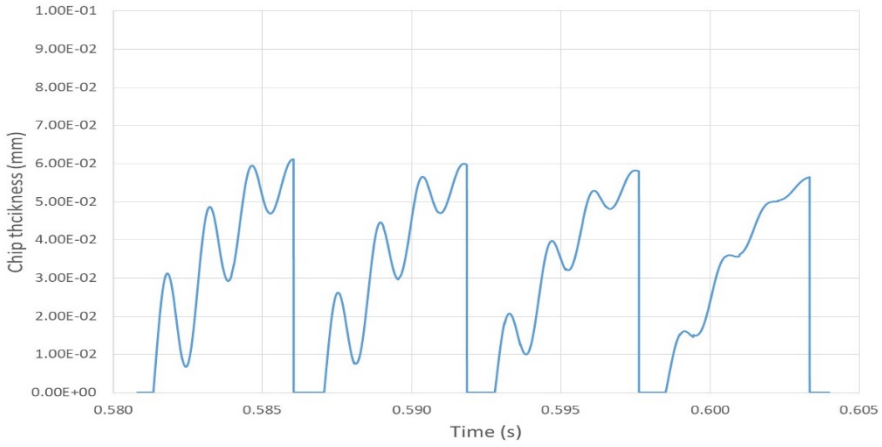

(c) Predicted chip thickness with 314 rad/s bandwidth speed controller at time 0.58 sec

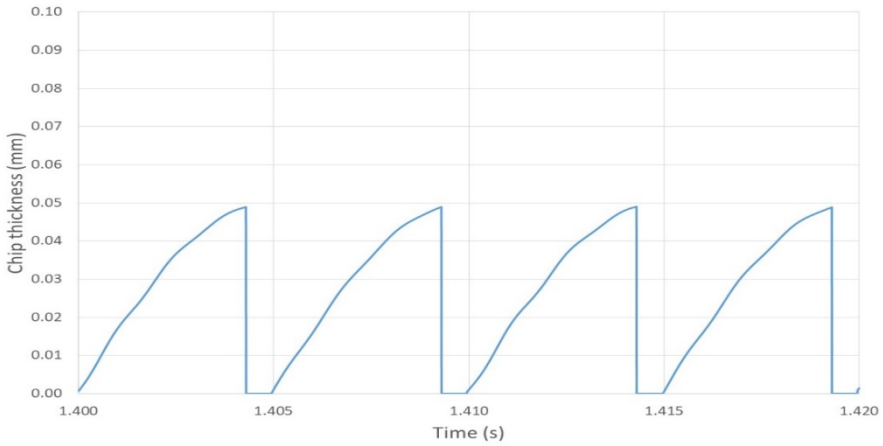

(d) Predicted chip thickness with 314 rad/s bandwidth speed controller at time 1.4 sec

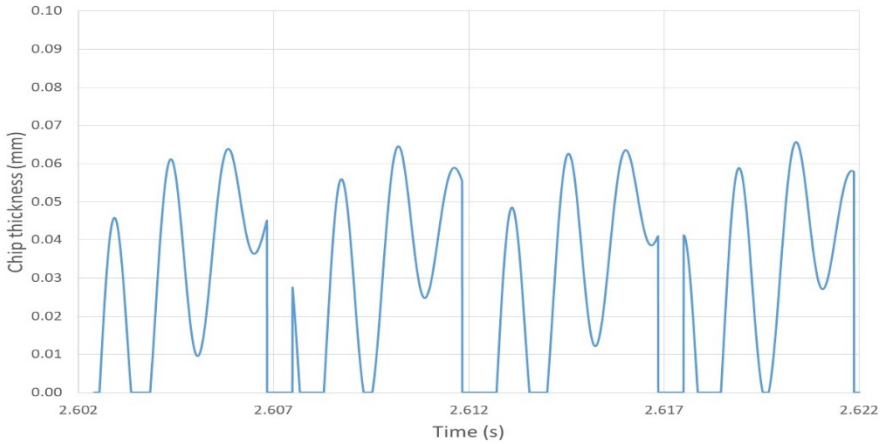

(e) Predicted chip thickness with 314 rad/s bandwidth speed controller at time 2.602 sec

Figure 22 the dynamic chip thickness at operating time shown in Figure 20 Predicted cutting force for a speed controlled drive (bandwidth of 314 rad/s) for a nominal rotational speed of 3000 rpm and a cutting depth of 14 mm (all other parameters as specified in Table 1)

2.4. Validation by comparison with published experimental measurements

Detailed experimental milling trials were reported by Insperger et al in [INS 03]. An instrumented work-piece mounting plate shown in Figure 23 was used to investigate vibration behaviour during milling, including assessing stability at a range of rotational speeds and depth of cut. It is worth noting that although speed measurements were logged, this was based on a simple once per revolution measurements.

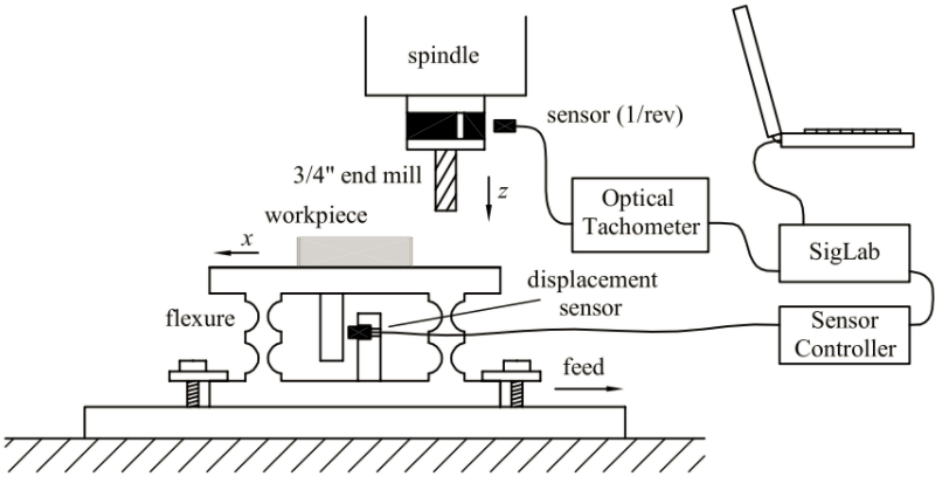

Figure 23 Schematic representation experimental arrangements used in [INS 03] (Source [INS 03])

Figure 24 shows the results of stability assessment performed at a series of discrete speeds between 3,300 rpm and 3,600 rpm and a number of cutting depths between 0.6 mm and 4 mm. Stable cutting combinations are designated by an ‘o’ while unstable cutting combinations are denoted by an ‘x’. Also shown in Figure 24 are the theoretical stability lobes predicted in [INS 03].

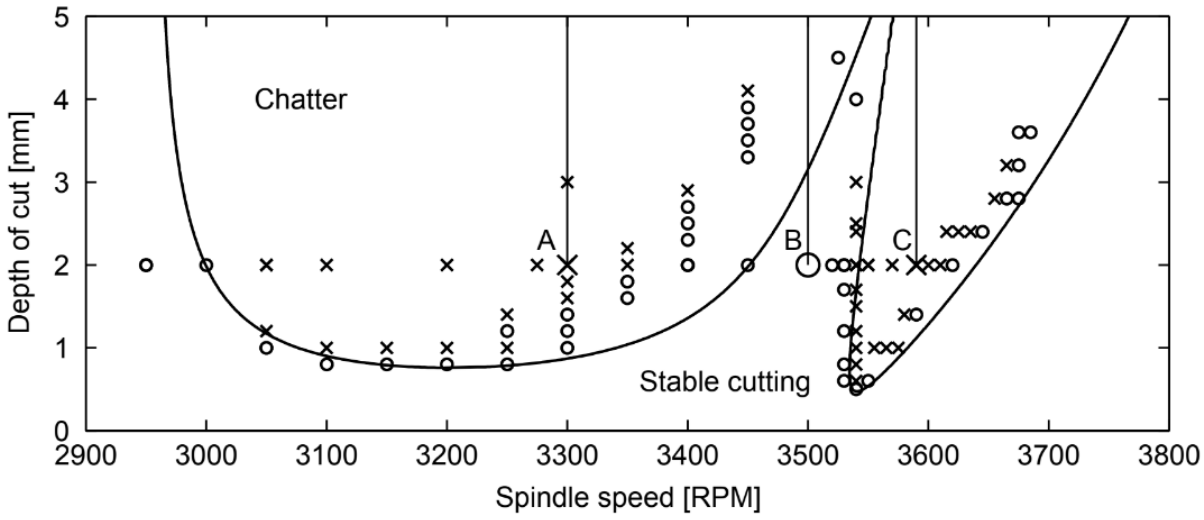

Figure 24 Experimental measurements of stability reported by Insperger (Source: [INS 03])

A series of simulations were performed with a speed stiff input into the cutting model described in section 2.2.4. The cutting parameters extracted from [INS 03] are summarised in Table 2. A series of simulations were performed at selected speeds that match those used by the authors of [INS 03]. Table 3 shows a summary of the simulated stability at a series of speeds and depths of cut alongside the measured indication of stability in [INS 03]. As shown, there is good agreement between the simulations performed and the measured results reported in [INS 03]. There are a few operating points, shaded in Table 3, in which there are some discrepancy. However several of these test points, e.g. 3530 rpm are on the transition between stable and unstable operation.

Table 2 Tool parameters and machine settings from [INS 03] for validation

Parameter	**Value**
Cutting tools radius	9.525 mm
Number of teeth	1
Feed rate	0.1016mm/tooth
Natural frequency	146.8 Hz
Stiffness	2.2×10^6 N/m
Damping Ratio	0.38%
Tangential cutting coefficient	1.9×10^8 N/m^2
Radial cutting coefficient	1.52×10^8 N/m^2
Helix angle	0°

Table 3 Comparison between stability predicted by the model in section 2.2.4 and measured stability in [INS 03]

(o – stable, x – unstable)

Speed (rpm)	Depth of cut (mm)	Stability from simulations	Stability measured in [INS 03]
3300	1.0	0	0
	1.2	0	0
	1.4	0	0
	1.6	0	x
	1.8	x	x
	2.0	x	x
3400	2.0	0	0
	2.3	0	0
	2.5	x	0
	2.7	x	0
	2.9	x	x

3500	2.0	0	0
3520	1.5	0	0
	2.0	0	0
3530	1.1	0	0
	1.2	x	0
	2.0	x	0
3540	0.5	0	0
	0.6	0	x
	0.8	x	x
	2.0	x	x
3550	0.6	0	0
	2.0	x	x
3560	1.0	0	x
	1.2	0	x
	1.3	x	x
	1.4	x	x
	1.5	x	x
3570	1.0	0	x
	1.4	0	x
	1.5	x	x
	2.0	x	x
3580	1.4	0	x
	1.6	x	x
3590	1.4	0	0
	2.0	x	x
3600	2.0	0	x

In addition to stability measurements, the performance at three specific points (designated as A, B and C in Figure 20) were measured. Figure 25 shows a comparison between the vibration at point A shown in Figure 25 and predicted with a speed-stiff input to the model described in section 2.2.4. Although the vibration in the predicted waveforms is not growing in magnitude, this combination of speed, depth of cut and feed rate produce unstable cutting as indicated from the contact loss accumulated work. The time sequences in Figure 25 have different start-up profiles (not provided in [INS03]) and hence it is only the vibration beyond 5 sec in the measured data can be compared with the simulation output. As shown, there is good agreement in terms of the magnitude of vibration.

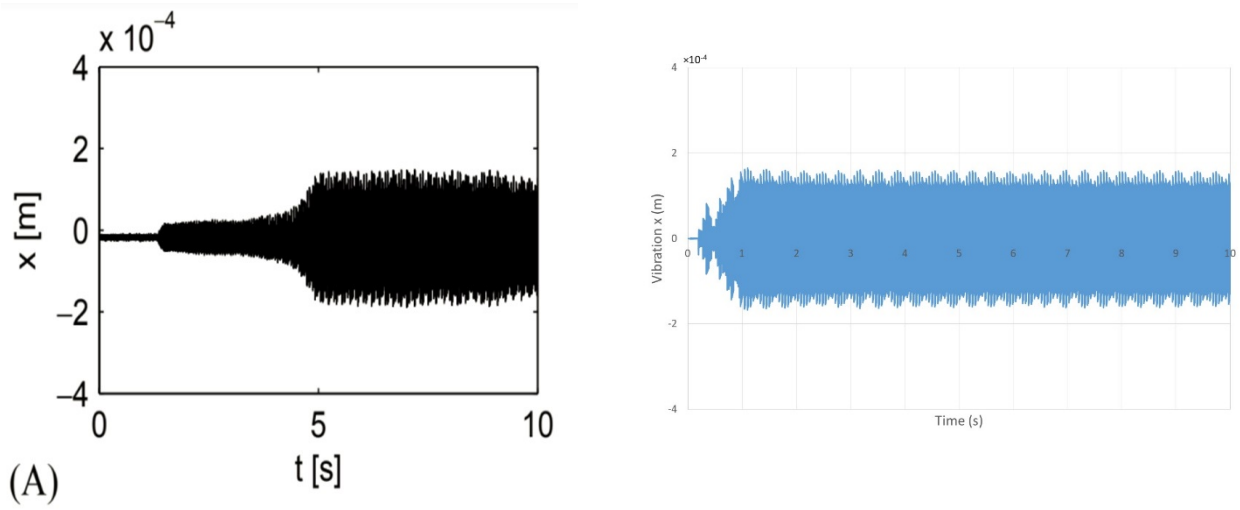

Measured from [INS 03] Predicted

Figure 25 Comparison between measured [INS 03] and simulated vibration at a rotational speed of 3,300 rpm and a depth of cut of 2 mm

2.5. Influence of time-step duration

One important consideration in determining the likely accuracy of a cutting model is the selection of an appropriate time-step for a given simulation. The authors of [KHA 13] used a fixed time step of 7.8×10^{-5} sec which they deemed to be appropriate, but did not provide comprehensive evidence to support their assertion of the suitability of the time-step duration selected. In order to both verify the model and understand the interactions between time step duration and model performance, a systematic study was undertaken using the model developed in this section.

Figure 26 shows the influence of simulation time step on the peak cutting force predicted for the same conditions of a depth of cut at 14 mm for a rotational speed of 3,000 rpm. The peak cutting force provides an indication of the degree of disturbance to the cutting torque profile and hence the level of vibration and whether chatter is developing. As shown by Figure 26, time steps

greater than 20μs tend to predict stable cutting, while a time step of less than 10μs is required to capture the full dynamics of the chatter. This is consistent with the selection of 7.8μs in [KHA 13].

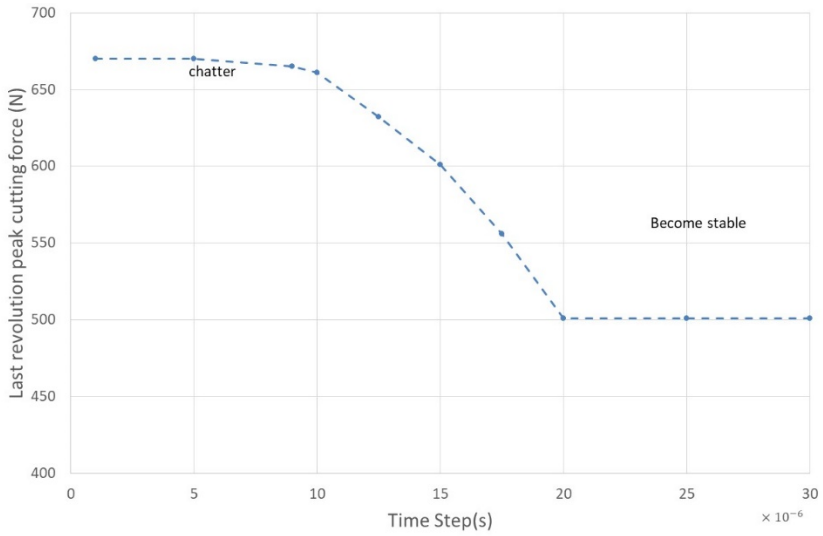

Figure 26 Influence of simulation time step on the peak cutting force at 3000 rpm and 14 mm depth of cut.

2.6. Calculation of average load torque on machine for different cutting conditions

The validated cutting model can be used to map the variation of the average cutting torque for a range of machine speeds and feed rates. As will be apparent from Table 1, the feed rate is expressed as a traversal distance per tooth, specifically 0.05 mm per tooth for the reference conditions of Table 1. This is an entirely logical definition in terms the detailed modelling of chip formation rather than specifying a traversal per unit time. The feed rate in terms of the advance per second, and hence the material removal rate, is proportional to the rotor speed. By way of example, at 3,000 rpm and a feed rate of 0.05 mm per tooth, the rate of tool advanced into the work-piece is 10 mm/s. These simulations were performed with the low bandwidth speed control (314 rad/s).

Figure 27 shows the variation of the average cutting torque per mm of cut depth as a function of rotational speed at four different feed rates. As would be expected from the equations (2-8) and (2-9) in section 2.2.2, as a given feed rate (expressed in mm/tooth) the torque is independent of the rotational speed while the average torque scales linearly with feed rate. Since these values were taken for a 1 mm depth of cut, all the conditions were for stable cutting. There are some very minor variations in the torque at a given feed-rate. The corresponding RMS values are shown in Figure 28.

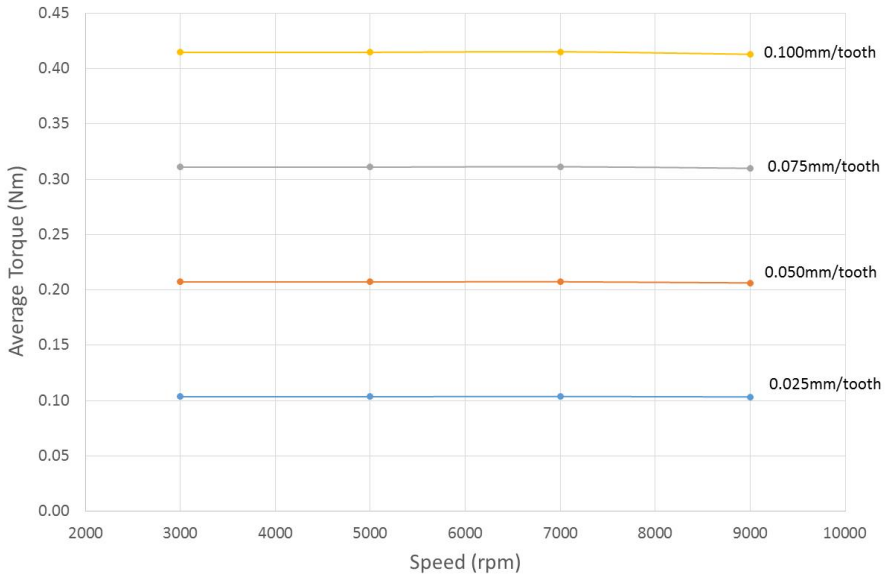

Figure 27 Predicted variation in average cutting torque per mm of cut depth as a function of rotational speed and feed-rate (feed rate expressed in terms of traversal per tooth passing)

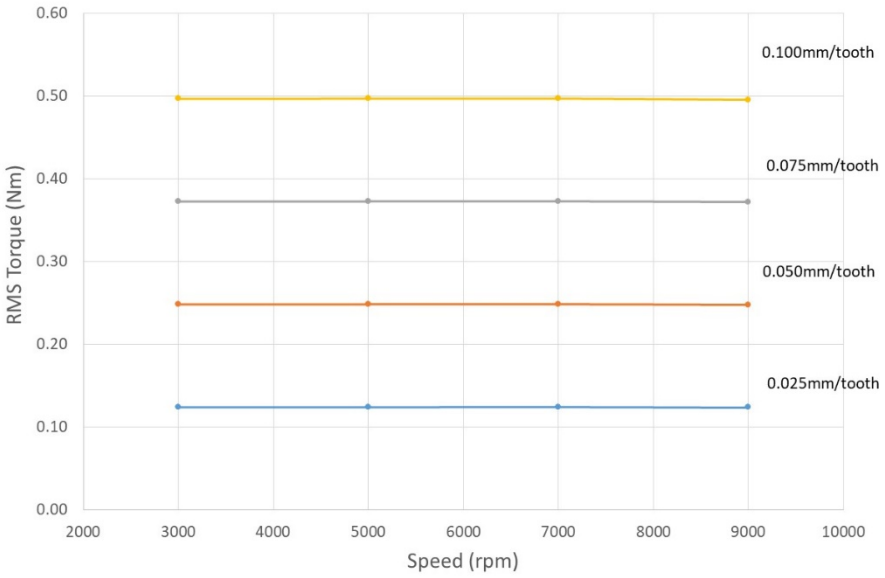

Figure 28 Predicted variation in rms cutting torque per mm of cut depth as a function of rotational speed and feed-rate (feed rate expressed in terms of traversal per tooth passing)

2.7.Influence of the inertia in the drive train system

From the equation (2-4), it is apparent that the inertia of the drive train would affect the result significantly. Assuming the inertia from the tool holder and other mechanical system is J_m. The equation (2-4) then can be rewritten as follows:

$$\frac{d\omega_m}{dt} = \frac{1}{J+J_m}(T_e - T_L - B\omega_m) \qquad (2\text{-}31)$$

Since inertia J is time irrelevant, hence the equation (31) can also be expressed as:

$$\omega_m = \frac{1}{J+J_m}\int (T_e - T_L - B\omega_m)dt \qquad (2\text{-}32)$$

Assume electromagnetic torque keeps constant at a small-time interval, under the same load torque characteristics, equation (32) shows the motor speed is inverse to the drive train inertia. The speed change would then affect the electromagnetic torque. Refer to the motor parameters from appendix A as an example, Figure 29 shows the peak to peak speed ripple versus drive train inertia, (scaled proportionally with the motor inertia), load with milling conditions from Table 1 at 10 mm depth of cut and 3000 rpm cutting speed. Figure 30 shows the peak to peak torque ripple versus drive train inertia under the same conditions from Figure 29. As the inertia in the whole drive train increases from 0.0003 kgm2 to twice the motor inertia, the peak to peak speed ripple reduces from 96 rpm to 48 rpm. This 50% speed ripple reduction results in 40% electromagnet torque ripple decrease. However, as the inertia further increases, the reduction of the speed ripple slows down. The speed ripple of the motor still could be as big as 12 rpm at 8 time the motor inertia. The techniques purposed in this thesis limits the overall inertia of the drive train within 2 times the motor inertia.

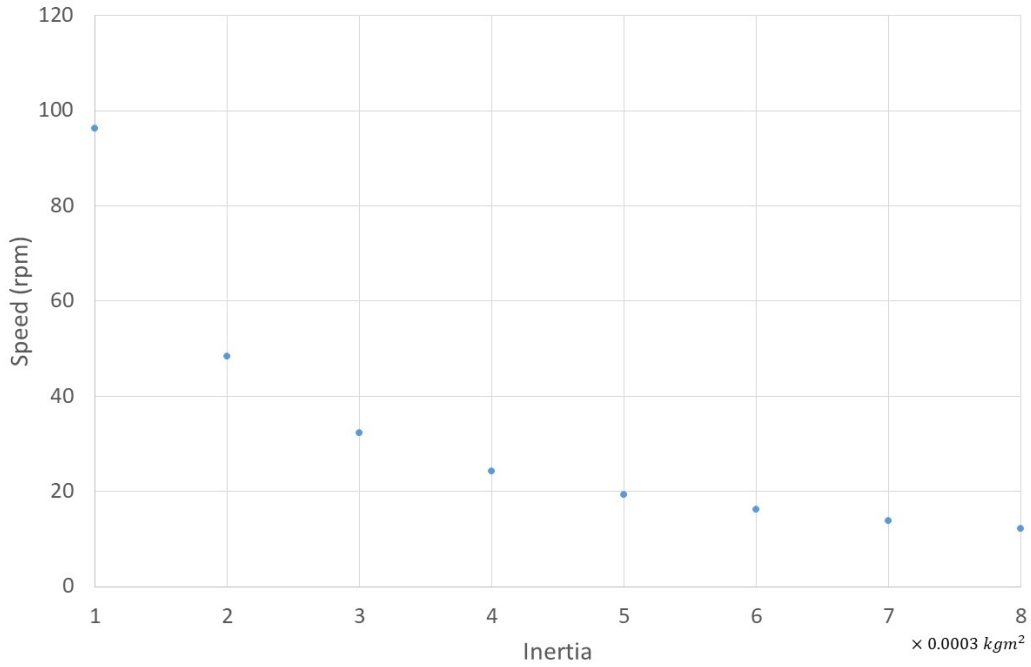

Figure 29 Peak to peak speed ripple versus drive train inertia with 3000 rpm and 314 rad/s speed controller bandwidth.

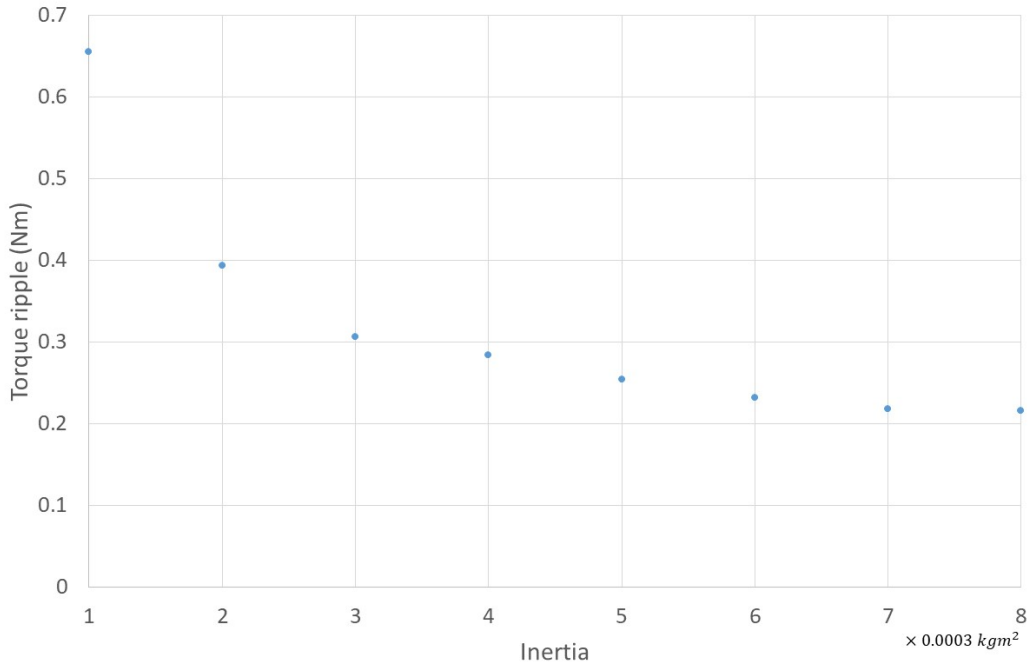

Figure 30 Peak to peak torque ripple versus drive train inertia with 3000 rpm and 314 rad/s speed controller bandwidth.

2.8.Stability lobe diagrams

The cutting model can be used to establish a so-called stability lobe diagrams (SLD). This type of diagram offers a convenient method for mapping the combinations of cut depth and rotational speed which result in stable operation. It is important to note that an SLD is specific to a particular tool feed-rate. Figure 31 shows a calculated SLD for the cutting parameters shown previously in Table 1 for the case of a speed-stiff input to the cutting mechanical model. Regions above the boundary line correspond to unstable operation while those below gives rise to stable operation. This type of stability lobe diagram is established by undertaking many simulations and is a very time-consuming process since each critical depth is established from many iterative simulations at each speed, i.e. many hundreds of individual simulations may be required depending on the resolutions of steps used in both speed and depth.

As shown by Figure 31, there are some speeds at which even small cutting depths are prone to instability for the parameters shown previously in Table 1, e.g. ~5 mm at 4,500 rpm. It is worth noting many of the depths for which stable cutting is predicted solely from essentially two-dimensional dynamic considerations may in practice be deeper than the tooth height. This is illustrated in Figure 31 by the superposition of the maximum 20 mm cutting depth of the tool in Table 1, a limit set by the height of the cutting teeth. It is also worth noting that many of the depths encountered results in an average cutting torque that exceeds the rating of the spindle drive.

Figure 32 shows a close-up of the predicted stability lobe diagram, onto which is superimposed a series of operating points from [KHA 13] which are denoted as stable and unstable. As shown, there is good agreement in terms the transition from stable to unstable cutting at this speed.

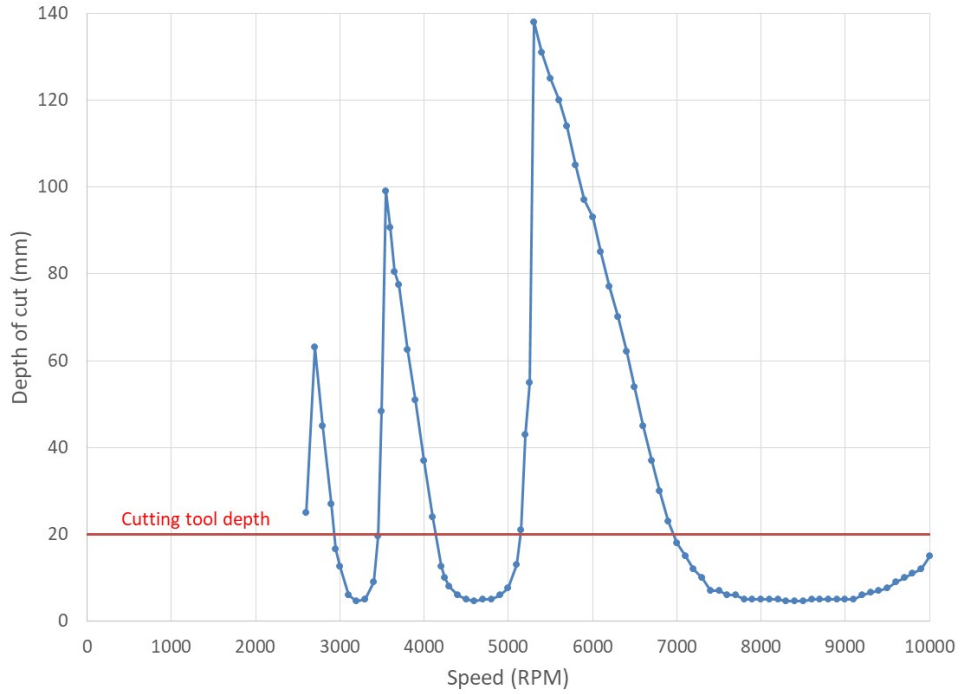

Figure 31 Predicted stability lobe diagram for cutting parameters in Table 1 with a speed-stiff input

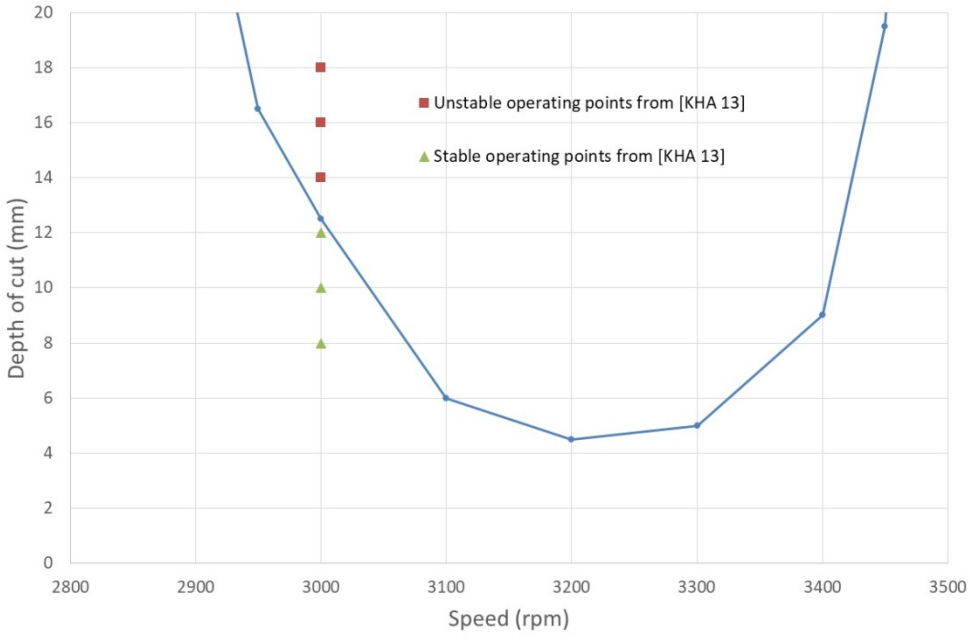

Figure 32 Zoom-in of predicted stability lobe with corresponding operating points from [KHA 13]

Chapter 3 - Dynamic behaviour with a range of control strategies

3.1. Introduction

Having developed and validated the system model developed in section 2.2, the model was employed in a series of configurations to explore several aspects of dynamic performance. The classical feedforward control system with PI controller alone cannot fully reject disturbance signal while keep a good reference signal tracking. To overcome this problem, the new control strategies are designed to reject disturbance signal caused by the milling operation, so the PI controllers can focus on keeping a good reference signal tracking. This chapter investigate the dynamic behaviour and maximum capability of the servo system and the effects that different control strategies might have on stability of the cutting process. In this chapter, three alternative control strategies are considered, in some cases in combination:

- Standard speed control
- Torque balance control
- Modulation of torque by rapid torque reversals

3.2. Standard speed control

3.2.1. Introduction

As noted previously, almost all commercial machine tool spindles operate with set-point speed control, although often in combination with some ramp rate settings. A block diagram of typical speed loop structure is shown in Figure 33. There is an outer speed loop which produces a torque demand for an inner current loop. In commercial spindle drives, the closed loop controllers are usually tuned quite conservatively with modest response time and therefore are likely to have little or no influence on the dynamic cutting behaviour. A key motivation in this series of

simulations is to establish whether more highly tuned speed control loops will enhance or diminish performance and stability, and whether factors such as the PWM nature of the converter output voltage or the dynamics of the converter current loop have an effect.

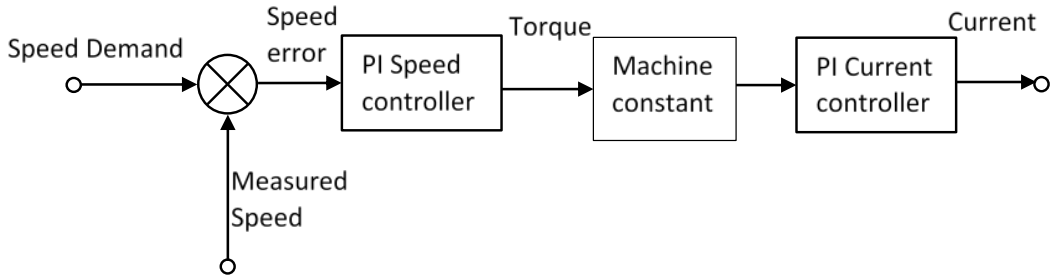

Figure 33 Block diagram of the speed controller

In each case, the aim was to demonstrate the intrinsic torque and speed ripple caused by the PWM behaviour of the converter or the current and speed controller. These simulations provide some in-depth knowledge of system performance for a typical PI controlled feedback system.

This section presents a series of simulations for three different control set-ups, i.e. open-loop set-point control and closed loop speed control with both high bandwidth and low bandwidth controller settings.

The series of simulations performed was based on various controller settings (of the same structure but with different gains and hence bandwidths) attempting to maintain a set point speed of 3,000 rpm with 10 mm depth of cut (stable cutting). In the case of SIEMENS SIMODRIVE 611 universal control, the default settings for closed-loop speed control derived from the operating manual are a speed control bandwidth of 314 rad/s and 50,000 rad/s bandwidth for the internal current loop

In this series of simulations, the PWM frequency is set at 50 kHz in this first instance. In the later simulations, presented in section 3.2.8, the influence of PWM frequency on overall performance is investigated. In order to establish the link between the PI speed controller bandwidth and the ability of the system to match the torque profile of the cutter in speed control mode within one cutting cycle, a series of combinations of gains were considered.

3.2.2. Open loop set-point control

This control strategy is not representative of commercial machine tools but is useful for predicting the baseline system response in the absence of closed loop speed control. As noted in section 2.6 , the cutting torque (which is the dominant contributor to the 'load' torque of the machine) varies as a function of cutter feed rate.

A nominal speed of 3000 rpm produced average cutting load torque of 2.08 Nm for a cutter depth of 10 mm (all cutter parameters are summarised in Table 1). A q-axis current set-point of 3.65A produces an essentially smooth electromagnetic excitation torque of 2.08 Nm which would balance this cutter torque at a nominal speed of 3000 rpm. In the simulation of this operating condition, the machine is fed from standstill with a q-axis current demand of 0.57A (d-axis current regulated to zero) and hence accelerates from standstill up to this balanced torque speed and then establishes a steady-state operating point for an interval as shown in Figure 34. However, this is an unstable equilibrium. Since the feed rate of the machine is fixed to nominal speed, i.e. 0.05 mm per tooth or 10 mm/s at 3000 rpm, then when the speed drops below 3000 rpm the cutting force increases and vice versa. Hence the speed of the machine eventually either decays until it reaches standstill or increases uncontrollably.

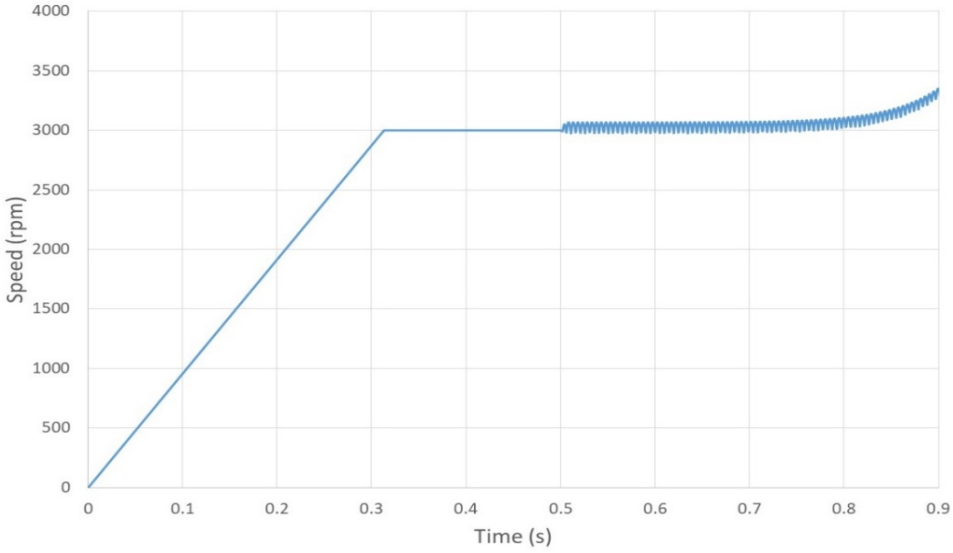

Figure 34 Transient start-up speed profile for a fixed q-axis demand current of 3.65A

The resulting variations in the electromagnetic and cutting torques are shown in Figure 35 along with the net accelerating torque that is simply the difference between the smooth applied electromagnetic torque and the cutting torque. As will be apparent, there is significant instantaneous mis-match in torque on the timescales of individual tooth passing events. This results in the speed variations shown in Figure 36.

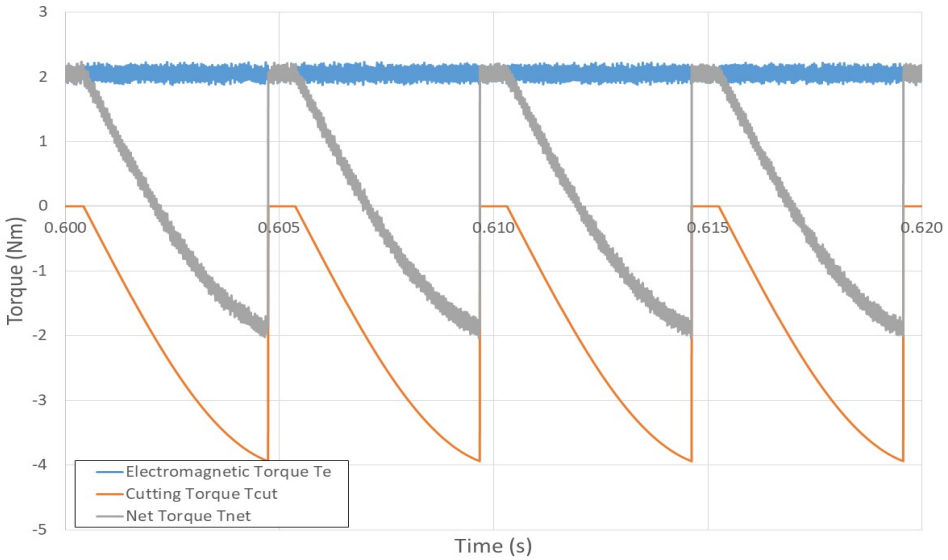

Figure 35 Predicted dynamic torque waveforms for a fixed controller demand torque of 2.08 Nm at 3000 rpm with a cutting depth of 10 mm

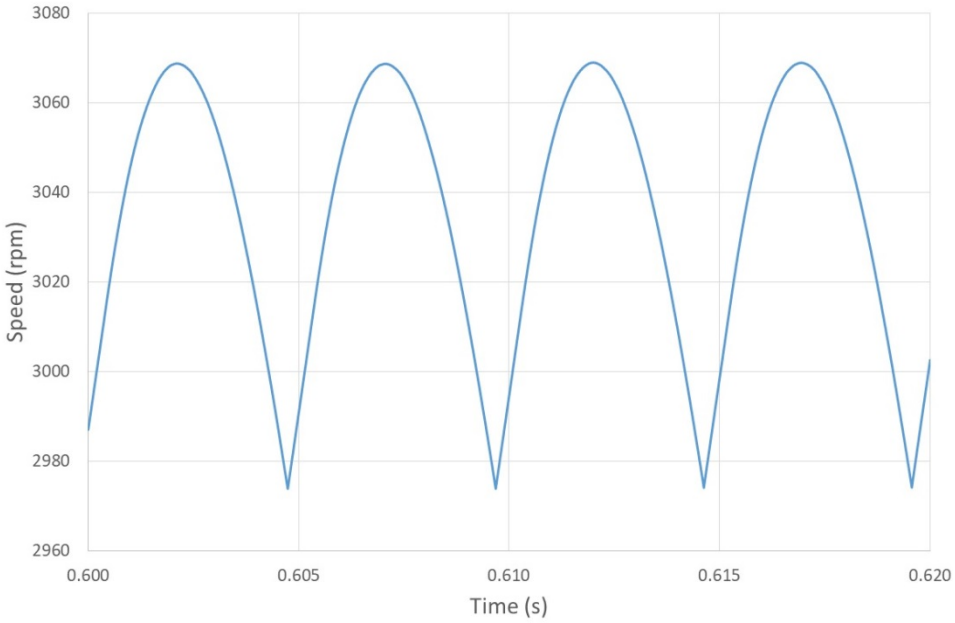

Figure 36 Simulation speed fluctuations for open-loop set-point control for a speed of 3,000 rpm and a cutting depth of 10 mm

3.2.3. Low bandwidth speed controller at 3000 rpm

The first case considered was with the motor running at 3000 rpm for a low bandwidth speed controller, using the manufacturer default bandwidth settings of 314 rad/s. The bandwidth of the inner current loop was set to 100,000 rad/s. As noted previously, this speed controller setting provides good set-point control of speed rather than any meaningful dynamic control, at least within individual passes of cutting edges. Figure 37 shows the predicted electromagnetic torque produced by the machine (T_e), the load torque on the cutter and the net accelerating torque (T_{net}). The resulting variation in the rotational speed is shown in Figure 38. As would be expected given the 50 Hz bandwidth of the speed controller and the 200 Hz disturbance forces generated by successive tooth passes, the speed controller does little to modify the torque during each tooth pass and the tool and motor are exposed to significant torque ripple. However, the moment of inertia ensures that the resulting speed variation is only ~98 rpm which is small in the context of the 3,000 rpm set-point. The three-phase currents for the same time interval are shown in Figure 39. As will be apparent, the fluctuations in the I_q demand generated by the speed controller

(which mirror the electromagnetic torque variation in Figure 37) cause the currents to fluctuate in magnitude even though the current is essentially in steady-state.

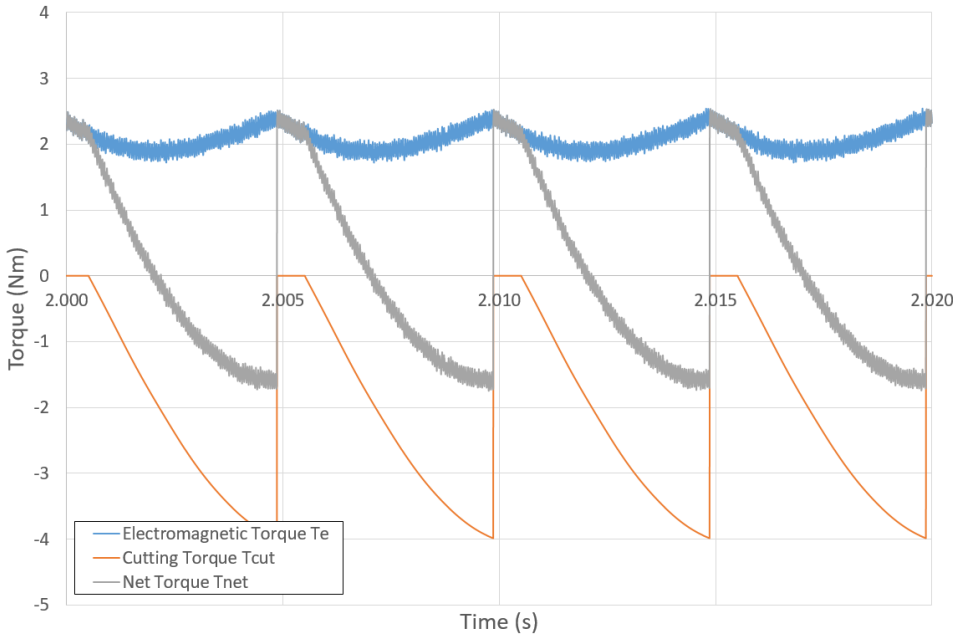

Figure 37 Instantaneous predicted load torque on cutter, electromagnetic torque produced by the machine and residual acceleration torque at 3,000 rpm for a speed controller with a speed loop bandwidth of 314 rad/s and torque loop bandwidth of 100,000 rad/s (10 mm depth of cut and tool parameters from Table 1)

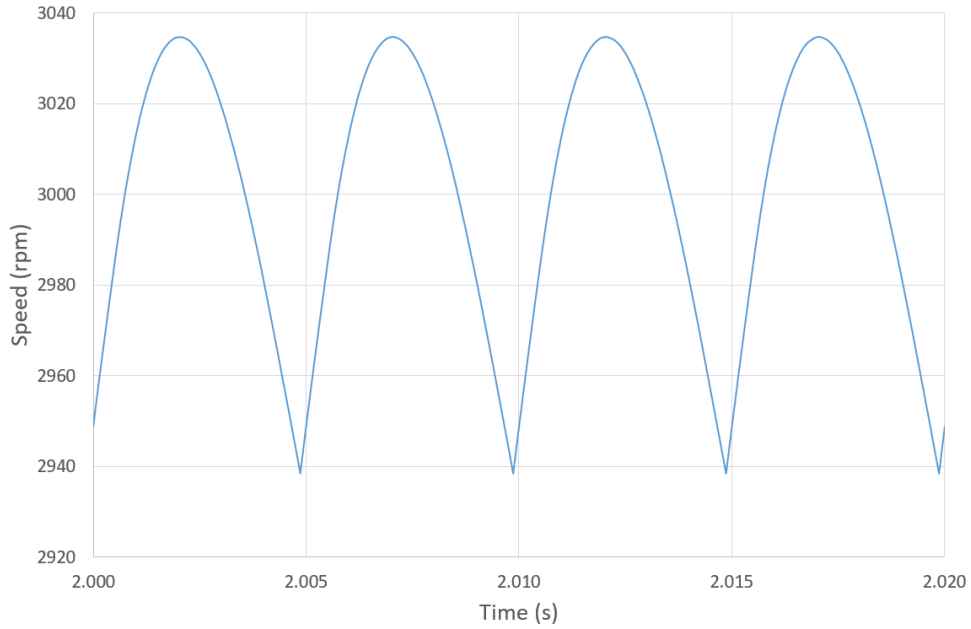

Figure 38 Instantaneous predicted speed variation around a set-point of 3,000 rpm for a speed controller with a speed loop bandwidth of 314 rad/s and a torque loop bandwidth of 100,000 rad/s (10 mm depth of cut and tool parameters from Table 1)

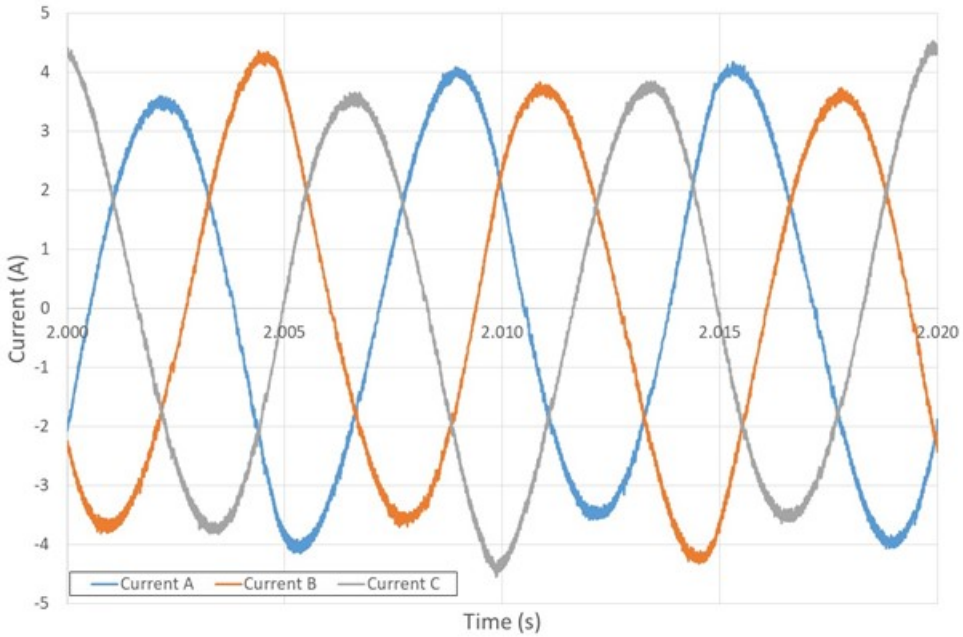

Figure 39 Predicted three-phase currents a set-point of 3,000 rpm for a speed controller with a speed loop bandwidth of 314 rad/s and a torque loop bandwidth of 100,000 rad/s operating at a PWM frequency of 50k Hz (10 mm depth of cut and tool parameters from Table 1)

3.2.4. High bandwidth speed controller at 3000 rpm

Although several intermediate speed controller bandwidths were simulated (the results from which are summarised later in Table 4), it is useful to consider the case of the highest bandwidth speed controller in detail. In this case, the control bandwidth for the speed control loop was set to 50,000 rad/s (corresponds to 16 kHz) and the inner current loop to 100,000 rad/s.

The resulting variation in the various components of torque are shown in Figure 40. In this case, there is significant modulation of the electromagnetic torque by the controller on the timescales of individual tooth passes and it is able to reduce the net accelerating torque from that shown previously in Figure 38 for the low bandwidth controller. This reduces the speed ripple to 5.9 rpm as shown in Figure 41. However, Figure 41 also demonstrates that the controller is unable to fully counteract the rapid drop in cutting torque as each tooth exits the work-piece. There is a rapid increase in speed which corresponds to an acceleration of ~6000 rad/s^2. This is a consequence of the use of a straight-edged cutter. A helical cutter would result in a less abrupt reduction in load torque and even some overlap with the next tooth.

The three-phase currents show an even more pronounced modulation than with a low bandwidth controller, as would be expected given the I_q demand that generates the electromagnetic torque variation in Figure 42.

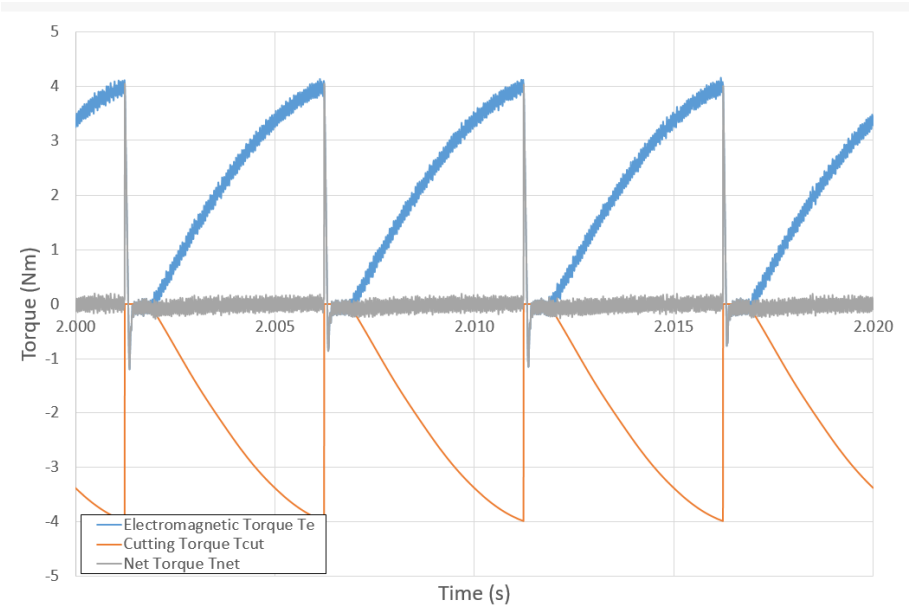

Figure 40 Instantaneous predicted load torque on cutter(T_{cut}), electromagnetic torque produced by the machine (T_e) and residual acceleration torque (T_{net}) at 3,000 rpm for a speed controller with a speed loop bandwidth of 50,000 rad/s and a torque loop bandwidth of 100,000 rad/s. (Depth of cut is 10 mm and tool parameters as listed in Table 1)

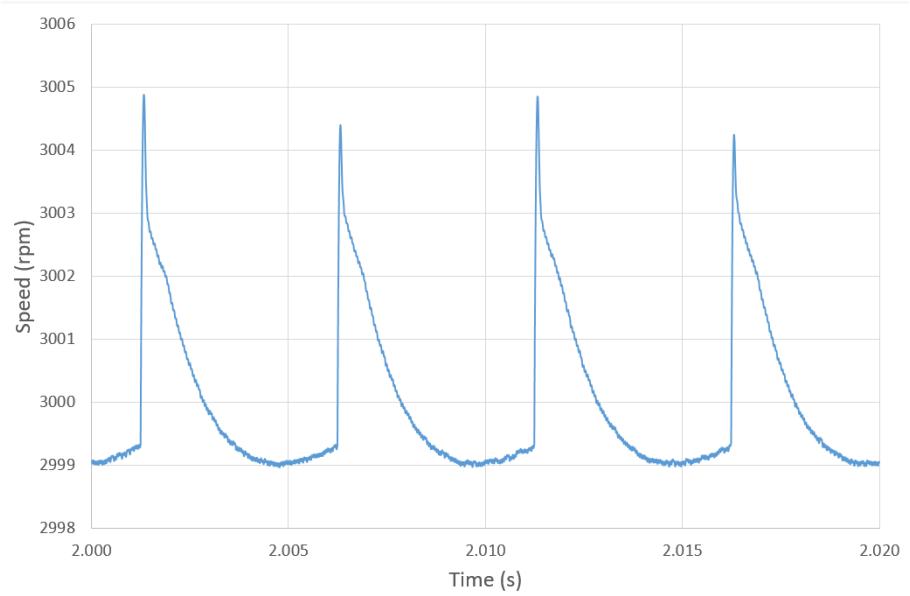

Figure 41 Instantaneous predicted speed variation around a set-point of 3,000 rpm for a speed controller with a speed loop bandwidth of 50,000 rad/s and a torque loop bandwidth of 100,000 rad/s (Depth of cut is 10 mm and tool parameters as listed in Table 1)

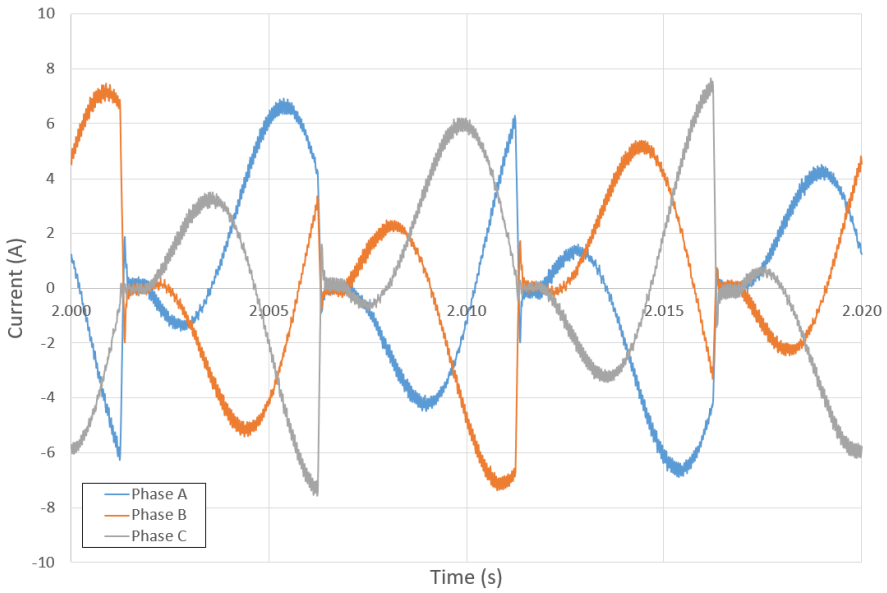

Figure 42 Predicted three-phase currents a set-point of 3,000 rpm for a speed controller with a speed loop bandwidth of 314 rad/s and a torque loop bandwidth of 100,000 rad/s operating at a PWM frequency of 50k Hz (10 mm depth of cut and tool parameters from Table 1)

3.2.5. Low bandwidth speed controller at 10,000 rpm

The preceding results for the low bandwidth speed controller in section 3.2.3 were for a speed of 3,000 rpm and a tooth passing frequency of 200 Hz. In this section, the speed is increased to 10,000 rpm which corresponds to a tooth passing frequency of 667 Hz. It is to be expected that the low bandwidth speed controller will exert even less influence on the timescales of individual tooth passing. Figure 43 shows the variation in the electromagnetic torque, the cutting torque and the net torque while Figure 44 shows the resulting variation in speed. The three-phase motor currents are shown in Figure 45 from which it is apparent that the level of fluctuations is far smaller than was the case at 3,000 rpm where the low bandwidth speed controller was able to exercise more control at the lower tooth passing frequency.

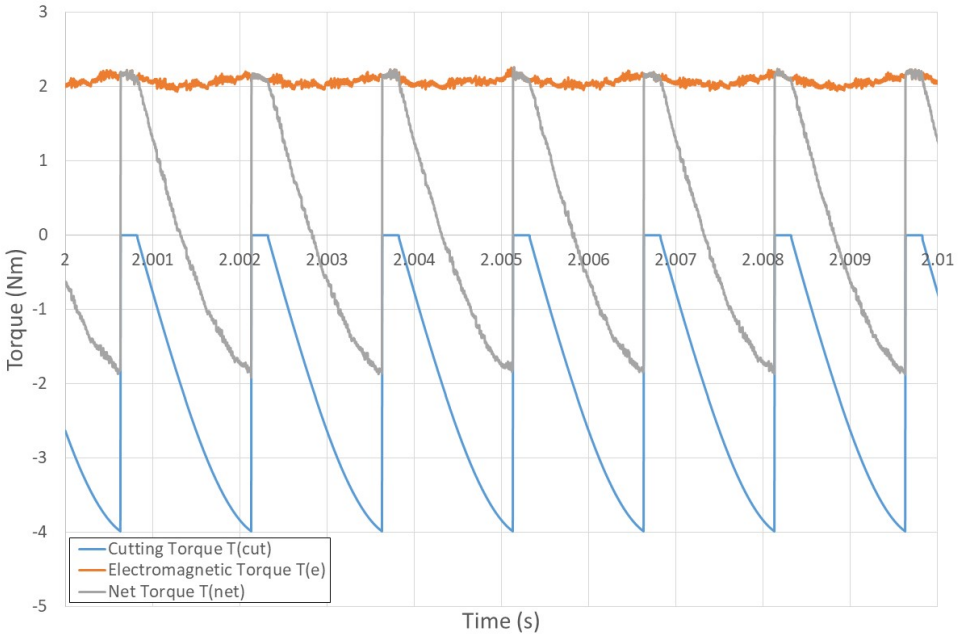

Figure 43 Predicted steady-state variations in cutting torque, electromagnetic torque and net accelerating torque at a 10,000 rpm speed demand set-point at a depth of cut of 10 mm for a low bandwidth speed controller (314 rad/s)

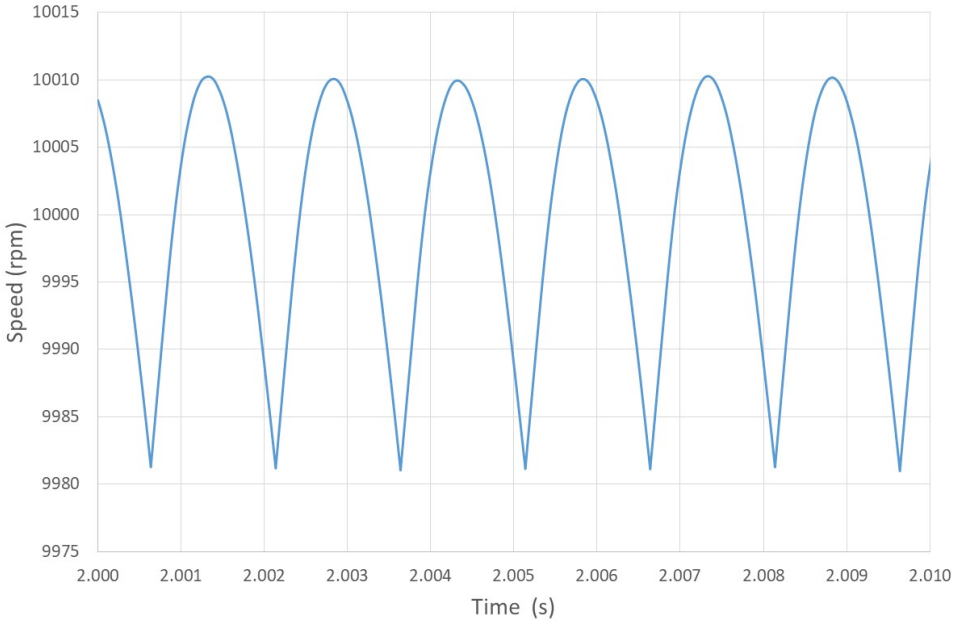

Figure 44 Steady-state speed fluctuations at 10,000 rpm for a depth of cut of 10 mm and a low bandwidth speed controller (314 rad/s)

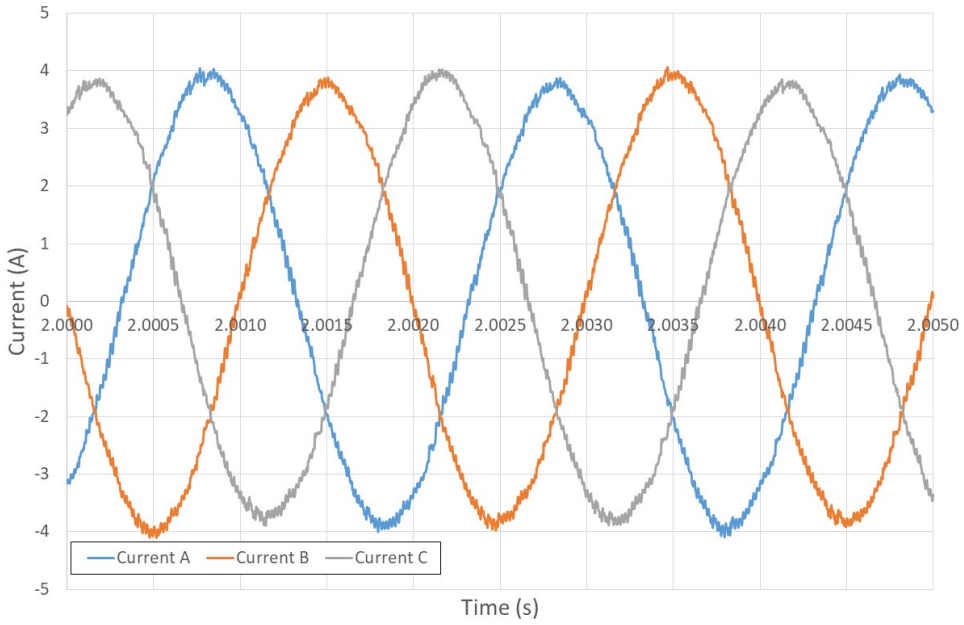

Figure 45 Three-phase currents at 10,000 rpm for a depth of cut of 10 mm and a low bandwidth speed controller (314 rad/s) and a PWM frequency of 50 kHz

3.2.6. High bandwidth speed controller at 10,000 rpm

The same conditions of a 10 mm deep cut at 10,000 rpm were simulated for the case of a high bandwidth (50,000 rad/s) speed controller. The resulting torques, speed variation and three-phase currents are shown in Figure 46 Figure 47 and Figure 48 respectively. As would be expected, although the tooth passing frequency is increased from 50 Hz to 166 Hz compared to the 3,000 rpm case, the high bandwidth speed controller is still capable of dealing with the disturbance force caused by the tool cutting into the work-piece, although again it struggles with the very abrupt drop in torque on the motor when the tooth exits the work-piece.

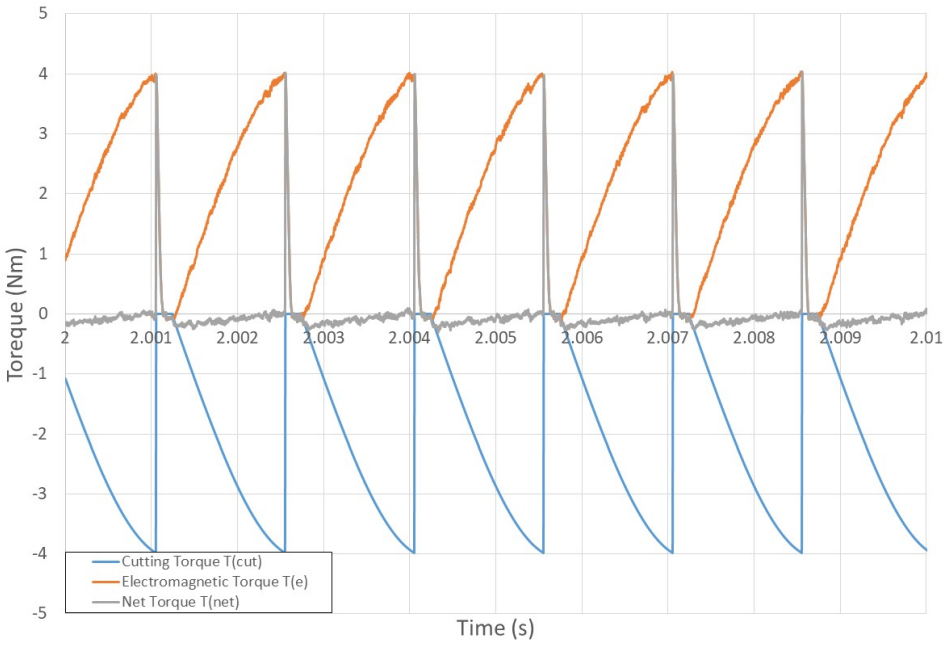

Figure 46 Predicted steady-state variations in cutting torque, electromagnetic torque and net accelerating torque at a 10,000 rpm speed demand set-point at a depth of cut of 10 mm for a high bandwidth speed controller (50,000 rad/s)

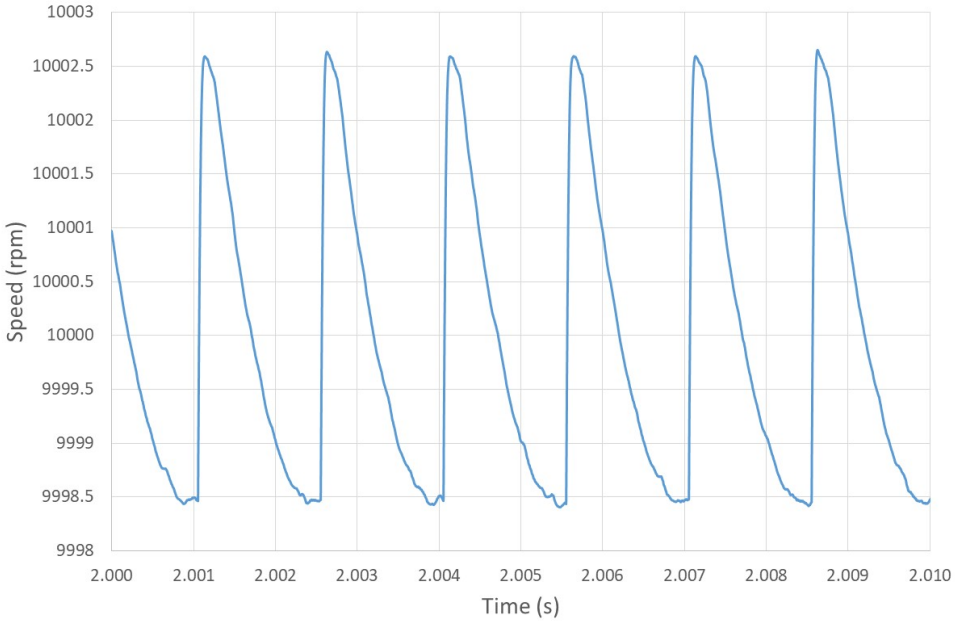

Figure 47 Steady-state speed fluctuations at 10,000 rpm for a depth of cut of 10 mm and a high bandwidth speed controller (50,000 rad/s)

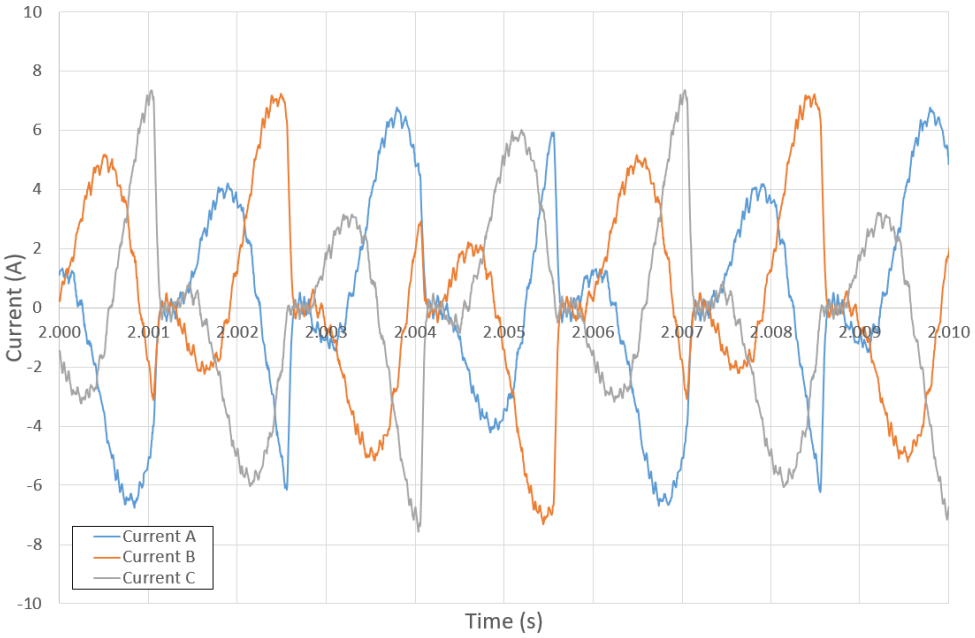

Figure 48 Three-phase currents at 10,000 rpm for a depth of cut of 10 mm and a high bandwidth speed controller (50,000 rad/s)

3.2.7. Summary of speed controller performance

The simulation results presented in sections 3.2.3 and 3.2.4 were for a series of speed loop control bandwidths from 314 rad/s up to 50,000 rad/s. Bandwidths beyond 50,000 rad/s could not be exploited as the controller saturated in terms of the available DC link voltage. The resulting variation in torque and speed ripple as a function of speed controller bandwidth is summarised in Table 4 for the case of a speed demand of 3,000 rpm.

Table 4 Predicted variation in speed ripple and accelerating torque for a range of speed controller bandwidths for a 10 mm depth of cut at a nominal speed of 3,000 rpm

Speed controller bandwidth (rad/s)	**Peak-to-peak speed ripple (RPM)**	**Peak-to-peak magnitude of T_{net} (Nm)**	**Standard deviation of Peak-to-peak magnitude of T_{net} (Nm)**
50,000	5.92	5.24	0.34
25,000	9.02	4.39	0.39
15,000	14.98	4.37	0.49
10,000	22.36	4.42	0.59
7,500	29.16	4.61	0.68
5,000	40.81	4.62	0.82
2,500	64.86	4.61	1.08
314	98.2	4.24	1.37

As it is apparent from the above table, even with a control bandwidth which is around 30 times higher than the default setting for commercial spindle drives, the ability of the speed controller to match the instantaneous cutting torque is limited. An inevitable feature of controlling speed is the lag between torque fluctuations caused by the cutter and the torque response of the spindle drive which is attempting to correct the speed error. The resulting speed fluctuations even with the low bandwidth controller are very small in comparison to the rated speed (30 rpm out of

10,000 rpm which corresponds to ~0.3%) and hence from a set-point control point of view, this performance would be deemed excellent.

3.2.8. Influence of PWM frequency on dynamic behaviour

There are several factors to consider when selecting a PWM frequency for a power converter. On the one hand, it is desirable to have a large separation in frequency between the fundamental electrical frequency and the PWM frequency, by at least an order of magnitude, in order to minimise the distortion of the stator current waveform. However, the switching losses in the power converter increase in direction proportion to the switching frequency. Hence, it is usual to establish a trade-off between the quality of the waveform and converter efficiency. Other considerations in a practical drive can include a desire to avoid the audible range (i.e. > 20 kHz), electromagnetic interference and filter size.

Figure 49 shows the motor current and speed response with 10 kHz, 20 kHz and 50 kHz PWM frequencies for a depth of cut of 10 mm and a speed demand set-point of 10,000 rpm. The fundamental frequency of the current at this maximum operating speed for this 6-pole machine is 500 Hz. As will be apparent, there is some distortion of the current waveform with the 10 kHz PWM frequency, but as would be expected with the 20:1 frequency difference, the distortion is small. Figure 50 shows an FFT of the 10 kHz PWM waveform.

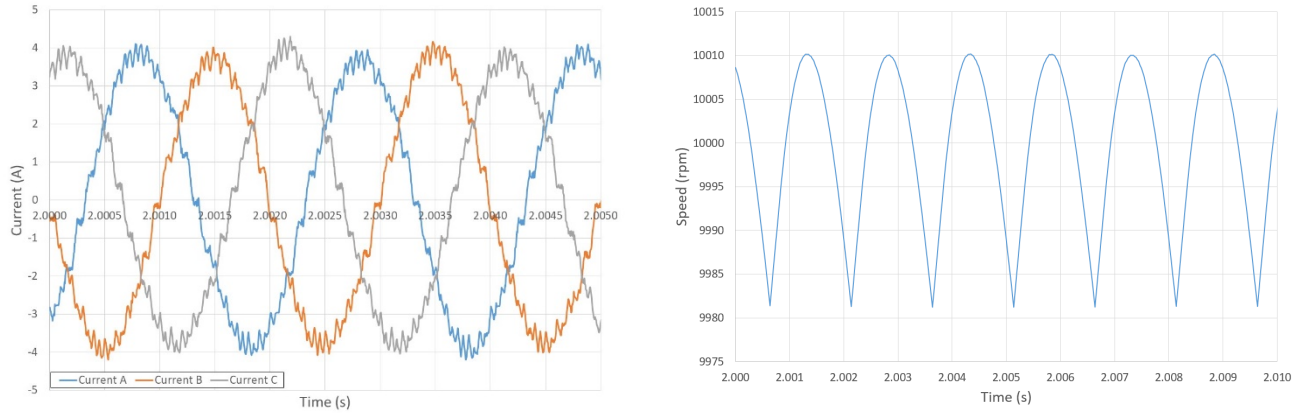

(a) 10 kHz PWM switching frequency

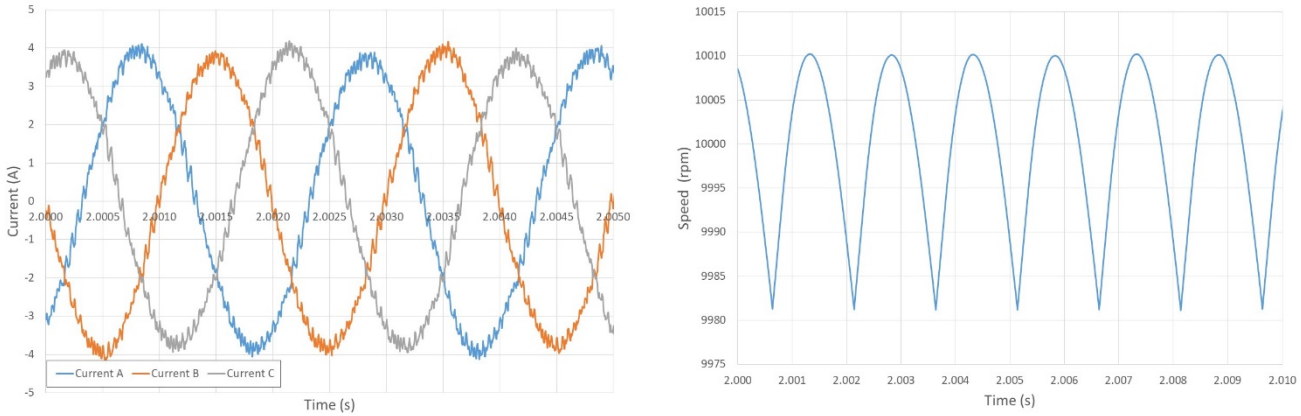

(b) 20 kHz PWM switching frequency

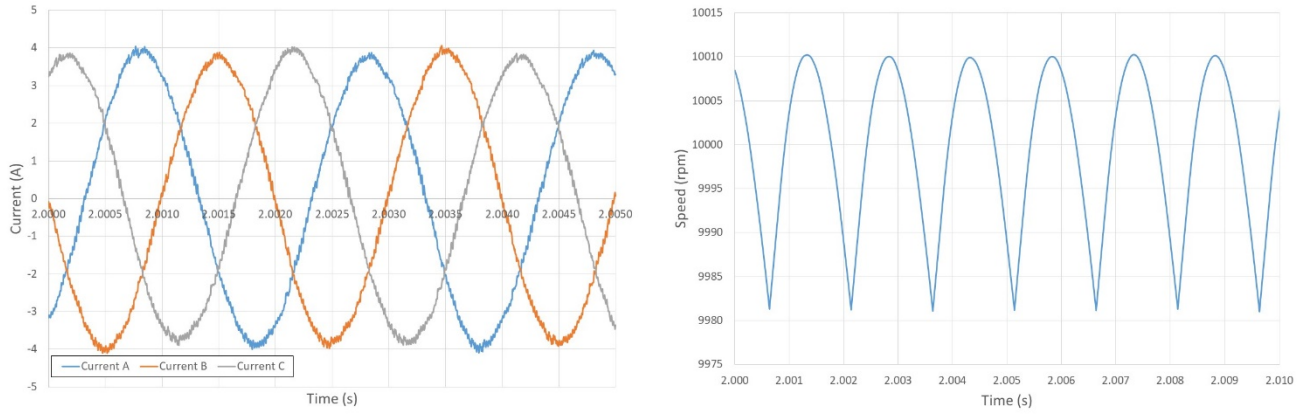

(c) 50 kHz PWM switching frequency

Figure 49 Current waveforms for converter switching frequencies of 10,20 and 50 kHz (10,000 rpm, 10 mm depth of cut with low bandwidth speed controller)

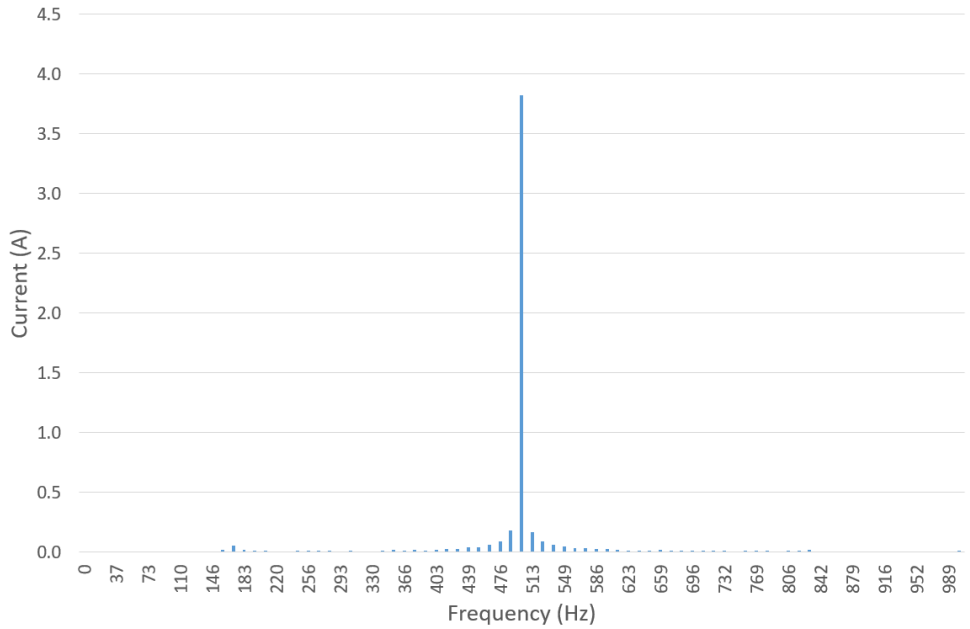

Figure 50 FFT spectrum of phase current for 10 kHz PWM

3.3. Open-loop torque matching

3.3.1. Description of the method

As shown previously in Figure 40 a high bandwidth speed controller (50,000 rad/s) is able to produce a torque that matches closely the cutting torque in response to speed error. However, there is a residual mismatch when each cutting tooth exits the work-piece and the cutting force falls rapidly, events that correspond to the rapid acceleration shown in Figure 38.

An alternative control strategy which can be used in conjunction with a low-bandwidth speed controller is to match the cutting torque in an open-loop manner with torque generated by a cutting torque model. This would be added on top of the set-point control torque demanded by the speed controller. This predicted cutting torque is generated on an open-loop basis solely from the depth of cut and the instantaneous angular position. The torque is calculated from vibration-free model presented in section 2.2.3 and hence is only applicable under stable cutting conditions. This should provide a reasonably well matched cutting torque prediction under normal stable cutting conditions and minimise the influence of tooth impact. There is no

published literature on the merits of instantaneous torque matching of the cutting force in terms of managing impact, tool wear or improving stability. Indeed, from a milling point of view there may be limited value in closely matching torque. It nevertheless provides an interesting case study in terms of the ability of the spindle drive to achieve very high dynamic response.

A key enabler for this approach is a means of predicting the depth of cut so that the normalised torque waveform in the controller can be scaled appropriately.

3.3.2. Depth prediction

The cutting model developed and validated in Chapter 2 which is based on a two-dimensional model assumes that the torque waveform remains fixed in shape with a magnitude that scales in linear proportions with the depth of cut. In order to apply a torque waveform to the spindle with the correct magnitude it is necessary to account for the depth of the cut at that instant. In principle, once a block of material has been completely traversed, then the CAD system will have knowledge of the form of the part and hence the cutting depth can be calculated. However, during initial passes over the stating piece, there is a need to reliably estimate cutting depth in real time. In order to achieve this without the need for any additional sensors, e.g. a proximity sensor running ahead of the tool, a method based on monitoring the power consumption of the motor can be employed.

The net electrical power over one electrical cycle can be readily and reliably calculated in a practical machine from the measured drive current and voltage. High performance permanent magnet spindles tend to exhibit high efficiency over much of their operating range (>95% being common) and hence a reasonable estimate of the mechanical output power could be derived from simply the electrical input power. However, it is relatively straightforward to account for copper loss in the machine (although some correction for coil temperature may be necessary). Iron loss, although more complex, could be accounted for with a rudimentary representation, e.g.

simple loss versus speed relationship based on open-circuit losses. With an estimate of average mechanical power (which can be updated every electrical cycle if required) then the depth which yields the correct power balance from the cutter force model can be established. A block diagram of the depth predicting model is shown in Figure 51.

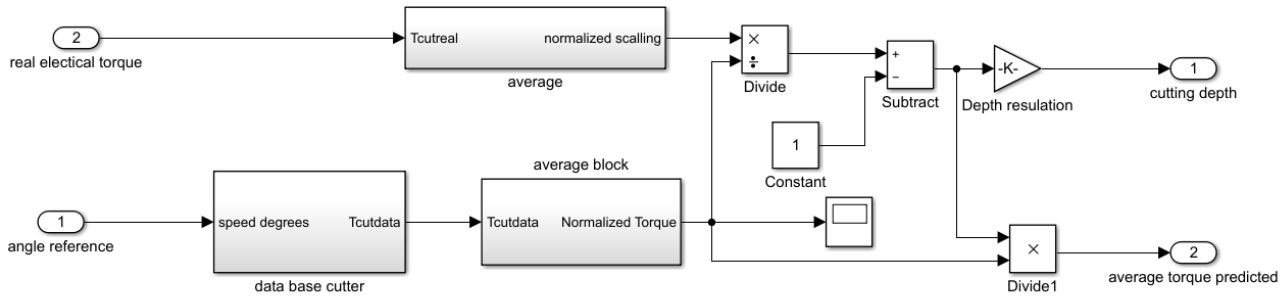

Figure 51 SIMULINK block diagram of cutting depth predictor

3.3.3. Simulation results for open-loop torque matching

In order to separate out the effect of the depth predictor and effect of the chatter model. Three different series of simulations were performed:

- In the most straightforward case, a fixed, known depth was fed into both the vibration free cutter force model which represents the mechanical load on the cutter and the vibration free cutter force model which is implemented within the controller to predict the torque to be added to the spindle demand.
- In the second series of simulations, a prescribed depth was set in the vibration-free cutting force model which represents the mechanical load on the cutter while the value used in the controller predictive load drew on the predicted depth.

- In the third series of simulations, the full cutting model which includes vibration represents the mechanical load while the predictive model within the controller is unchanged with depth of cut feed in from the depth predictor.

The first two series of simulations, the model was run under different parameters of control bandwidth, ranging from 314 rad/s to 50,000 rad/s. This series of simulations was performed at a rotational speed of 10,000 rpm. Figure 52 show the speed ripple and net accelerating torque between electromagnetic torque and cutting torque with 'stiff' torque match function at 10,000 rpm at 10 mm depth of cut with both 315 rad/s and 50,000 rad/s band width speed controller.

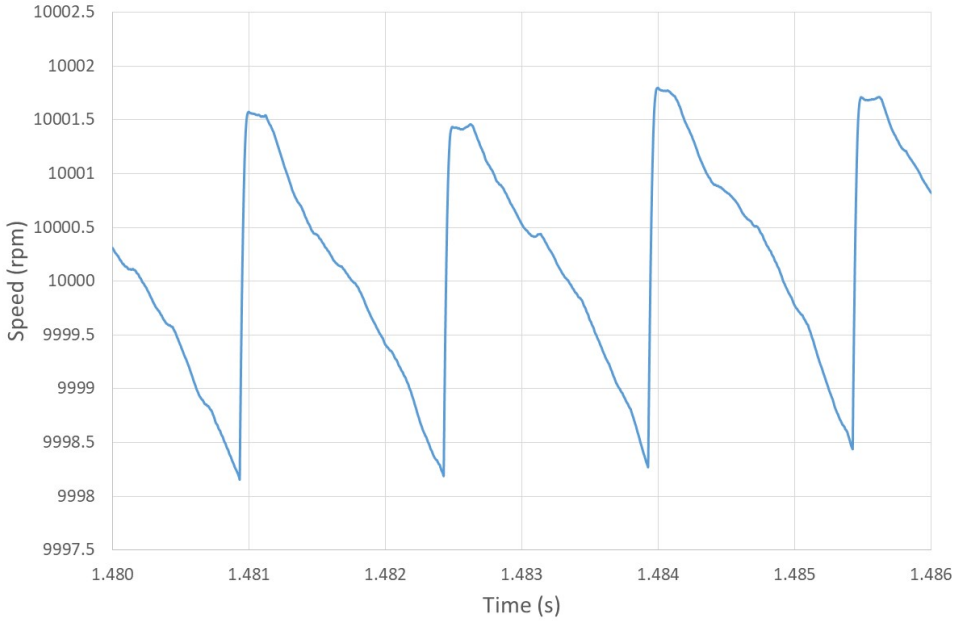

(a) Speed ripple at 10,000 rpm depth of cut 10 mm with 314 rad/s speed controller and stiff torque match

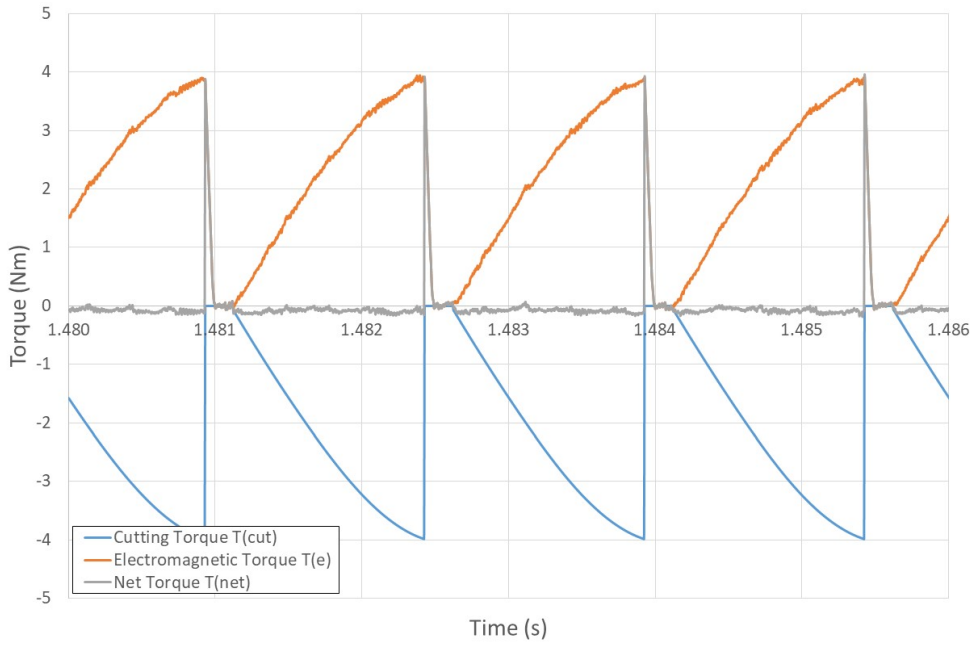

(b) Torque wave from at 10,000 rpm depth of cut 10 mm with 314 rad/s speed controller and stiff torque match

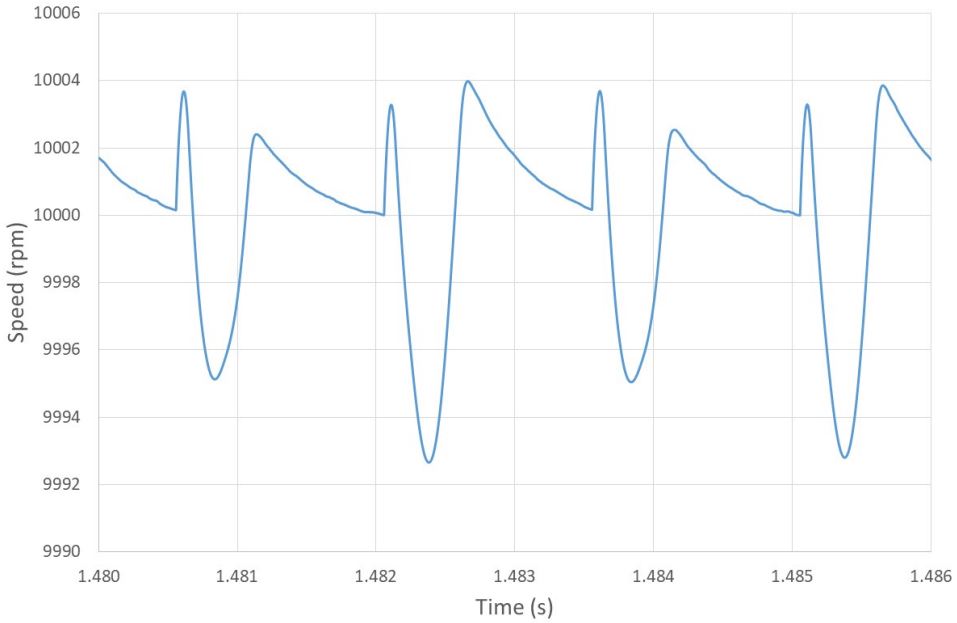

(c) Speed ripple at 10,000 rpm depth of cut 10 mm with 50,000 rad/s speed controller and stiff torque match

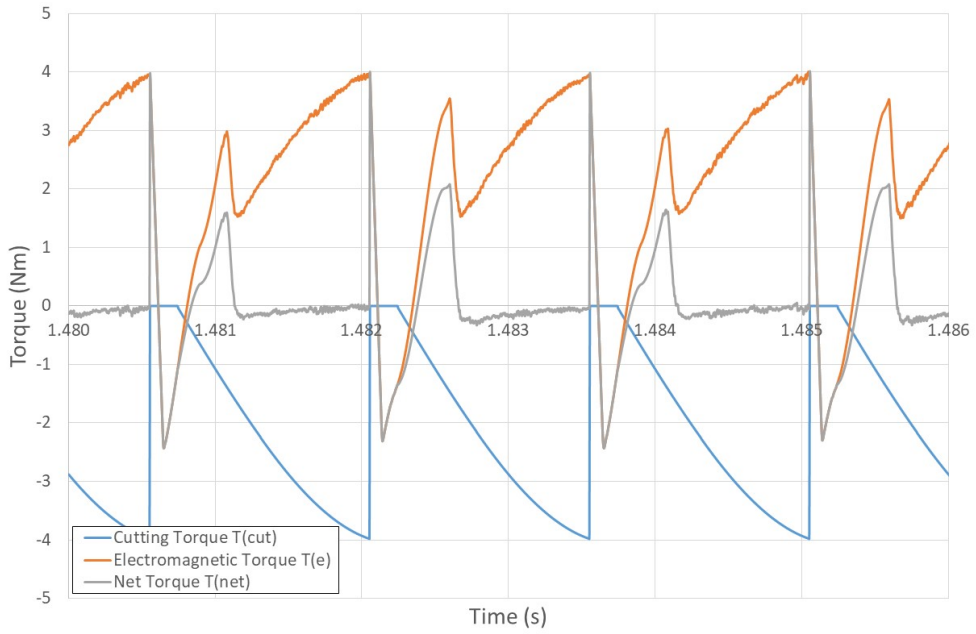

(d) Torque wave from at 10,000 rpm depth of cut 10 mm with 50,000 rad/s speed controller and stiff torque match

Figure 52 Speed ripple and net accelerating torque between electromagnetic torque and cutting torque with 'stiff' torque match function

There is a very abrupt reduction in cutting torque when the tool exits the work-piece which the motor fails to track precisely. The response of the motor is limited by the dynamics of the current controller. This is due to a combination of the PI controller bandwidth and the maximum current slew rate which can be achieved given the available maximum converter output voltage, the back emf and the inductance of the winding. In an attempt to remedy this problem, the torque match profile was reduced by half an electrical time constant 3×10^{-5} sec as shown in Figure 53.

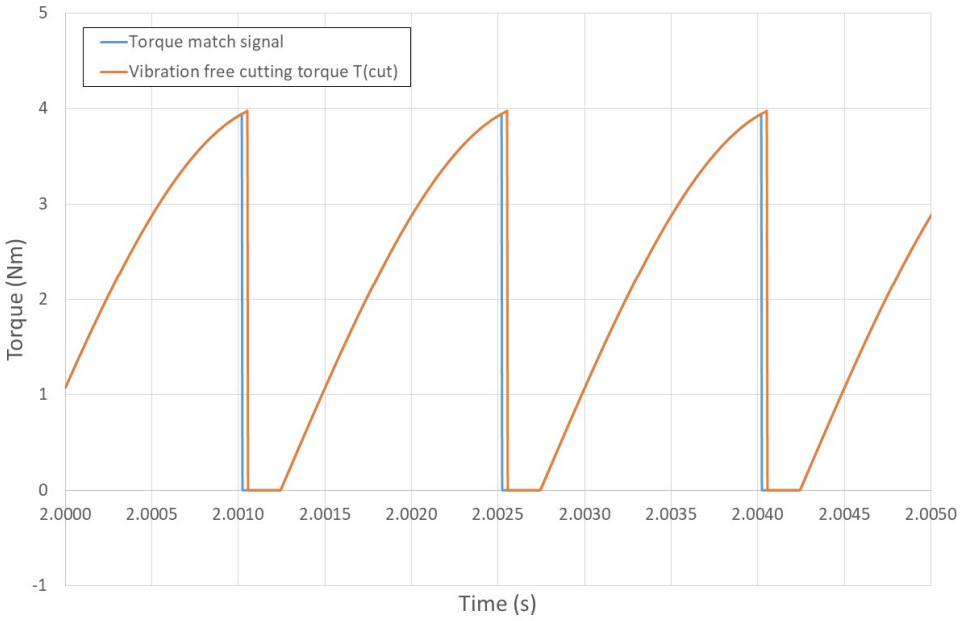

Figure 53 Modified torque match profile

Table 5 summarise the speed ripple for both a prescribed known depth set in the model and a depth predicted from the electrical power. As between torque ripple, speed ripple and control bandwidth.

Table 5 Torque ripple, speed ripple under different control bandwidth at 3000 rpm with a 10 mm depth of cut

Speed bandwidth (rad/s)	Speed Ripple (RPM)		Net accelerating Torque ripple (Nm)	
	Predicted depth	Prescribed depth	Predicted depth (Standard deviation)	Prescribed depth/ Standard deviation
50,000	2.08	2.08	3.96 (0.17)	3.96 (0.17)
25,000	2.16	2.15	4.25 (0.17)	4.23 (0.17)
15,000	2.25	2.23	4.27 (0.17)	4.24 (0.17)
10,000	2.27	2.26	4.28 (0.18)	4.24 (0.17)
7,500	2.35	2.32	4.29 (0.19)	4.26 (0.18)
5,000	2.62	2.58	4.34 (0.22)	4.29 (0.20)
2,500	3.52	3.45	4.37 (0.23)	4.30 (0.20)
314	4.40	4.38	4.37 (0.26)	4.31 (0.20)

Table 6 Torque ripple, speed ripple under different control bandwidth at 10000 rpm with a 10 mm depth of cut

Speed bandwidth (rad/s)	Speed Ripple (RPM)		Net accelerating Torque ripple (Nm)	
	Predicted depth	Prescribed depth	Predicted depth / Standard deviation	Prescribed depth/ Standard deviation
50,000	1.5	1.5	3.87/0.25	3.86/0.23
25000	1.6	1.5	3.88/0.25	3.86/0.23
15000	1.6	1.6	3.88/0.25	3.86/0.23
10000	2.01	1.97	4.14/0.26	4.12/0.25
7500	2.03	1.99	4.16/0.27	4.14/0.25
5000	2.07	2.05	4.18/0.27	4.17/0.25
2500	2.18	2.12	4.21/0.27	4.18/0.26
314	2.37	2.3	4.21/0.27	4.18/0.26

Table 5 and Table 6 demonstrates the accuracy on depth predictor, although it should be noted that the mechanical model which represents the physical system is that same as that used to predict the depth which results in some inevitable self-consistency.

The key results from a third series of simulations are shown in Figure 54 which shows the electromagnetic torque ripple, cutting torque and net accelerating torque at 3,000 rpm speed demand with depth of cut of 10 mm operating with 50,000 rad/s speed control and 100,000 rad/s current control loop. Figure 55 shows the speed ripple for the same conditions. In comparison, Figure 56 and Figure 57 below shows the torque ripple and speed ripple at 3,000 rpm speed demand with depth of cut of 10 mm and operating with a 314 rad/s speed control and 100,000 rad/s current control loop.

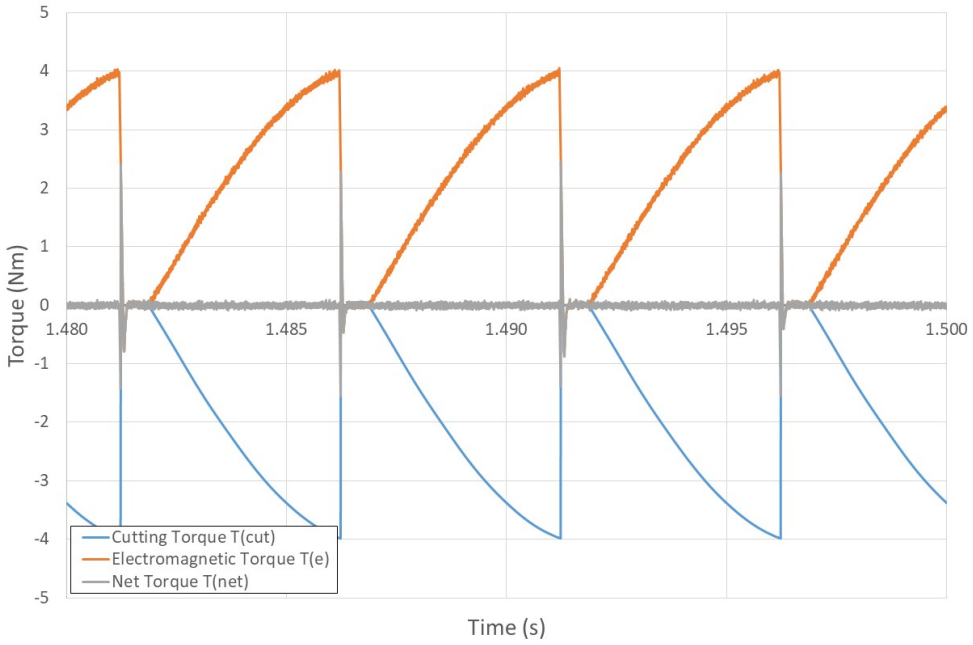

Figure 54 Predicted steady-state variations in cutting torque, electromagnetic torque and net accelerating torque at a 3,000 rpm speed demand set-point at a depth of cut of 10 mm for a high bandwidth speed controller (50,000 rad/s)

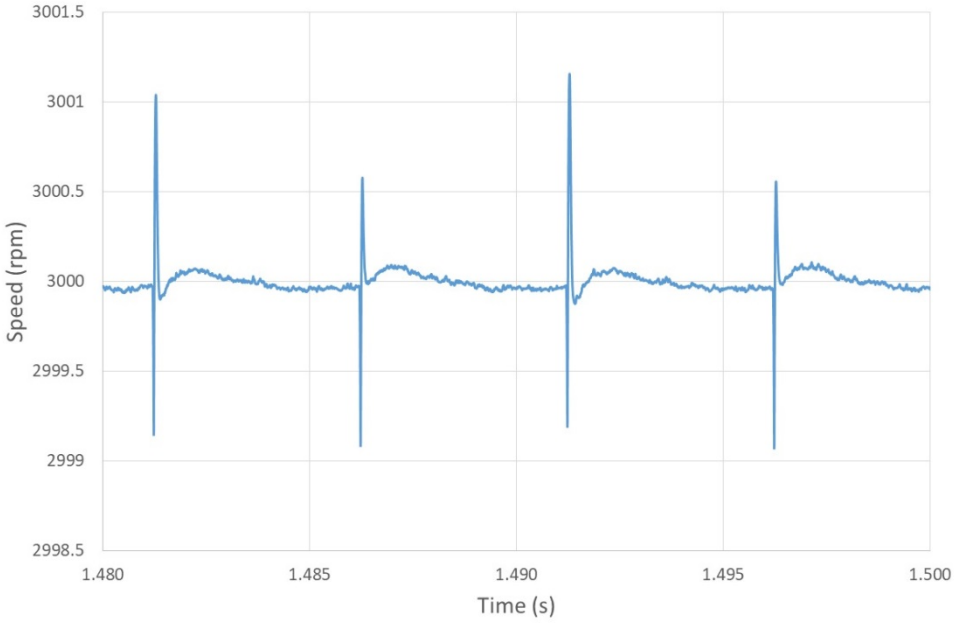

Figure 55 Predicted stead-state speed ripple at a 3,000 rpm speed demand set-point at a depth of cut of 10 mm for a high bandwidth speed controller (50,000 rad/s)

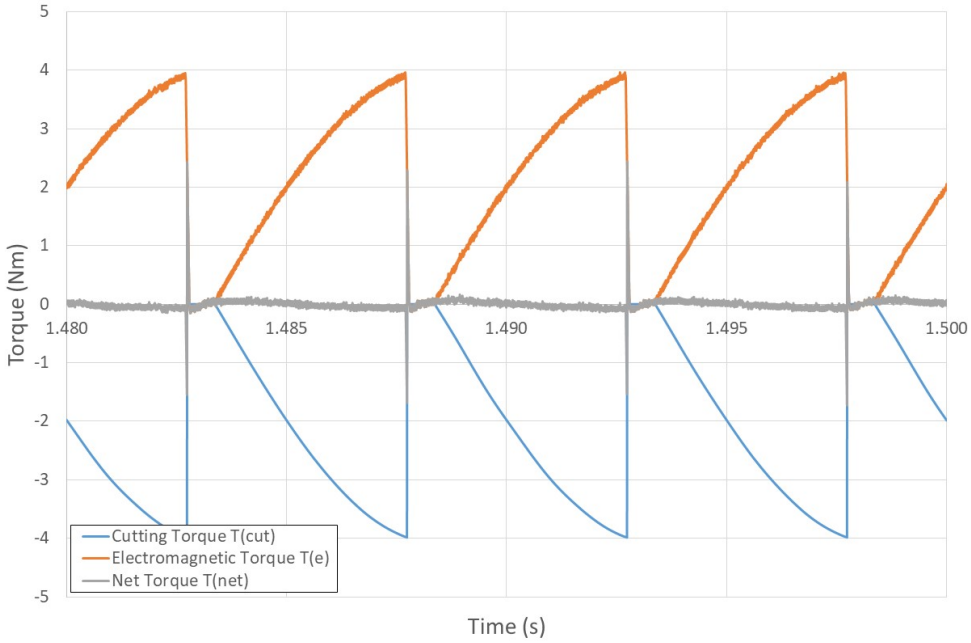

Figure 56 Predicted steady-state variations in cutting torque, electromagnetic torque and net accelerating torque at a 3,000 rpm speed demand set-point at a depth of cut of 10 mm for a low bandwidth speed controller (314 rad/s)

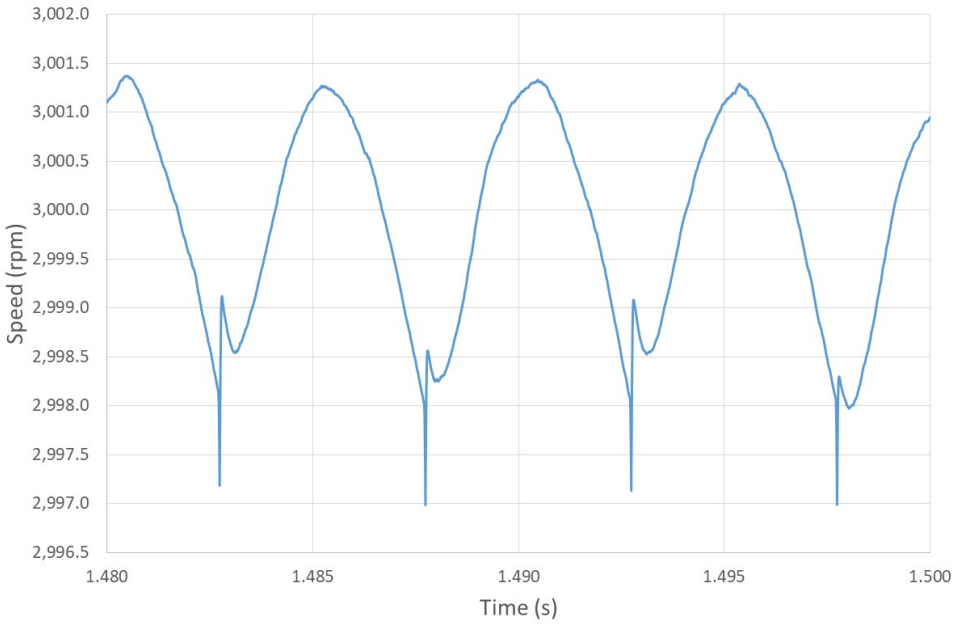

Figure 57 Predicted stead-state speed ripple at a 3,000 rpm speed demand set-point at a depth of cut of 10 mm for a low bandwidth speed controller (314 rad/s)

As will be evident from the results shown above, the speed ripple and torque ripple can be reduced significantly by adding in an open-loop torque match, although the issue of self-consistency in a ‘perfect’ mechanical representation of the load is recognised.

In order to establish whether torque matching would yield some benefits in terms of reducing chatter, a large number of simulations were performed with this torque match controller for speeds between 2,600 rpm and 10,000 rpm. At each discrete speed, the depth of the cut was increased until chatter was detected. This series of simulations were performed with a speed-stiff input and did not limit the depth of cut to either the physical height of the cutter teeth (20 mm) or the maximum torque rating of the machine. The resulting stability lobe diagram for this torque match is shown in Figure 58 along with the SLD calculated previously for a simple speed stiff input to the model with no torque match. As shown, there is negligible difference in terms of stability and hence torque match offers very little in terms of reducing vibration.

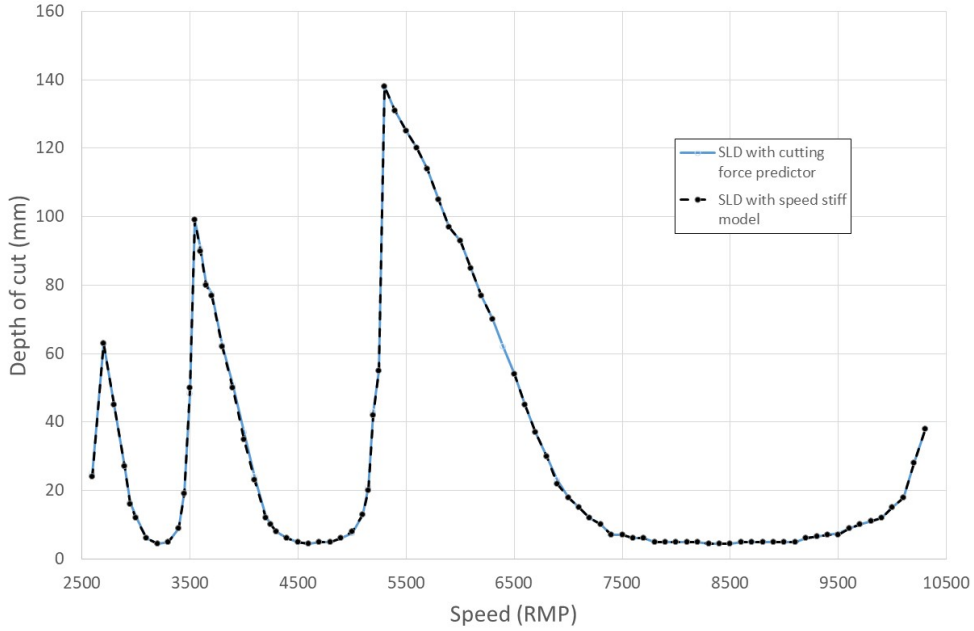

Figure 58 Stability lobe diagram with cutting force predictor

3.4. Rapid torque modulation

3.4.1. Description of method

As noted previously, conventional variable-speed milling tends to involve relatively slow modulation of the spindle speed, with cycles in the range of a second to a few seconds. The method described in this section involves rapid torque modulation and is intended to achieve significant changes in speed on the timescales of tens of milliseconds. In order to achieve the maximum rates of deceleration and acceleration around a set-point, an open-loop square wave torque demand is added to the torque demand from the speed controller as shown in the block diagram of Figure 59. The new open-loop torque modulation works in combination with a low bandwidth closed loop speed controller (314 rad/s) and a model of the cutting force to regulate the average speed.

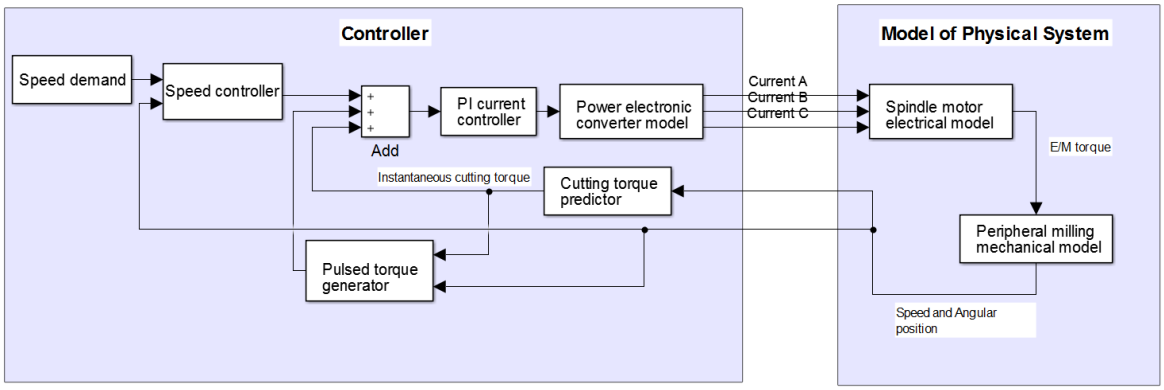

Figure 59 Block diagram of controller for implementing open-loop square wave torque modulation with torque match

It is important to note that although the torque pulsations are applied in an open-loop manner, their magnitude is limited by the operating conditions, specifically in terms of the average cutting torque. All electrical machines have maximum continuous torque ratings, usually determined by thermal limits. The maximum magnitude of the square wave torque pulsations which can be applied are limited by the torque rating and the proportion of the torque rating

which is used to overcome the average cutting force. Figure 60 shows a cycle of torque modulation which is centred around a net positive torque which matches the average cutting torque, T_c. In order to assist with maintaining the desired speed set point, the modulating torque has a 50:50 duty cycle such that the acceleration and deceleration introduced by these pulsations are balanced.

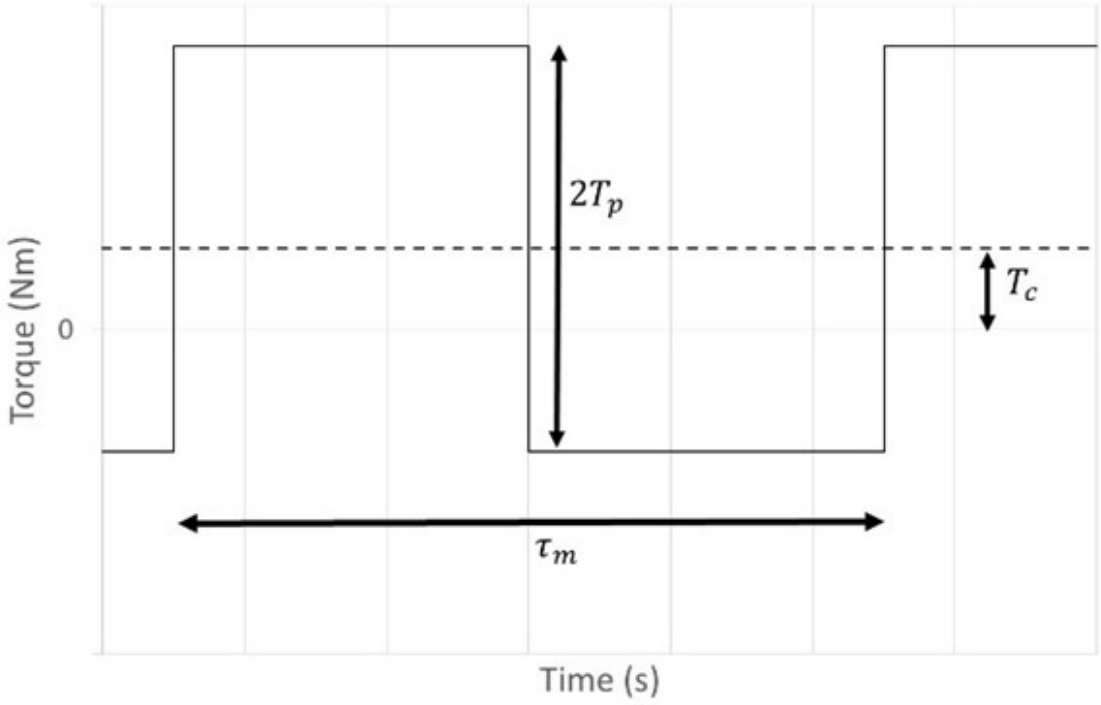

Figure 60 General form of torque waveforms used to rapidly modulate speed

It is important to recognise that these torque pulsations will inevitably affect the efficiency of the machine. Many high performance permanent magnet machines achieve efficiencies of 95%+ at their maximum rated operating point. Since the torque waveform of Figure 60 only contributes a net torque equal to T_c. Providing the power converter has regenerative capability the additional power consumption of this mode of control is determined only by the losses and not any additional work done (at least when process damping forces are neglected). It is nevertheless important to minimise the losses associated with this torque modulation and hence it is useful to

establish the minimum value of T_p which ensures stable cutting rather than use the maximum available T_p.

As will be apparent from the block diagram, the torque modulation block and the speed controller operate alongside a cutting torque predictor. The speed controller is in conflict with the torque modulation function as it attempts to maintain the speed at the set-point while the torque pulsations are introduced in order to modulate the speed. Clearly, a high bandwidth speed controller would be more effective in counteracting the effect of the torque pulsations. However, a modest bandwidth speed controller will tend to yield very poor dynamic response with a high propensity for instability. Hence, a balance must be struck between ensuring sufficient speed control action to regulate the average speed while not introducing excessive speed control action which counteracts the effect of the torque pulsations. Hence, a cutting force model, which provides an output which should match to a reasonable degree the cutting force, was added into the control scheme to assist the low-bandwidth speed controller in maintaining the average set-point speed over an extended timescale. This compensation of the cutting force greatly enhances the ability of the speed controller to regulate the average speed of the cutter with a modest bandwidth.

As the cutting torque, T_c, increases, the maximum available accelerating and decelerating torque must be reduced to remain within the maximum thermal rating of the machine. For a given RMS cutting torque of T_c and a rated RMS motor torque of T_r, the peak flat top, $50{:}50$ duty cycle, the maximum torque which can be applied to remain within the thermal rating of the machine is given by:

$$T_p = \sqrt{{T_r}^2 - {T_c}^2} \qquad (3\text{-}1)$$

As noted previously, this is a maximum available T_p rather than the value that needs to be used to achieve stable cutting. The key to minimising the additional losses associated with the torque modulation is to use the minimum value of T_p which ensures stable cutting.

Rather than specifying the duration of the torque modulating cycle, τ_m, in terms of a time interval, this study defined τ_m in terms of multiples of the tooth passing intervals. In the case of the 4 tooth cutter with the parameters shown previously in Table 1, one tooth pass corresponds to a quarter of a mechanical revolution.

3.4.2. Simulation results

A series of simulations were performed with progressively increasing values of the cycle duration τ_m for the spindle operating at 4500 rpm (all other parameters as specified in Table 1). A baseline for this new speed point was established for the case of no torque modulation and a low bandwidth (314 rad/s) speed controller. The depth of cut at which there is an onset of chatter was determined from the stability lobe diagram shown previously in Figure 31. For this speed and tool parameter combination, the maximum depth of cut is only 5 mm. As will be apparent from the stability lobe diagram, this is one of the most challenging speeds in terms of stability.

A large number of simulations were performed to quantify the benefits of torque modulation. At a given depth of cut and a given value of τ_m, the magnitude of T_p was progressively increased in increments of 1 Nm until stable cutting was achieved. For these simulations, the torque was not hard limited in the simulations to the maximum available value T_p, i.e. torques greater than the rated torque of the machine was allowed at the largest cutting depth to explore the behaviour, although it was recognised that this may not be achievable in practice.

Figure 61 to Figure 64 show the variation in the minimum value of T_p required to achieve stable cutting and a feed rate of 0.05 mm/tooth for values of τ_m between 4 and 16 tooth passes. Also shown in the characteristics is the limiting contour of T_p calculated from the cutting

torque per mm of cut depth shown previously in Figure 27 and equation (3-1). As would be expected, the available modulation torque decreases with cutting depth because of the increased cutting torque required.

As will be apparent, for all values of τ_m, there is a significant increase in the cutting depth compared to the standard speed controller with no torque modulation. Only the very short duration τ_m which corresponds to 4 tooth passes, is unable to reach the full tool cutting depth of 20 mm (limited by length of the teeth).

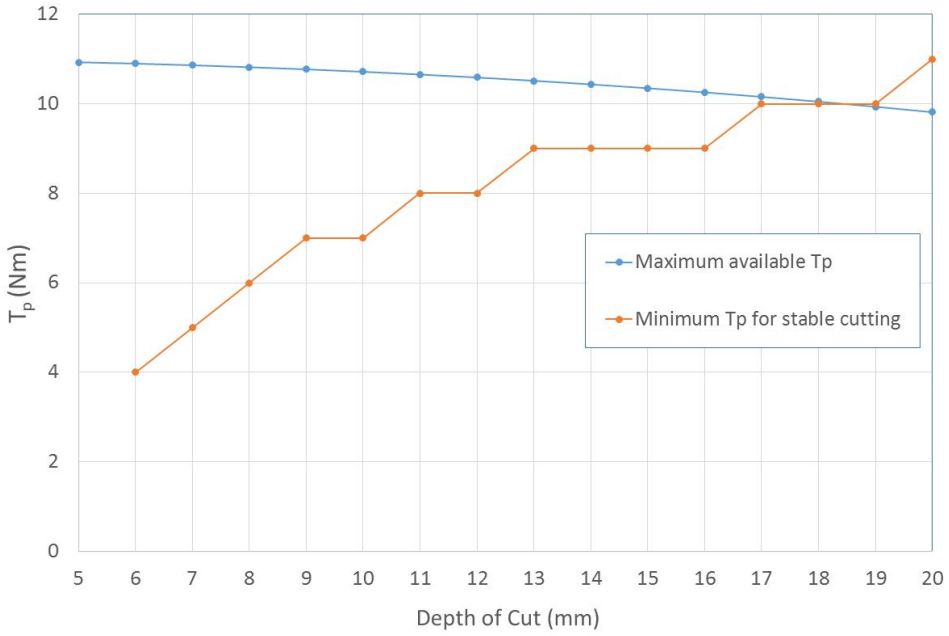

Figure 61 Variation in minimum T_p to achieve stable cutting at 4,500 rpm at a series of cutting depths and a modulation cycle duration, τ_m, of 4 tooth passes

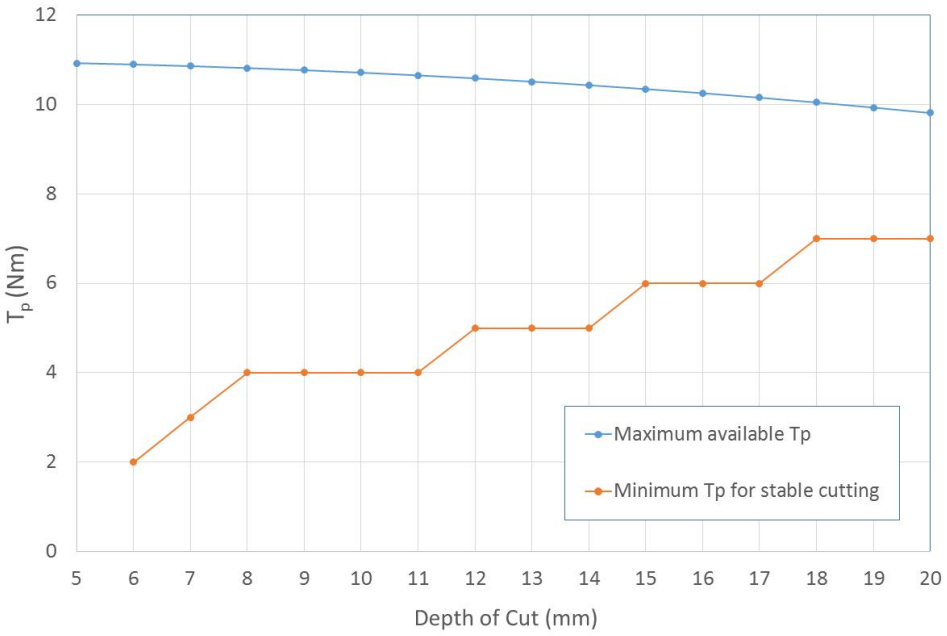

Figure 62 Variation in minimum T_p to achieve stable cutting at 4,500 rpm at a series of cutting depths and a modulation cycle duration, τ_m, of 8 tooth passes

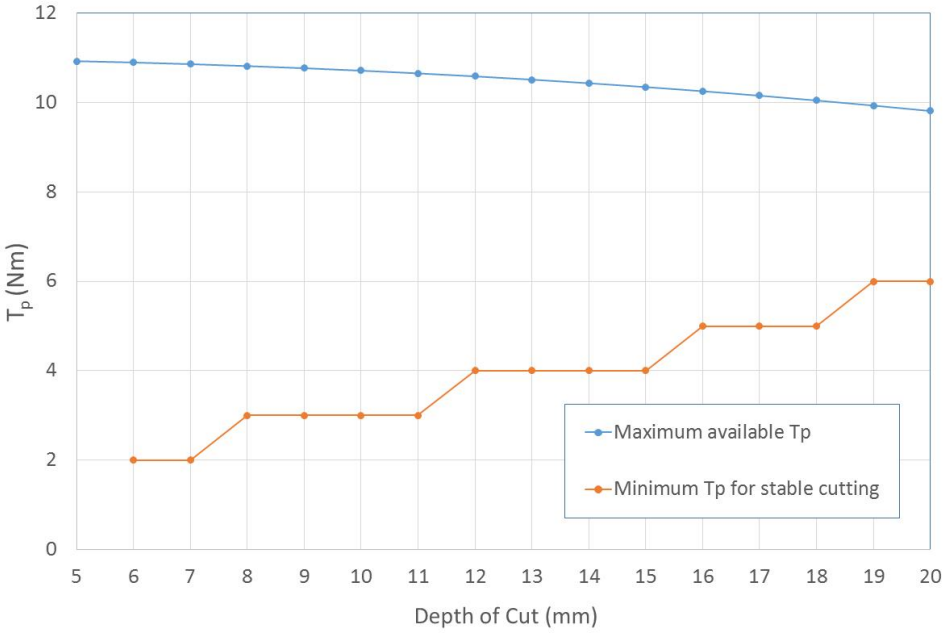

Figure 63 Variation in minimum T_p to achieve stable cutting at 4,500 rpm at a series of cutting depths and a modulation cycle duration, τ_m, of 12 tooth passes

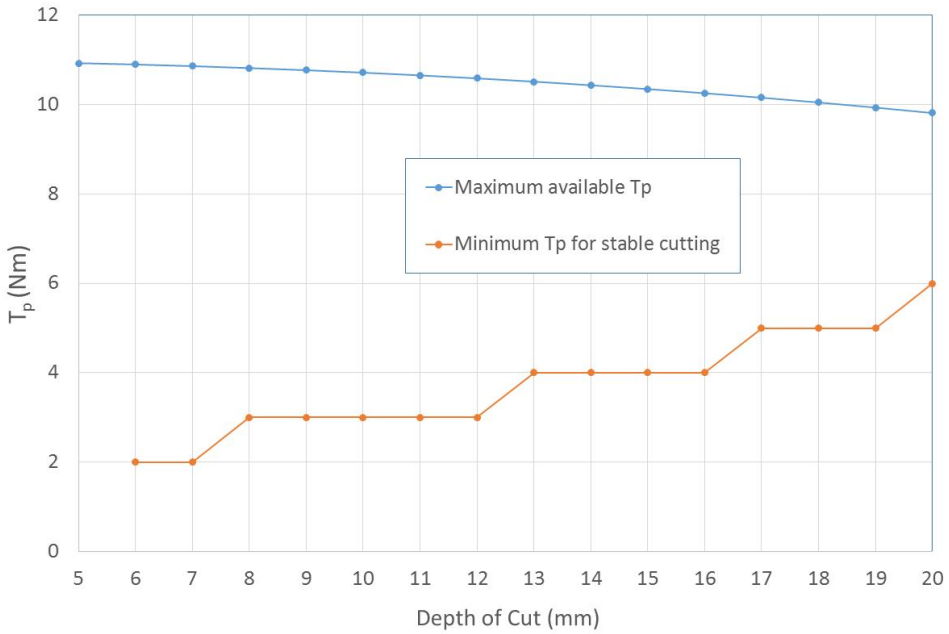

Figure 64 Variation in minimum T_p to achieve stable cutting at 4,500 rpm at a series of cutting depths and a modulation cycle duration, τ_m, of 16 tooth passes

Table 7 shows a summary of the variation in the critical cutting depths at 4,500 rpm which are at the limit of stability as a function of τ_m along with the minimum value of T_p required and the maximum and minimum speeds achieved during the simulations.

As will be apparent, all the combinations in Table 7 result in an increased critical depth compared to the original baseline condition of no torque modulation in which the critical depth was only 5.5 mm. It is also apparent, that there are joint optima on this resolution, with value of τ_m which corresponds to 12 or 16 tooth pass intervals and frequencies of 25 Hz and 18.7 Hz respectively. Finally, it is interesting to observe that for the longer duration pulses, the speed controller begins to exercise increasing control over the speed, limiting the speed excursion to less than would be expected from the relative durations of the acceleration and deceleration intervals.

Table 7 Predicted variation of critical cutting depth with duration of torque modulating pulses

τ_m (ms)	Number of tooth passes in τ_m	Calculated torque T_p (Nm)	Maximum speed (rpm)	Minimum speed (rpm)	Speed change (pk-to-pk rpm)	Critical depth of cut (mm)
6.67	2	11	5100	3938	1162	7
13.34	4	8	5241	3754	1487	12
26.68	8	6	5372	3622	1750	16
40.02	12	5	5359	3642	1717	18
53.36	16	5	5393	3612	1781	18
66.70	20	6	5580	3413	2167	16
80.04	24	6	5604	3395	2209	16

* - Based on thermal rating and equation

Regardless of the speed controller action, this open-loop torque modulation still results in very large speed changes which are centered around the steady-state set-point speed.

Of all the cases considered a τ_m value of ~40ms (corresponding to 12 and 16 tooth passes) results in the maximum critical cutting depth, with a near four-fold increase in the depth of cut compared to a standard speed set-point controller. At this depth of cut, operated within the machine's thermal rating, the pulsed torque waveform with minimum T_p of 5 Nm.

Figure 65 to Figure 68 show a series of time variations for key quantities in the model for the case of the optimal cycle duration of 12 tooth passes at a cutting depth of 18 mm. As will be apparent from the rotational speed waveform of Figure 65, the deceleration element of the modulating torque pulse train results in a large transient drop in speed at the tool engages the work-piece. However, once this initial transient is overcome, the speed settles into a steady cycle between ~3600 rpm and ~5400 rpm.

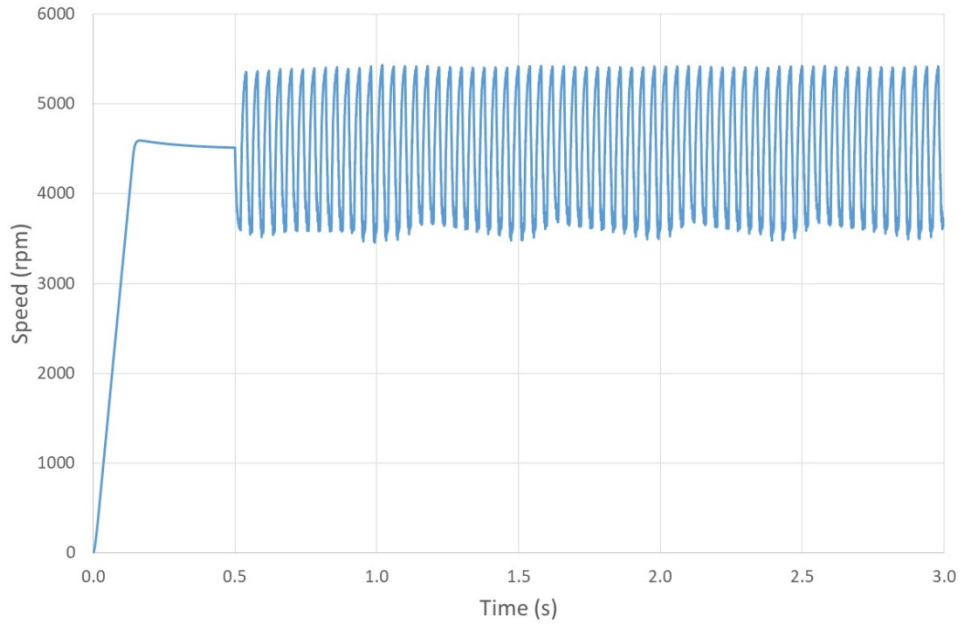

Figure 65 Predicted rotational speed of machine for $\tau_m = 40.02$ ms, $T_p = 5Nm$ and cutting depth of 18 mm at 4500 rpm spindle speed

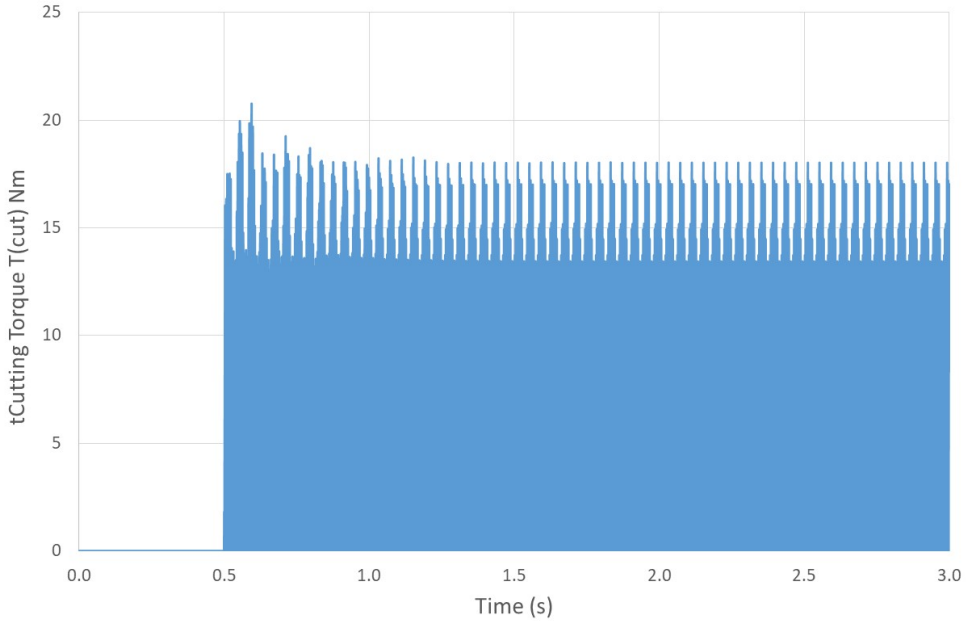

Figure 66 Predicted cutting torque waveform for $\tau_m = 40.02$ ms, $T_p = 5Nm$ and cutting depth of 18 mm at 4500 rpm spindle speed

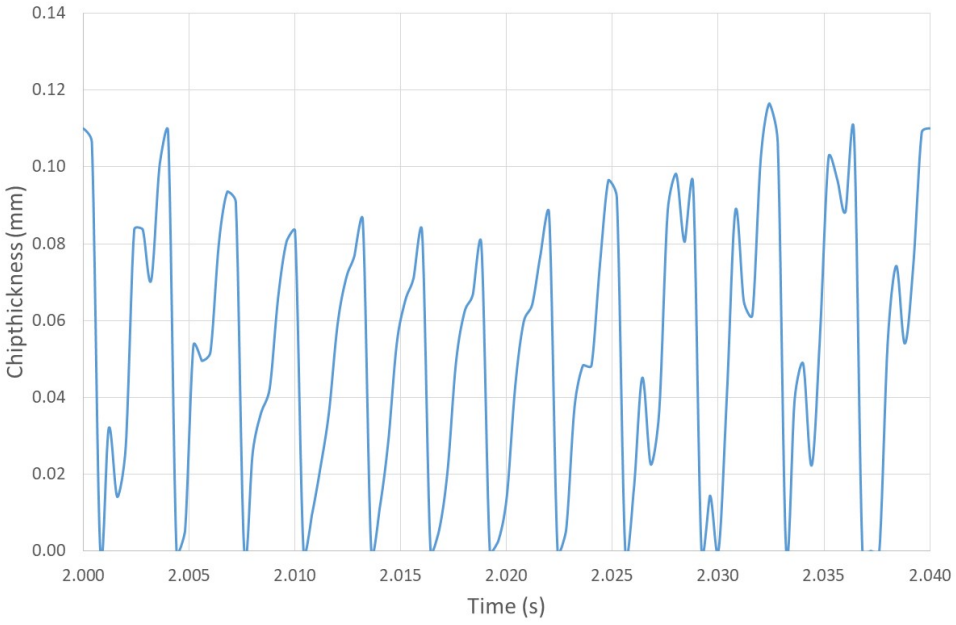

Figure 67 Predicted chip thickness waveform for $\tau_m = 40.02$ms, $T_p = 5Nm$ and cutting depth of 18 mm at 4500 rpm spindle speed

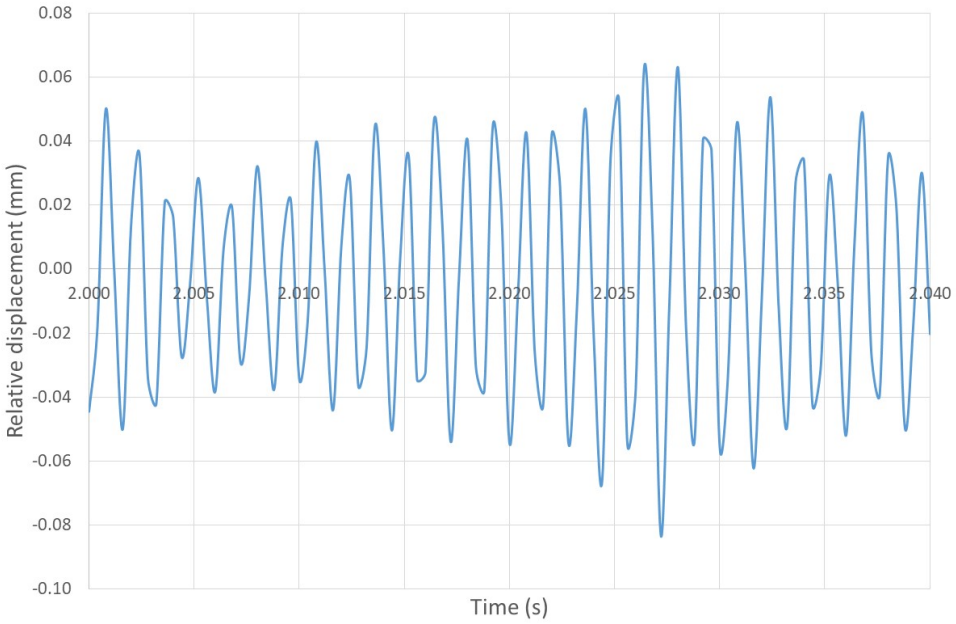

Figure 68 Predicted displacement in the direction of feed for $\tau_m = 40.02$ ms, $T_p = 5Nm$ and cutting depth of 18 mm at 4500 rpm spindle speed

It is interesting in terms of understanding the role of the torque modulation to consider an unstable case which leads to chatter in the same detail. This can be achieved by considering the case of the same speed controller (bandwidth 314 rad/s) at 4,500 rpm with no torque modulation and the same cutting depth of 18 mm.

Figure 69 shows the variation in rotational speed over a 3s interval, which includes the initial acceleration ramp to 4500 rpm followed by engagement of the tool with the work-piece at 0.5 sec. As will be apparent this engagement results in a marked speed drop which the speed controller recovers over a period of ~0.4 sec. As will be apparent from the cutting torque waveform in Figure 71 and the corresponding variation in chip thickness in Figure 72, there is significant chatter with increasing mismatch between the applied electromagnetic torque and the cutting torque. This leads to the growing speed fluctuations between 1 sec and 1.5 sec in Figure 69. Eventually at ~1.7 sec there is a significant increase in rotational speed

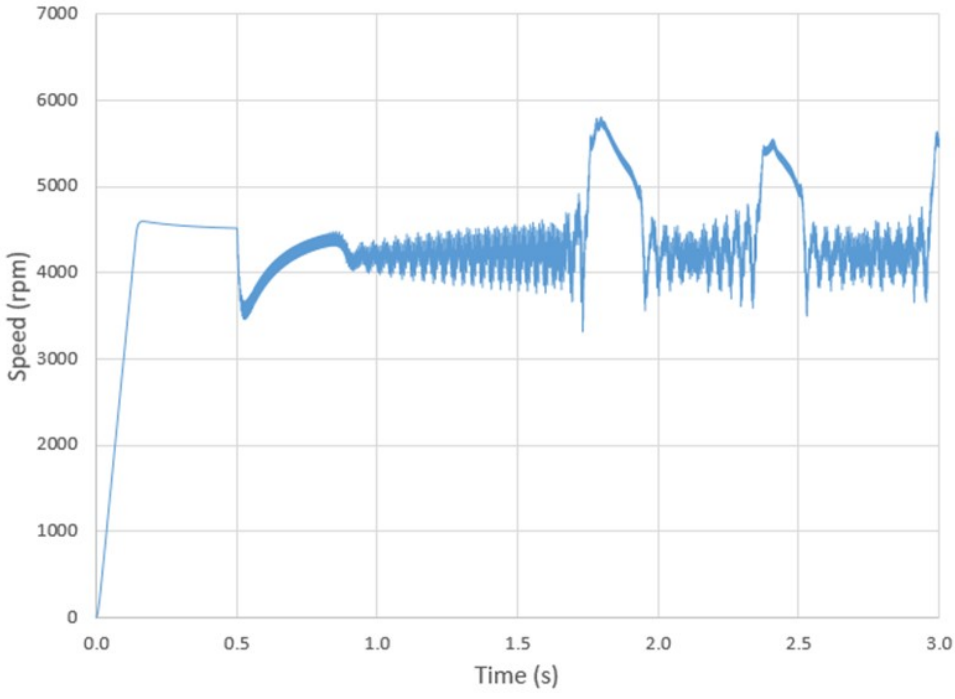

Figure 69 Predicted rotational speed of machine for a standard set-point speed control (314 rad/s controller) at a depth of 18 mm and a 4500 rpm spindle speed

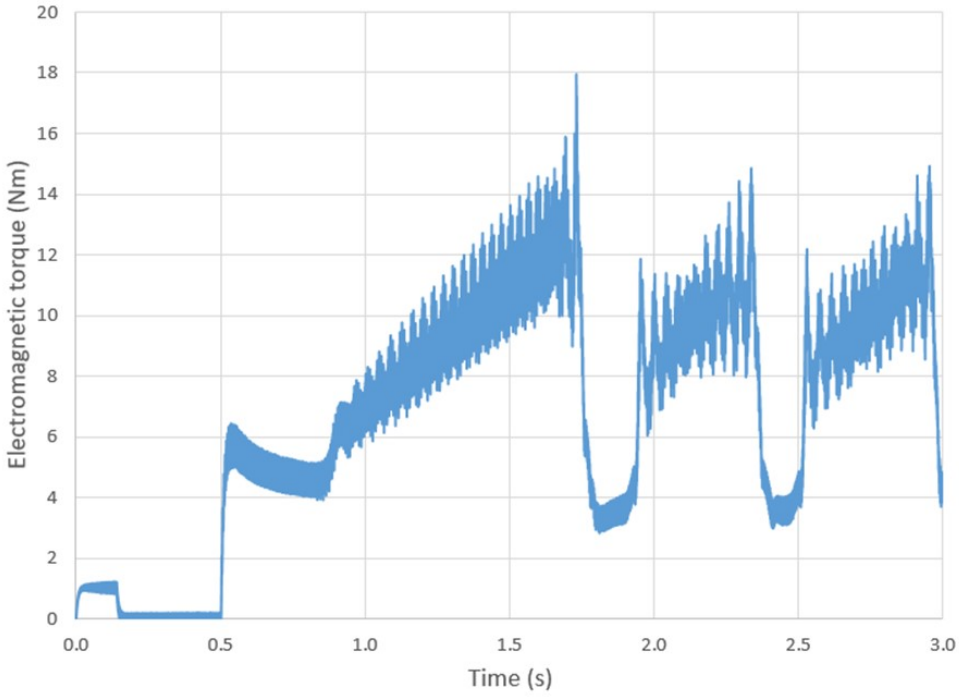

Figure 70 Predicted electromagnetic torque output for a standard set-point speed control (314 rad/s controller) at a depth of 18 mm and a 4500 rpm spindle speed

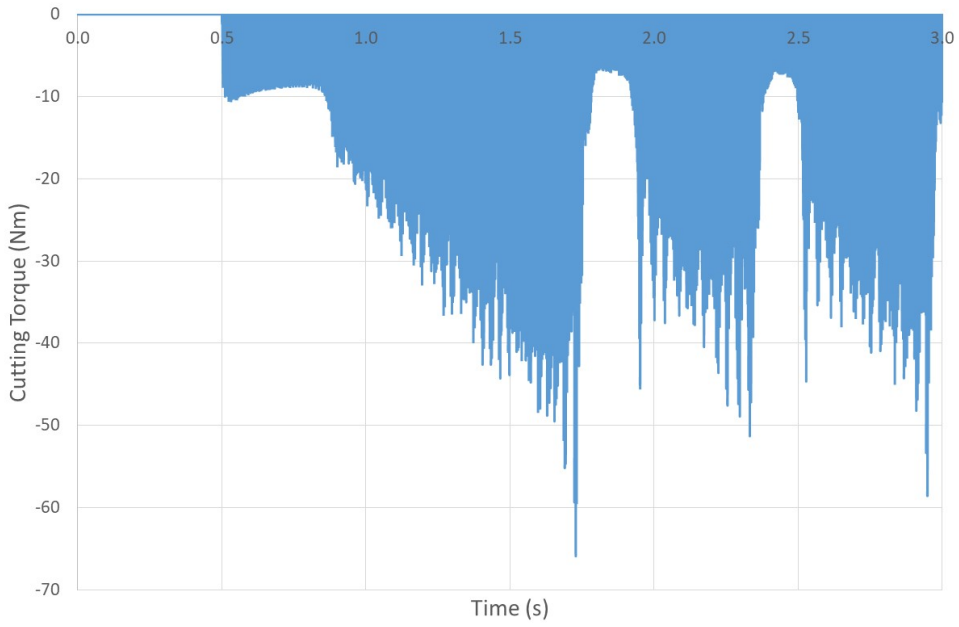

Figure 71 Predicted cutting torque waveform for a standard set-point speed control (314 rad/s controller) at a depth of 18 mm and a 4500 rpm spindle speed

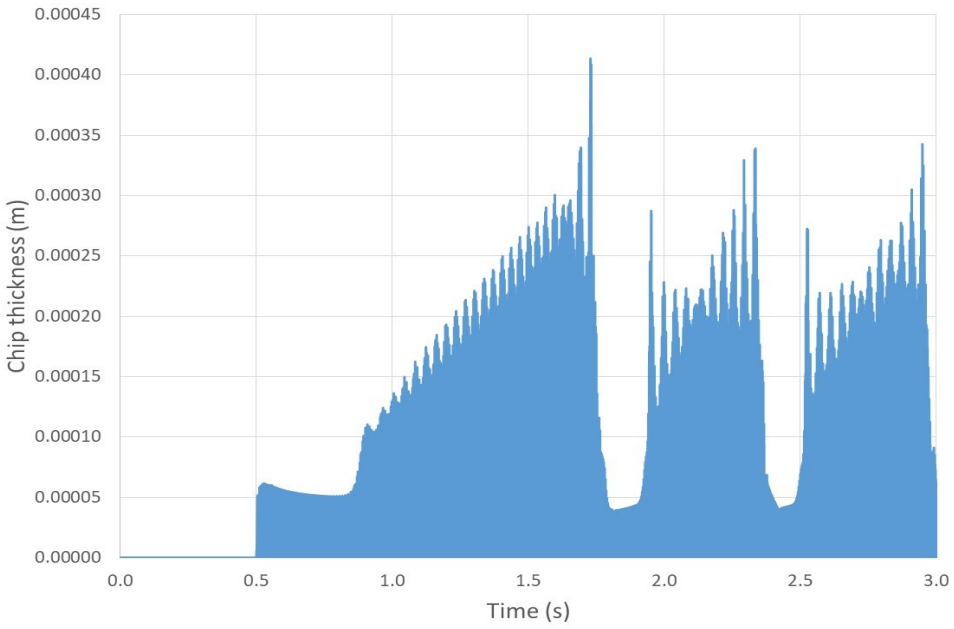

Figure 72 Predicted chip thickness variation for a standard set-point speed control (314 rad/s controller) at a depth of 18 mm and a 4500 rpm spindle speed

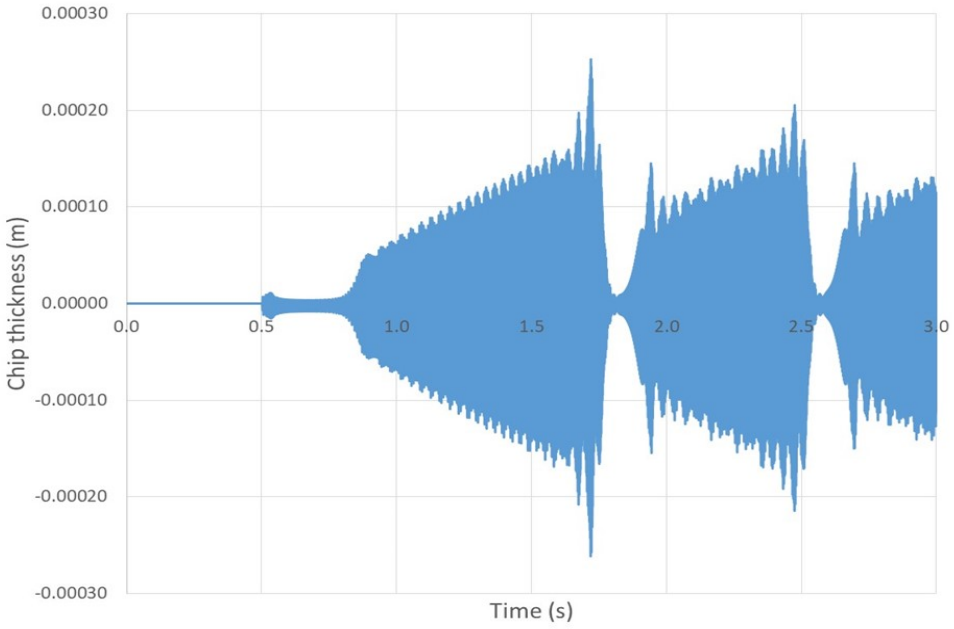

Figure 73 Predicted variation in displacement in the feed direction for a standard set-point speed control (314 rad/s controller) at a depth of 18 mm and a 4500 rpm spindle speed

The waveforms in Figure 69 to Figure 73 show typical behaviour with chatter, recalling that the critical depth for a standard speed controller at this speed and feed rate is only 5.5 mm and hence

a cutting depth of 18 mm is well beyond the point at which chatter is problematic. The cutting torque waveform of Figure 71 shows a progressive increase in torque after 0.8 sec as the vibration builds up as shown in Figure 73. However, at ~1.75 sec, the vibration suddenly drops and the cutting shows signs of approaching stability. However, this is short-lived and the vibration and cutting torque begins to grow once more. In order to understand this behaviour, it is useful to consider a few key factors.

- The feed rate is fixed throughout the simulation at a rate that is equivalent to 0.05 mm/tooth for the nominal speed of 4,500 rpm. This corresponds to a 15 mm/s and this feed rate does not vary as the speed changes around the nominal speed during the simulation. As a consequence of this constant feed rate with respect to time, a speed above the nominal set-point results in a reduced feed rate in terms of mm/tooth. This lower feed rate per tooth is likely to assist in maintaining stable cutting.
- As the speed changes, the system moves along the SLD shown previously in Figure 31, although the varying feed rate caused by speed changes will modify the SLD to some degree. At the nominal speed of 4,500 rpm the SLD indicates a critical depth of 5.5 mm. However, at 5,700 rpm, which is the maximum speed achieved in this series of simulations, the critical depth on the SLD increases to ~115 mm (which is a theoretical value given that the height of the cutter is only 20 mm).

The combined effect of these two factors is that for speed increases above the nominal set-point, there will a tendency for the cutting to become more stable. A zoom-in of the speed variation between 1.7 sec and 2.0 sec is shown in Figure 74 while Figure 75 shows the corresponding variation in the cutting force.

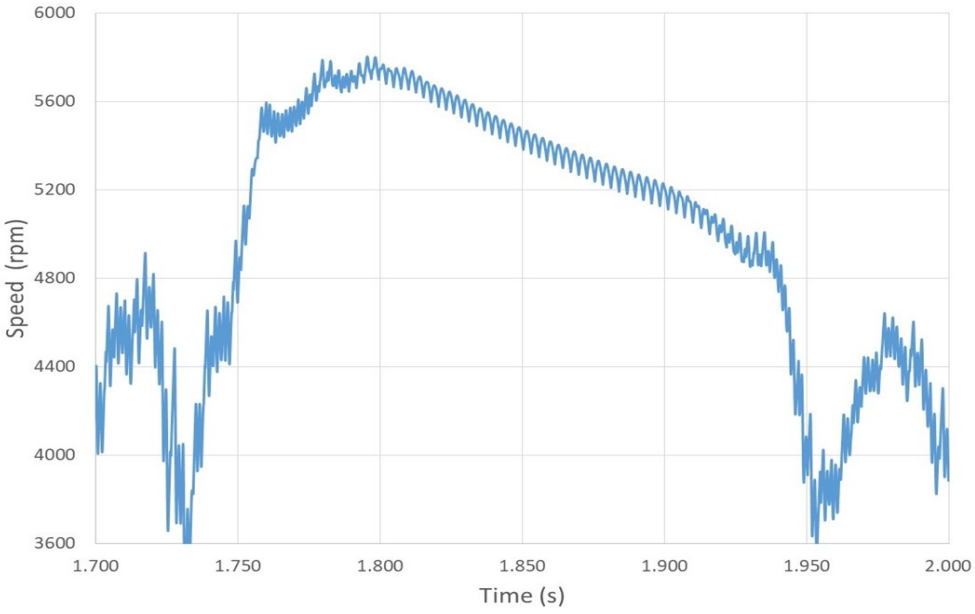

Figure 74 Zoom-in of predicted rotational speed of machine for a standard set-point speed control (314 rad/s controller) at a depth of 18 mm and a 4500 rpm spindle speed

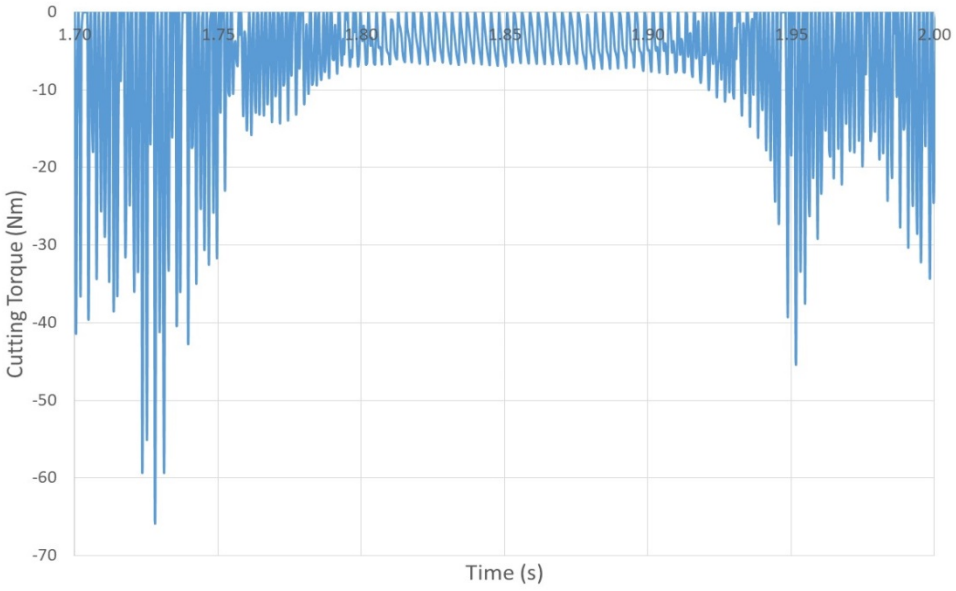

Figure 75 Predicted cutting force between 1.7 sec and 2.0 sec for a standard set-point speed control (314 rad/s controller) at a depth of 18 mm and a 4500 rpm spindle speed

3.4.3. Comparison with standard variable-speed milling

Another useful reference case is to employ more standard variable speed milling approach using the guidelines described in [KHA 13] [JAY 00] [SAS 02]. For this case, no torque modulation was applied, but the demand to the speed controller was cycled as shown in Figure 77. Hence, the dynamics of the speed controller also come into play. Figure 76 shows the block diagram of a system for standard variable speed milling. This was deemed a more realistic representation than forcing the speed profile directly into the cutting model. The demand speed variation corresponds to ±10% from the nominal 4,500 rpm set-point with a cycle frequency of 1 Hz. The depth of cut was progressively increased until chatter was observed. The resulting critical depth of cut at which the system remains just stable with conventional approach to variable speed milling is only 7 mm, i.e. an increase of only 2 mm compared to fixed speed demand.

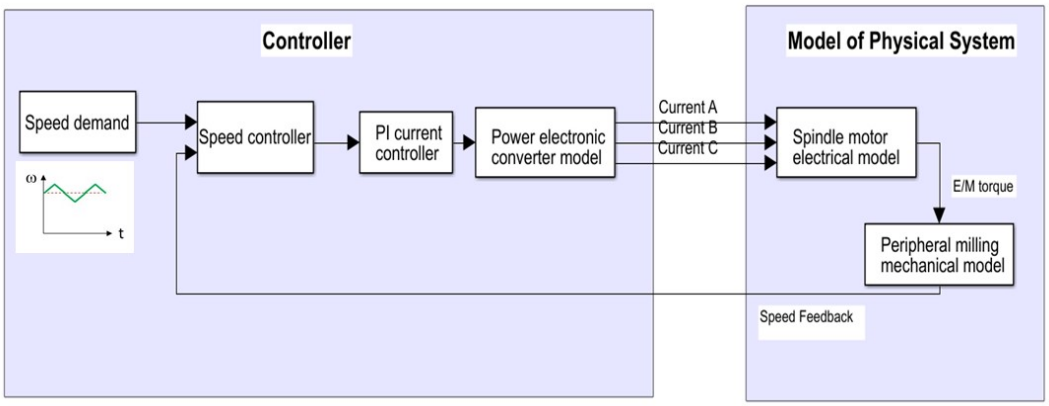

Figure 76 Block diagram of system used for standard variable-speed milling

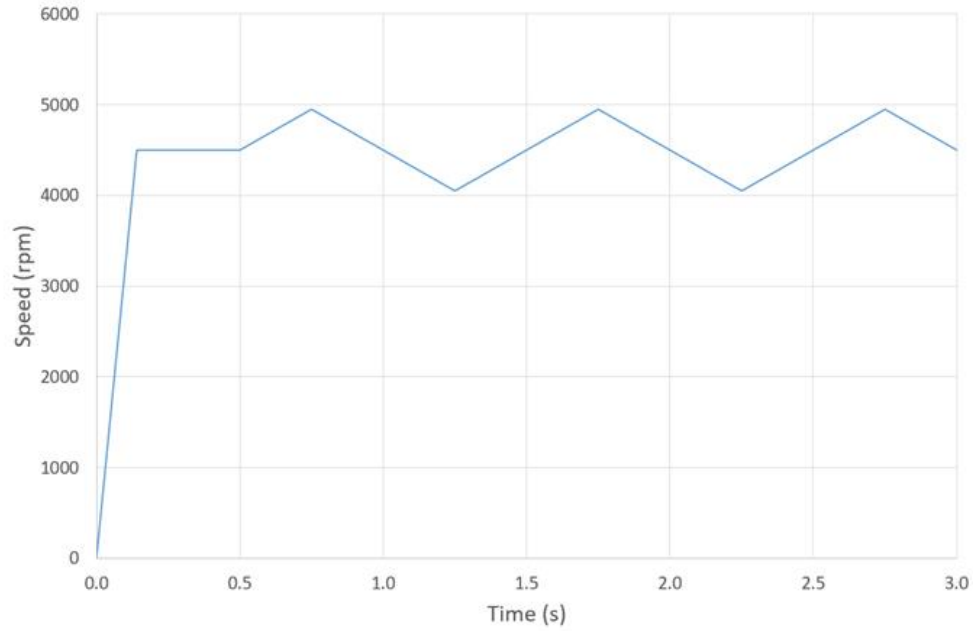

Figure 77 Demand speed profile used in simulation of conventional variable-speed milling

The resulting variations in some key time-varying quantities for the critical depth of cut are shown in Figure 78 to Figure 82.

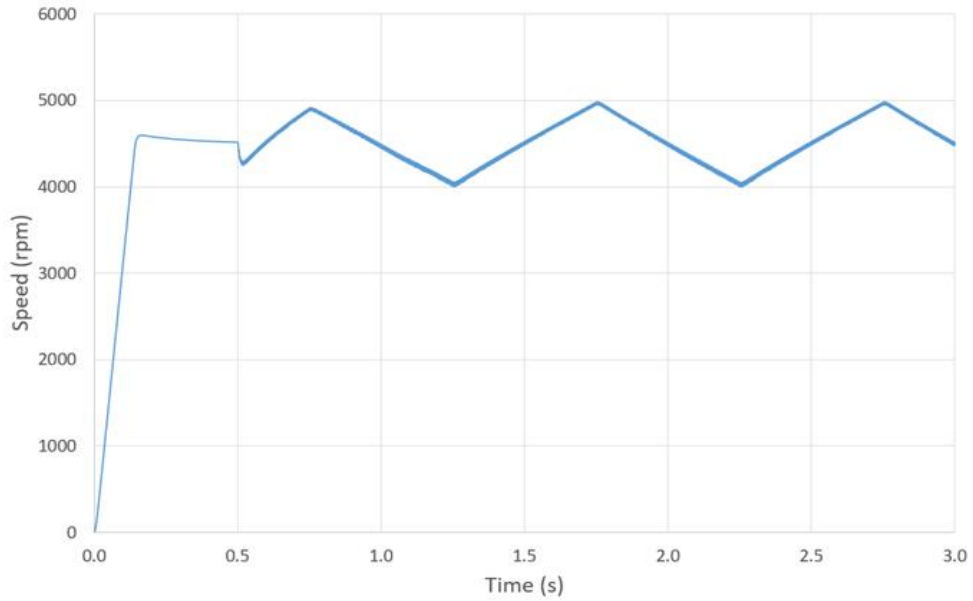

Figure 78 Predicted rotational speed of machine with standard variable speed milling with the demand speed profile of Figure 77 (314 rad/s controller) at a depth of7 mm and a 4500 rpm spindle speed

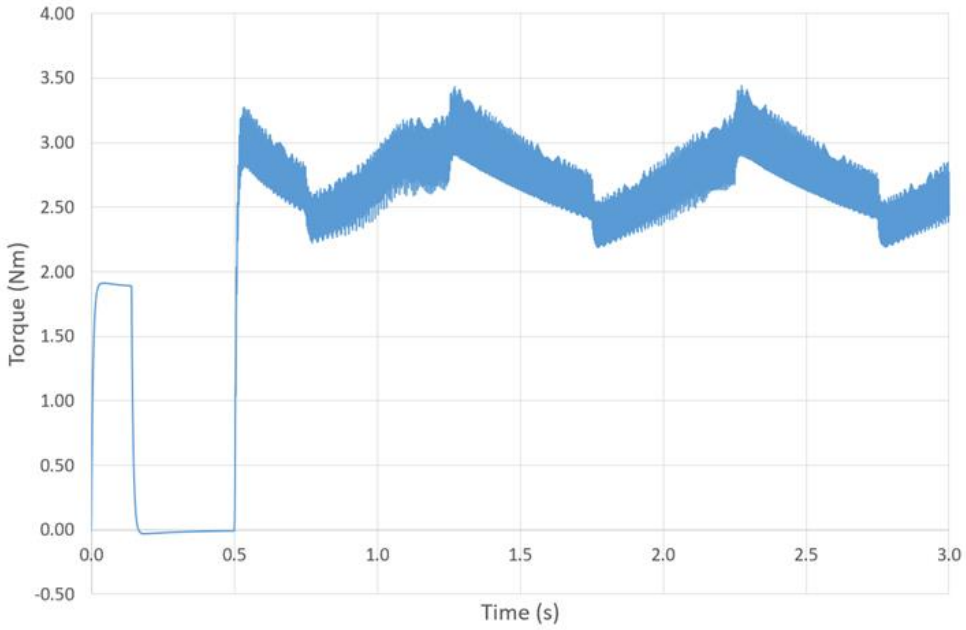

Figure 79 Predicted speed controller torque output for standard variable speed milling with the demand speed profile of Figure 77 (314 rad/s controller) at a depth of 7 mm and a 4500 rpm spindle speed

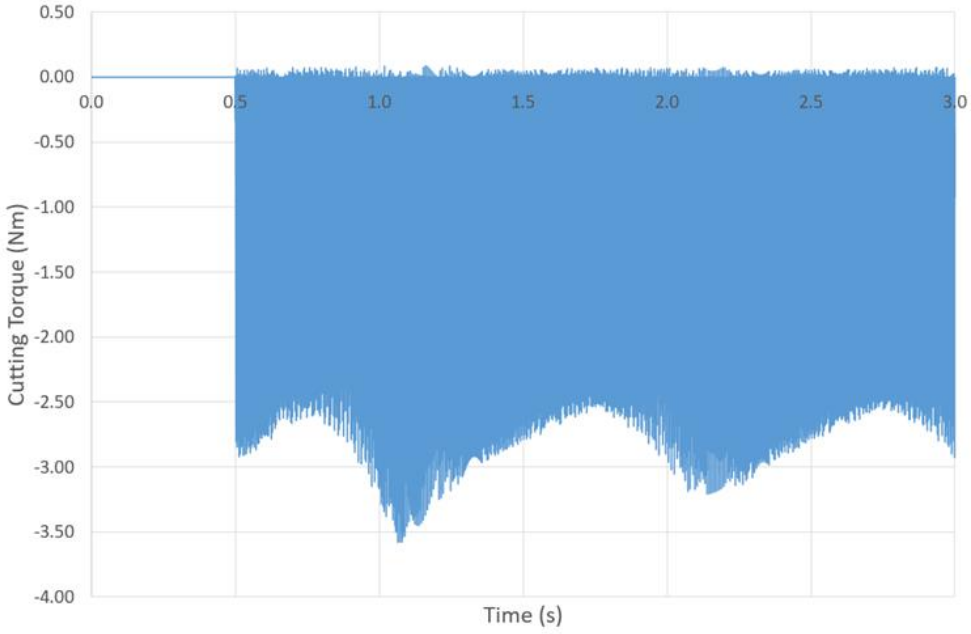

Figure 80 Predicted cutting torque waveform for standard variable speed milling with the demand speed profile of Figure 77 (314 rad/s controller) at a depth of 7 mm and a 4500 rpm spindle speed

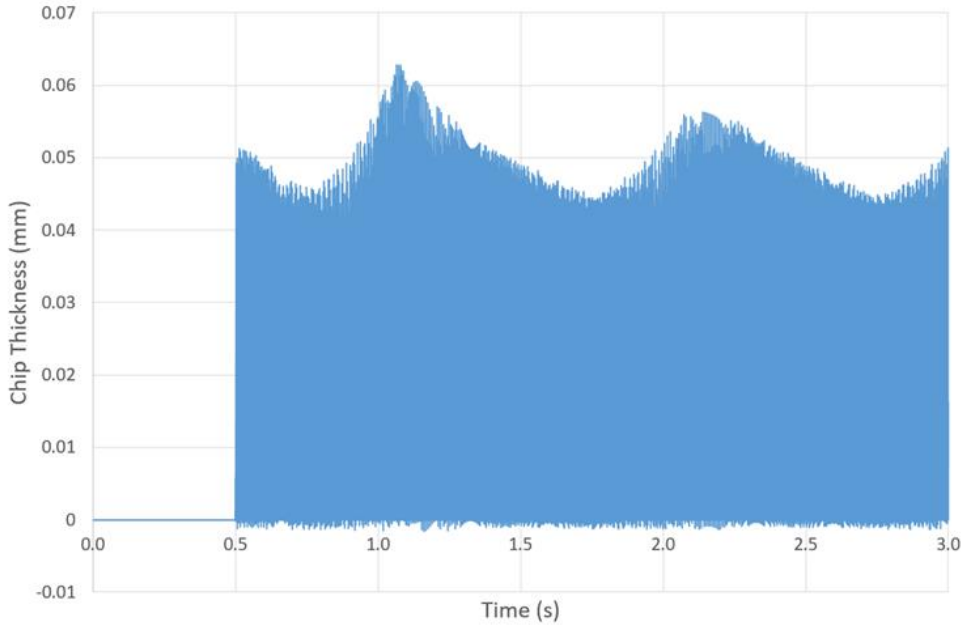

Figure 81 Predicted chip thickness variation for standard variable speed milling with the demand speed profile of Figure 77 (314 rad/s controller) at a depth of 7 mm and a 4500 rpm spindle speed

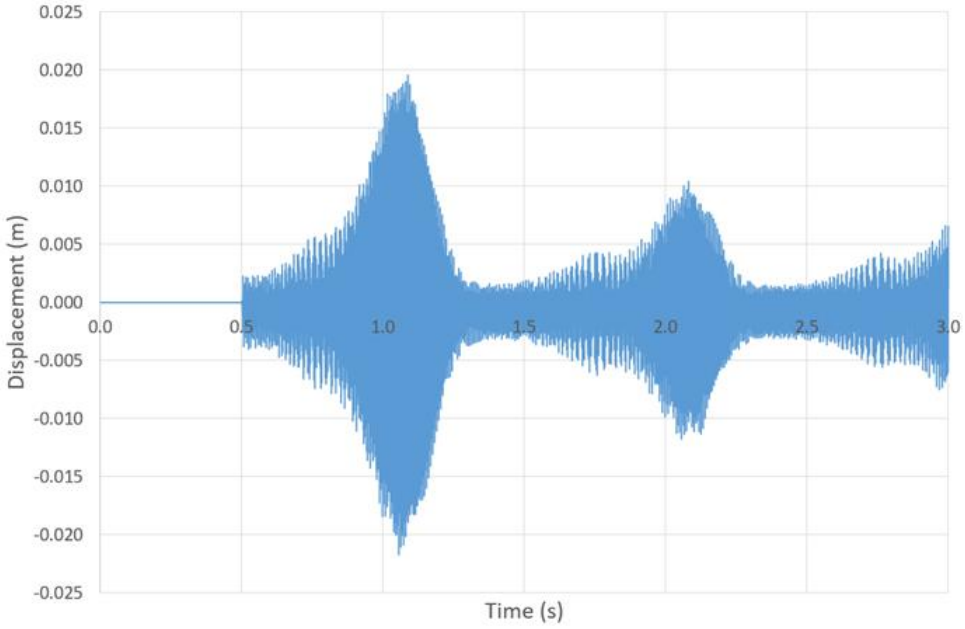

Figure 82 Predicted variation in displacement in the feed direction for standard variable speed milling with the demand speed profile of Figure 77 (314 rad/s controller) at a depth of 7 mm and a 4500 rpm spindle speed

The simulations were repeated for a total of five additional combinations of magnitude (±10%, ±15% and ±20%) and frequency of triangular modulation of the speed demand (1 Hz and 2 Hz), in all cases the nominal speed of 4,500 rpm. Table 8 shows a summary of the resulting critical cutting depths for these five combinations along with the earlier 1 Hz, ±10%, combination. As will be evident, there is a modest benefit of increased critical cutting depth from increasing the frequency but a reduction in critical depth with increased magnitude of speed modulation. However, in all cases the critical cutting depths are far smaller than predicted for the rapid torque modulation.

Table 8 Summary of critical cutting depths for triangular modulation of speed for a nominal speed demand of 4,500 rpm

Speed variation	Critical cutting depth for 1 Hz modulation (mm)	Critical cutting depth for 2 Hz modulation (mm)
±10%	7	8
±15%	6	7
±20%	6	6

This series of simulations has demonstrated that rapid torque modulation offers a significant improvement in avoiding chatter as the material removal rate is increased compared to the more standard approach to variable-speed milling. This is achieved well within the torque capability of the machine, although there is inevitably an increase in machine copper loss. Finally, it is worth recalling that at the critical depth, although the cutting is stable according to the work done by the loss of contact, there may still be excessive vibration if a high-quality surface finish is required.

Chapter 4 - Real-time chatter detection

4.1. Introduction

To maximise the material removal rate, it is necessary to operate the cutter at the maximum possible depth and feed rate while also avoiding chatter. One means of achieving this optimal performance is to continuously monitor the cutting process to detect the onset of chatter, at which point remedial action can be taken to avoid the build-up of chatter, e.g. reduce the feed rate and/or change the spindle speed [TEK 05]. There are many possible means of detecting chatter such as monitoring of acoustic emissions [WEC 75] [DEL 92] [SCH 01] [SCH 02] [WEI 06], direct measurement of vibration [HAS 96] [RVA 98] and multisensory approaches to detection chatter [FAA 03] [KUL 08] [KUL 09]. It is desirable that any method for detecting chatter in real-time satisfies the following criteria:

1. Minimum influence on overall system stiffness.
2. Minimum or no change to milling machine structure.
3. Robust to changes in cutting conditions.
4. Mechanically and environmentally robust system

This chapter will first investigate existing methods for real-time chatter detection. After comparing all the various methods published in literature, a new method for real-time in-process chatter detection based on detecting changes in speed will be presented.

On-line chatter detection has attracted significant interest as a research topic in recent years. Although a stability lobe diagram (SLD) provides some valuable a-priori guidance, it is specific to a combination of cutting parameters which may well vary during the manufacture of a component. The cutting parameters such as cutting coefficient, structural damping ratio and

natural frequency are all likely to vary during the milling process. In an attempt to address these limitations, this chapter discusses the potential for real-time chatter detection.

4.2. Review of methods for real-time chatter identification

Several methods for detecting the onset of chatter have been reported, and in all cases, chatter detection is achieved through the introduction of an additional sensor. Amongst the sensors that have been reported are microphones [DEL 92], accelerometers [DIM 00], laser displacement sensors [RVA 98] [GRA 05], eddy current gap sensor [DEV 07], and dynamometers [TAN 12] [ISM 97].

The monitoring of changes in the acoustic emissions with microphones during cutting provides a practical method of detecting the onset chatter during milling process [DEL 92]. According to the findings in [DEL 92], microphones can be set-up to be sensitive to chatter onset. However, microphones also have limitations, including modest frequency response (typically as low as 1000 Hz in 1992's while chatter frequencies can be up to 5000 Hz) and a potential for false triggering due to external acoustic disturbances.

Riviere et al. [RIV 06] improved this method by integrating the microphone itself into the tool holder which make it more immune to external disturbances, but this did not resolve the problems of modest frequency response. D.E. Dimlaet al. [DIM 00] and F.Ismael et al. [ISM 97] employed accelerometers and plate dynamometers to measure vibrations caused during milling, but this is a complex arrangement that does not lend itself to widespread adoption in production machines.

M. Hashimoto et al. [HAS 96] and A. Devillez et al. [DEV 07] investigated eddy current displacement sensors while O. Ryabov [RVA 98] and J. Gradisek [GRA 05] considered laser displacement sensor. In both cases, the aim was to monitor displacement of the tool relative to some datum as a means of tracking vibration. E. Kuljanic et al. [KUL 08] considered a

multi-sensor approach for chatter detection to increase the effectiveness and robustness of the detection. Although some of these studies reported promising results, they were all based on the introduction of bespoke sensors into a very harsh environment local to the cutting tool, in which coolant or swarf may be present

For the various signal sources reported in literature, four signal processing method have been employed to extract key information: Fast Fourier transform (FFT), power spectral density (PSD), wavelet transform (WT), and Pattern recognition. Although interest has been focused on wavelet transform due to its ability to extract information in both the time domain and frequency domains. [CHO 03] [YAO 10] [WAN 09], it can only be readily applied when the chatter frequency is known in advance. With an unknown chatter frequency, wavelet methods have difficulty in determining both mother wavelet function and sufficient number of levels of decomposition. In the case of pattern recognition algorithms, these have two very significant problems, in that it either requires long learning or adaptation before being deployed and moreover it cannot identify the chatter frequency [TAN 12].

The limitation of classical Fourier Transform and power spectrum density analysis is that these methods can only identify the chatter frequency when regenerative chatter has occurred [13]. To reduce the effect of this retrospective approach, the use of short time Fourier transform (STFT) has been proposed. The essence of STFT is to create a short duration ‘window’ in which the Fourier transform analysis is performed rather than on the entire data set. To apply this method, the sampling frequency and time length of the ‘window’ need to be carefully considered.

In this chapter, a novel chatter detection method based on identifying small variations in rotational speed is developed using an STFT algorithm.

4.3. Utilisation of measured rotational speed for chatter detection

A key element for the servo control of a spindle machine is the speed feedback loop, which is usually reliant on a speed sensor that is sufficiently precise to provide high fidelity position and speed data for the system controller. The onset of chatter will change the nature of the cutting force on the tool, which will result in a change in the instantaneous torque mismatch between the spindle machine and the load and hence intervals of acceleration / deceleration. The closed loop speed controller will try to correct these speed fluctuations, but is unlikely to fully suppress higher frequency speed fluctuations, particularly if the speed controller has a modest bandwidth compared to the frequency of the speed variation caused by chatter. In principle, the detection of changes in speed fluctuations provides a means of detecting chatter, e.g. by tracking the growth of a frequency in the spectrum of the speed signal. In many regards, a high-resolution speed sensor provides a convenient and practical means of detecting chatter:

- The method does not require additional sensors - although a higher performance replacement position/speed sensor than a standard sensor may need to be fitted
- No modifications required to spindle machine, tool-holder or work-piece base-plate. There will therefore more robust and do not require additional information
- Well established mechanistic analysis of dynamics of both motor rotational speed and milling process.

When chatter occurs, the average cutting torque tends to increase in magnitude at the chip thicknesses.

The classical equation of rotational motion for a non-salient PMSM machine is:

$$\omega_n = \frac{1}{J}\int (T_e - T_L - B\omega_m)dt \qquad (4\text{-}1)$$

while the electromagnetic torque generated by the motor is given by:

$$T_e = K_t i_{sq} \qquad (4\text{-}2)$$

where K_t is the machine constant.

Due to the nature of servo control system, the Fourier expansion of T_e consists of two elements: slow reacting PI controller $C_{pid}(t)$ and very high PWM switching frequency f_{sw}:

$$T_e(t) = C_{pid}(t) + \sum_{k=N_{sw}}^{N_{sw}} P_k e^{2\pi j k f_{sw} t} \qquad (4\text{-}3)$$

where N_{sw} is the harmonic number for switching frequency. P_k is the amplitude of the harmonic.

Since in idealized machining process, the load torque T_L is equal to:

$$T_L = \begin{cases} T_c & on\ stable \\ T_c + T_{chatter} & on\ chatter \end{cases} \qquad (4\text{-}4)$$

The cutting torque T_c is generated by cutting force F_c applied on the machine tool. As established in (4-3), and take periodic rectangular function from(4-4) into account, Fourier expansion of $F_t(t)$, the total force acted on the motor shaft, consists of three parts: tooth passing frequency f_{tpass}, chatter frequency $f_{chatter}$, and white noise (e.g. noise in sensor) :

$$F_t(t) = \sum_{k=N_{tpass}}^{N_{tpass}} A_k e^{2\pi j k f_{tpass} t} + \sum_{k=N_c}^{N_c} [B_k^+ e^{2\pi j (f_{chatter} + k f_{tpass}) t} + B_k^- e^{2\pi j (-f_{chatter} - k f_{tpass}) t}] + w(t) \qquad (4\text{-}5)$$

where A_k and B_k are amplitudes for the harmonic of cutting reaction and chatter reaction. N_{tpass} and N_c are the harmonic numbers. In practice, only limited order of harmonics are considered, because of the 90% of the energy are distributed in the first 3 harmonics [TES 05], hence higher orders of harmonics can neglected.

By combining (4-3) and (4-4) and substituting into (4-5), the Fourier expansion of the rotational speed can be rewritten as:

$$\omega_n = \sum_{k=N_{sw}}^{N_{sw}} K_t i_{sq} e^{2\pi j k f_{sw} t} + \sum_{k=N_{tpass}}^{N_{tpass}} A_k e^{2\pi j k f_{tpass} t} + \sum_{k=N_c}^{N_c} [B_k^+ e^{2\pi j (f_{chatter} + k f_{tpass}) t} + B_k^- e^{2\pi j (-f_{chatter} - k f_{tpass}) t}] + w(t) + C_{pid}(t) \qquad (4\text{-}6)$$

This equation reveals the spindle speed contains five potential sources of information:

- High frequency and small motion changes due PWM switching frequency
- Periodic motion reaction on the shaft due the normal machining process
- Motion disturbance due to the regenerative effect in machining
- Motion change due to speed controller trying to maintain the commanded speed
- White noise due to the measuring system

Although the method proposed in this chapter deals with the full spectrum of the speed signal, it is useful to consider the contributions from the five terms in equation (4-6). Around the frequencies of interest, i.e. those associated with the dominant mechanical dynamics of the system, the first term associated with PWM disturbance will be very low in comparison to the remaining terms. Under nominal steady-state speed conditions, the disturbance from PI speed controller will tend to modest and, in the case of the speed controller with a bandwidth of 314 rad/s, will tend to exert the majority of its control action below 50 Hz. When the machining process is stable, i.e. no chatter, then the spindle load force will be dominated by the normal cutting force. As the chatter starts to build up, the regenerative element will start to build up and eventually dominate the total force unless some reactive action is taken.

The thesis employed short time Fourier transform (STFT) to analysis the instantaneous signals during the milling process. STFT is a form of Fourier transform used to analysis the frequency and amplitude of a signal as it changes over time [SEJ 09]. Hence short time Fourier transform is

well-suited to producing a moving spectrum of speed during the milling operation. To achieve a useful resolution of STFT, a once per revolution sampling strategy (OPRS) strategy was employed.

To analyse a signal using STFT, requires the specification of a sampling frequency. The length of the data set, and the overall sampling frequency sets the resulting resolution of the spectrum. As an example, if the sampling frequency is at 25 kHz, and the data length at 2048 points, then the resolution of the frequency is 25 kHz/2048 = 12.21 Hz per data point.

4.4.Simulation and results

To explore the speed disturbances which result from chatter, a simulation of a representative unstable cutting was performed. A particular focus is the frequency spectrum of the speed variation. In this first series of simulations, a 'perfect' speed signal was used, i.e. the continuous variable within the SIMULINK model that is used for all the mechanical elements. Representations of a system with a more realistic speed signal is described in later in this chapter. The simulations employed in this chapter use the same reference set of cutting parameters that used throughout this thesis, and which were shown previously in Table 1. In the first series of simulations, the low bandwidth speed controller (i.e. bandwidth of 314 rad/s) was used. This low-bandwidth speed controller was chosen as it is less likely to correct the higher frequency speed fluctuations caused by chatter and hence mask the signal of interest.

4.4.1. Low bandwidth speed controller

The first simulation performed was for the operating point with a rotational speed of 3,000 rpm and a depth of cut of 14 mm, conditions that are known to give rise to chatter and instability with both an ideal speed stiff input and a standard speed controller. The speed demand profile consisted of a start from standstill, acceleration up to the demand speed of 3,000 rpm, followed by engagement of the tool with work-piece at 0.5 sec. The simulation was then run for a further

2.5 sec to allow sufficient time for the chatter to fully develop. Figure 83 shows the variation in the rotational speed during the simulation. The initial ramp up from standstill to the set-point results in a small overshoot which settles. When the tool engages, there is an abrupt drop in speed which the speed controller gradually corrects over ~0.4 sec. Also, apparent in the speed profile is a gradual growth in the speed variation, which is indicative of chatter. However, it is useful to note that the magnitude of this speed variation is smaller than the disturbance which occurs when the tool engages with the work-piece and hence simply measuring deviations from the demand speed is unlikely to provide a robust indication of chatter.

At this speed, the tooth passing frequency is 200 Hz. Figure 84 shows the speed variation during the interval 2.00 sec to 2.02 sec. The dominant variation in speed is at the tooth passing frequency of 200 Hz, with some smaller variations at higher frequency. In the speed variation in the later interval between 2.5 sec and 2.52 sec which is shown in Figure 85, this 200 Hz variation is still very evident but the influence of the higher frequency variation from the growing chatter are more apparent.

The corresponding variation if the electromagnetic torque produced by the machine is shown in Figure 86. As will be apparent, there is a much greater change in the electromagnetic torque required to regulate the speed than a change in speed. However, the direct measurement of torque is both challenging and likely to require significant modification to the mechanical structure of the machine. There is an option to monitor the trend in the q-axis current, which would simply be a scaled version the torque waveform. Almost all power converters, at least those that have current control capability, have some form of built-in current sensor and hence establishing q-axis current from measured phase currents is straightforward. However, tracking the magnitude of the q-axis current may not be a robust indicator of chatter under all conditions since for example, a change in cutting depth.

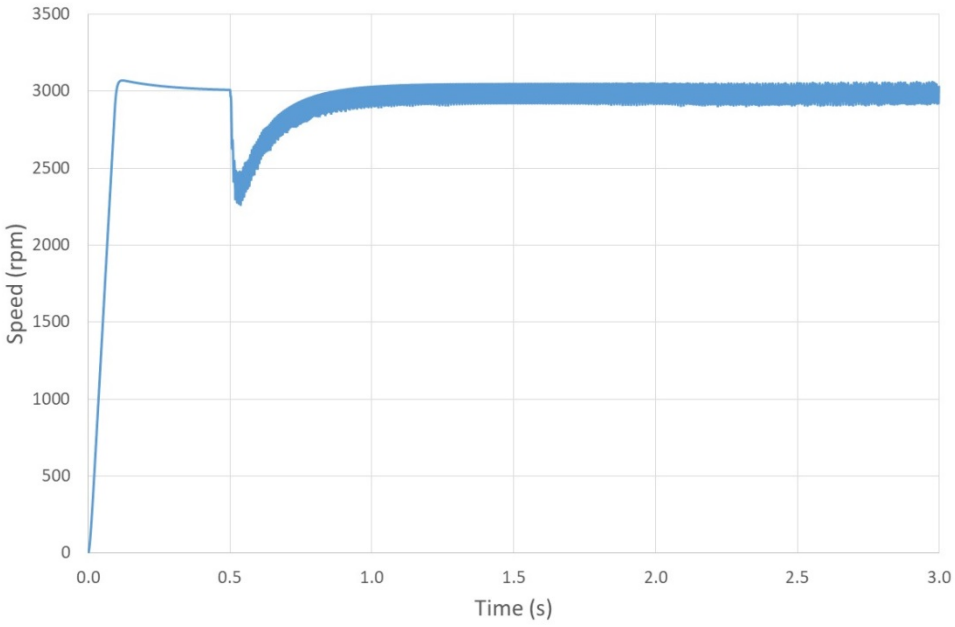

Figure 83 Predicted speed variation during simulation for a cutting depth of 14 mm at a nominal demand set-point of 3000 rpm with a 314 rad/s bandwidth speed controller (tool and cutting parameters as Table 1)

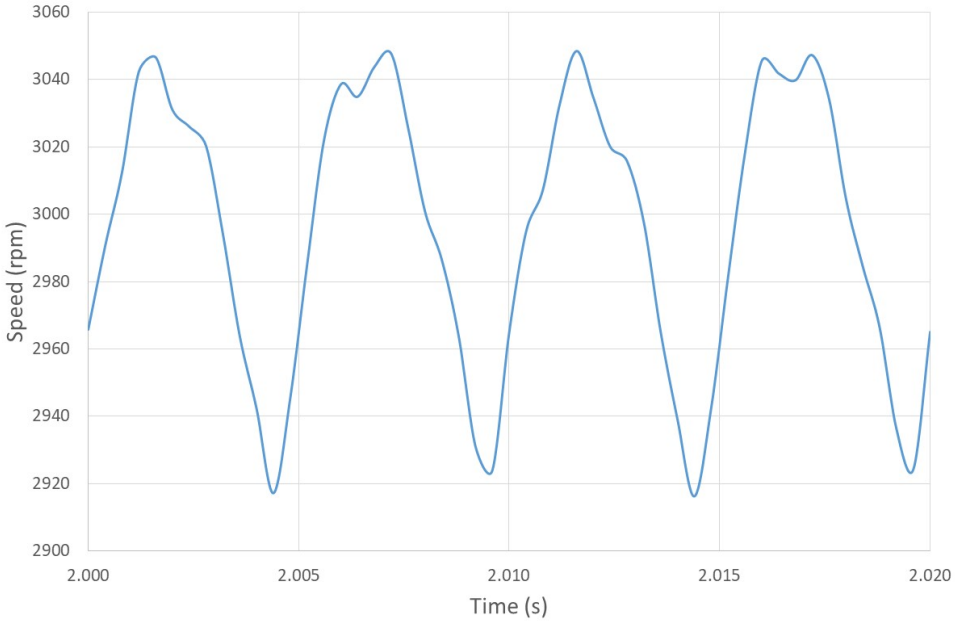

Figure 84 Close up view of interval between 2.0 sec and 2.02 sec

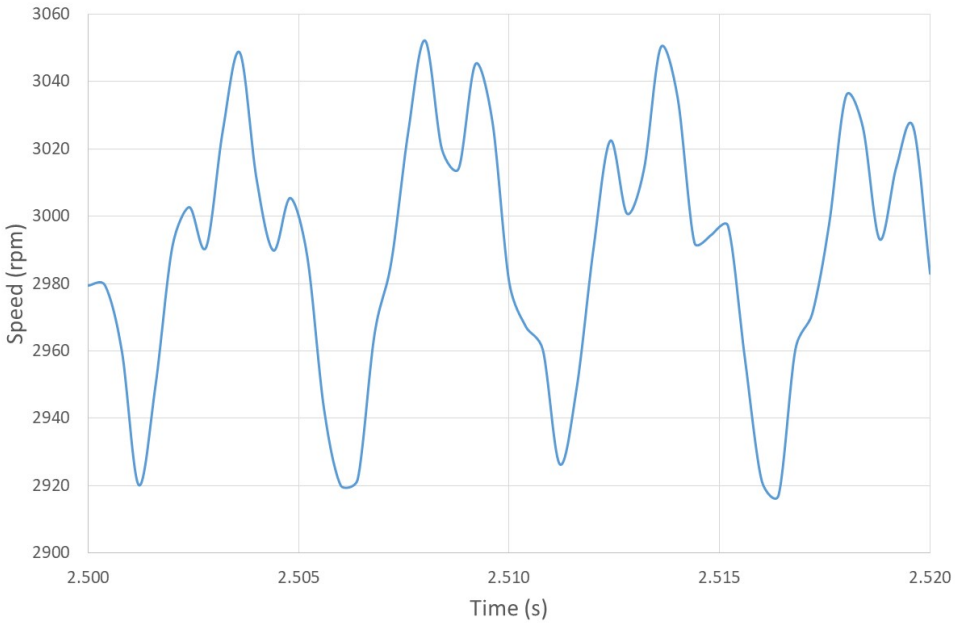

Figure 85 Close up view of interval between 2.50 sec and 2.52 sec

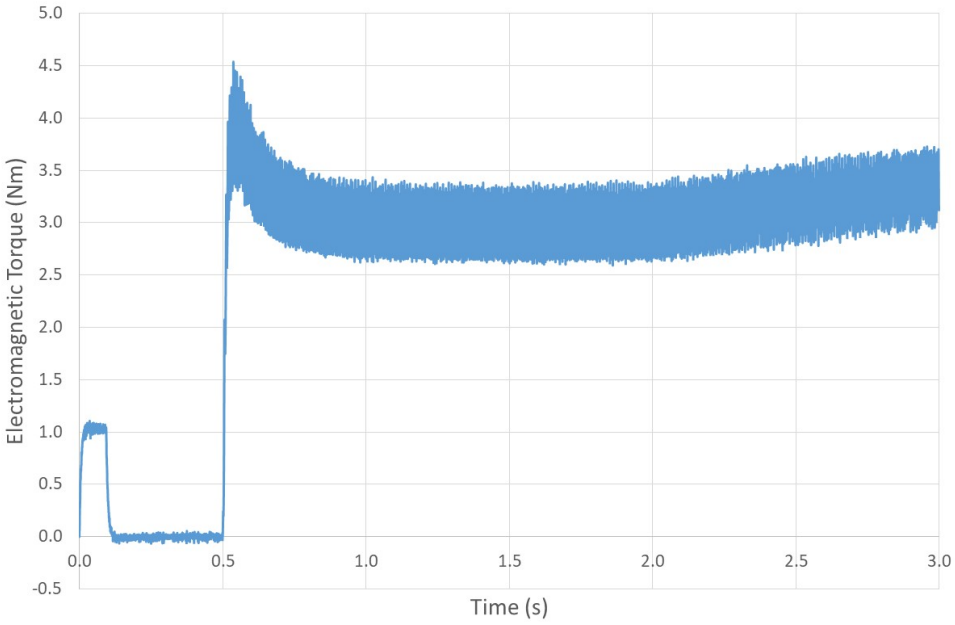

Figure 86 Predicted electromagnetic torque variation during simulation for a cutting depth of 14 mm at a nominal speed set-point of 3000 rpm with a low bandwidth speed controller (314 rad/s) -tool and cutting parameters as Table 1

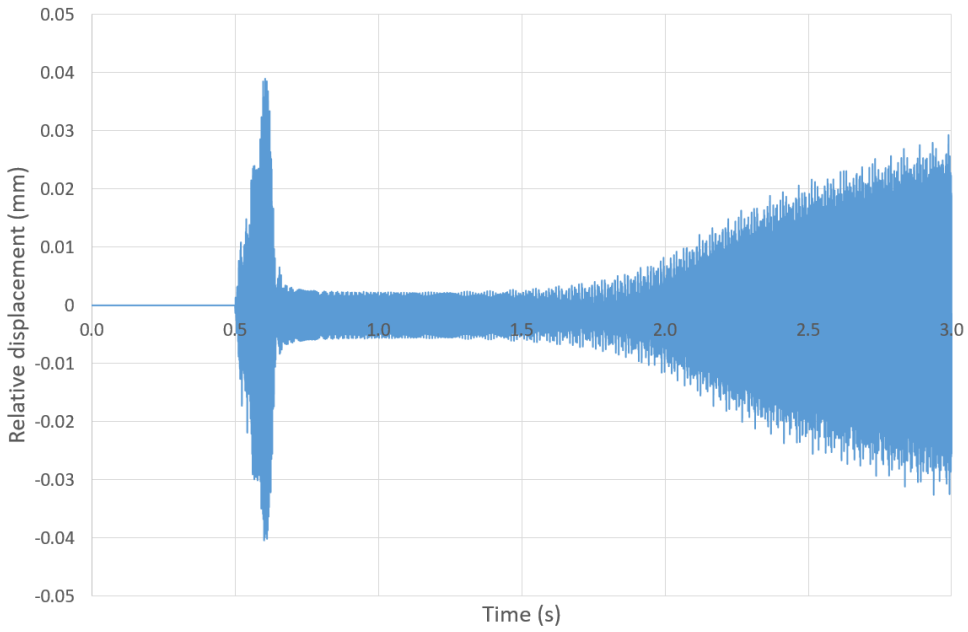

Figure 87 Predicted displacement in the direction of feed for a cutting depth of 14 mm at a nominal speed set-point of 3000 rpm with a low bandwidth speed controller (314 rad/s) - tool and cutting parameters as Table 1

In order to explore the information with the measured speed signal, a Fourier analysis was employed, more specifically an STFT method which was introduced earlier in this chapter. In chapter 3, it was noted that the typical time taken for chatter to build up is at least 5 to 10 tooth passes. Figure 88 shows the time evolution of a STFT of the speed over time. There is an initial low frequency component which relates to the dip in speed which occurs as the tool first engages with the work-piece.

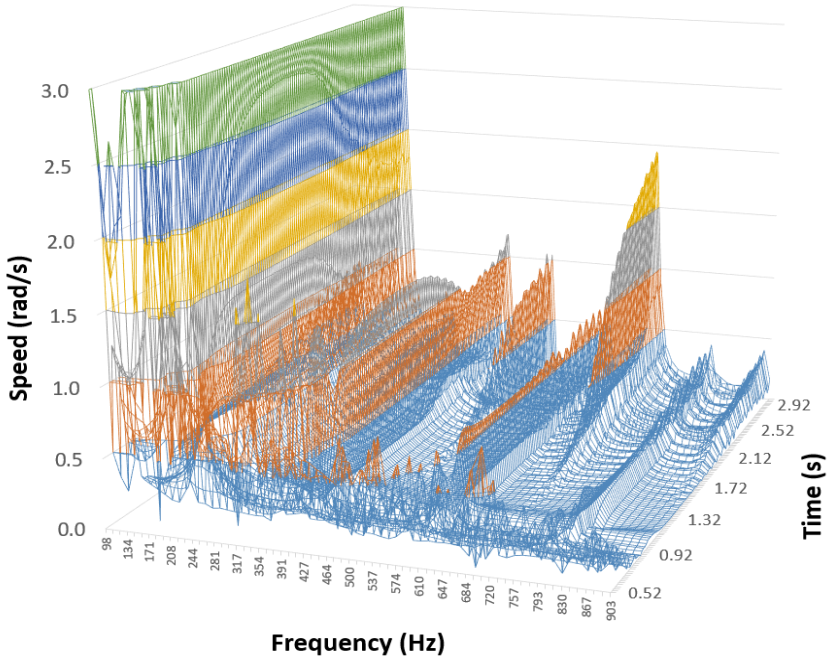

Figure 88 Evolution of the short-time Fourier transform of the speed - cutting depth of 14 mm at a nominal speed set-point of 3000 rpm (tool and cutting parameters as Table 1)

As will be apparent, when the tool is cutting, and the initial speed dip has been recovered, i.e. after 1 sec or so, there are several notable harmonics. These harmonics are summarised in Table 10. As will be apparent, the most significant harmonic in terms of magnitude is associated with the tooth passing frequency and the impact of the straight edged-tool with the work-piece.

The key to detecting of chatter is a reliable method for identifying from the STFT spectrum the main chatter frequency and detecting that it is growing in magnitude. In order to assess whether there is any variation in chatter frequency with rotational speed, a series of simulations was undertaken for a series of speeds between 3,000 rpm and 10,000 rpm. For each speed, it was necessary to use a depth of cut that resulted in chatter. This selection was undertaken using the SLD for these cutting conditions shown previously in Figure 31. In two cases (4,000 rpm and 6,000 rpm) the depth of cut required to ensure chatter is much greater than the depth of the cutting tool, would require a torque that is greater than the capability of the machine and a

voltage that is higher than the maximum converter. Hence, chatter at these speeds could not be initiated within the constraints of the system.

Table 9 shows the chatter frequency identified from the resulting STFTs for the remaining speeds, with a frequency resolution of 12.2 Hz. As shown Table 1, the chatter frequency (underlined) remains more or less constant over this range of speeds.

Table 9 Influence of rotational speed on chatter frequency for low bandwidth speed controller (cutting parameters as per Table 1). Main chatter frequency underlined.

Rotational speed (rpm)	Depth of cut simulated* (mm)	Nominal tooth passing frequency (Hz)	Components in spectra (Hz)	
			Tooth passing and multiples (Hz)	Others
3,000	14	200	195, 403, 598	98, 293, 488, <u>684</u>
4,000	38	Depth of cut required exceeds system capability		
5,000	7	333	330, 659	73♦,366, <u>696</u>
6,000	93	Depth of cut required exceeds system capability		
7,000	20	467	476	232, <u>671</u>
8,000	8	533	537	171, <u>696</u>
9,000	8	600	598	110,<u>696</u>
10,000	14	667	659	37,<u>696</u>

*** Selected to ensure unstable cutting - values greater than 20 mm exceed tool depth**
♦- Magnitude only 0.43 rad/s.

For speeds above 6,000 rpm there are only three components which exceed the threshold of a magnitude of 0.5 rad/s or at the time where the regenerative effect is fully developed. Taking 8,000 rpm as an example, and recalling that the exact frequencies have a resolution of ±12 Hz, the following components are present in the STFT:

- A component that matches to the tooth passing frequency of 533 Hz.

- A large and growing component at 696 Hz which corresponds to the main chatter frequency
- A component at 171 Hz that corresponds to the difference between the chatter frequency and the tooth passing frequency, i.e. 696 Hz – 533 Hz.

This pattern repeats for all the speeds from 7,000 rpm upwards. In cases, where only three harmonics that follow this pattern are present, the identification of chatter is straightforward. However, it is important to note that the robust setting of the threshold to 0.5 rad/s on an a-priori basis may be problematic.

In the cases of speeds below 6,000 rpm there are additional components which exceed the selected threshold of a magnitude of 0.5 rad/s, with the greatest number of harmonics at 3,000-rpm. Table 10 shows the magnitude of the various harmonics from which it is apparent that the three largest components correspond to the pattern observed for speeds of 6,000 rpm and above, i.e. the tooth passing frequency, the main chatter frequency a and a frequency which corresponds to the difference between these two frequencies. Of the remaining components, 403 Hz and 598 Hz are multiples of the tooth passing frequencies, which could be readily screened out. The remaining components correspond to the frequency difference between the main chatter frequency and the multiples of the tooth passing frequency, i.e. 98 Hz ≈ 684 Hz – 98 Hz, 293 Hz ≈ 684 Hz – 403 Hz and 488 Hz ≈ 684 Hz -195 Hz. In the case of 5,000 rpm, there is a component at 73 Hz which more or less satisfies the pattern, but this had not reached 0.5 rad/s threshold.

Table 10 Summary of harmonics in STFT of 3000 rpm with a magnitude greater than 0.5 rad/s at a time of 2.7 sec

Frequency component (Hz)	Magnitude (rad/s) at t=2.0 sec	Magnitude (rad/s) at t=2.7 sec
98	0.16	0.50
195	4.7	4.05
293	0.25	0.5
403	1.26	1.01
488	0.35	0.93
598	0.61	0.58
684	0.5	1.69

These findings are consistent with those reported by Insperger et al [INS 03] who investigated the origin of the multiple frequencies present during chatter. This demonstrated the strong link between tooth pass frequency harmonics and chatter frequency.

4.4.2. High bandwidth speed control

The same condition of 3000 rpm and a 14 mm deep cut was simulated with a high bandwidth speed controller (50,000 rad/s). It would be expected that the higher bandwidth controller is more effective in counteracting the speed variations at chatter frequency, hence masking out the signal that would is useful for monitoring the onset of chatter. However, it is important to recognise that the speed controller bandwidth is not the only factor that dictates how well the speed is controlled in response to high frequency speed fluctuations. The machine has a torque limit dictated by thermal limitations and is likely to be implemented as a hard-instantaneous torque limit. In addition, the controller could also saturate when the converter output voltage reaches its maximum limit.

The variation in speed and electromagnetic torque from the start of the simulation are shown in Figure 89 and Figure 90 respectively. As will be apparent from the gradual increase in the speed variation and the significant increase in the electromagnetic torque (which at some instants hits the torque limit). However, as would be expected, the much higher bandwidth of the speed controller reduces the speed error significantly as shown in the STFT of Figure 92, which is plotted on the same vertical scaling as the corresponding STFT for the low bandwidth speed controller. Although there is some evidence of a chatter signature at ~680 Hz, this is not sufficiently pronounced to be a reliable indicator of chatter.

However, the control action applied by the speed controller to counteract the speed variation provides a useful indicator of chatter. Figure 93 shows the STFT of the torque output of the speed controller that provides the demand for the PI current controller. As shown, there is a much more pronounced signal at the chatter frequency which could be tracked in the same manner at the speed error was for the low bandwidth speed controller.

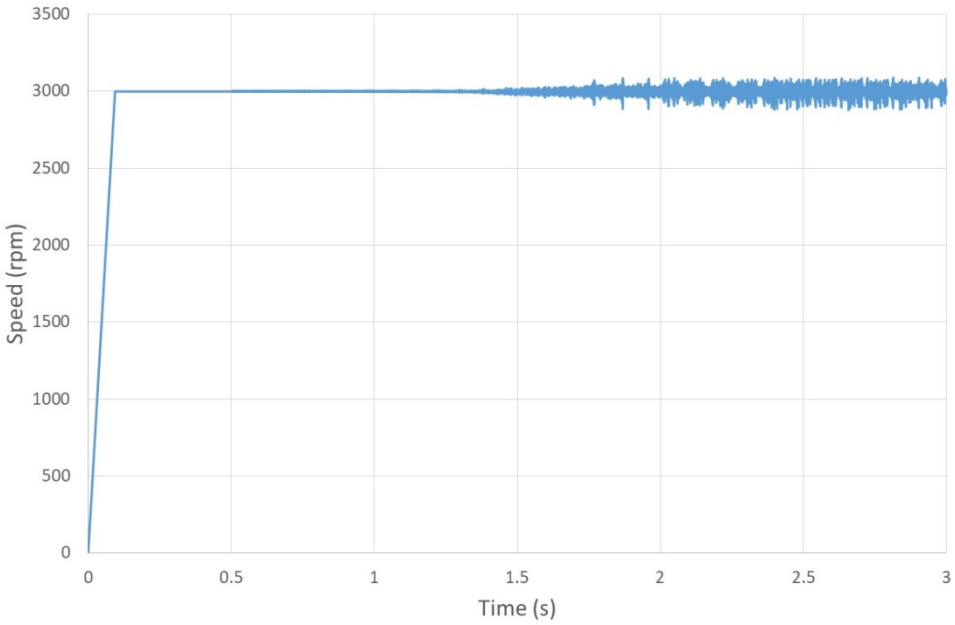

Figure 89 Predicted speed variation during simulation for a cutting depth of 14 mm at a nominal demand set-point of 3000 rpm with a 50,000 rad/s bandwidth speed controller -tool and cutting parameters as Table 1

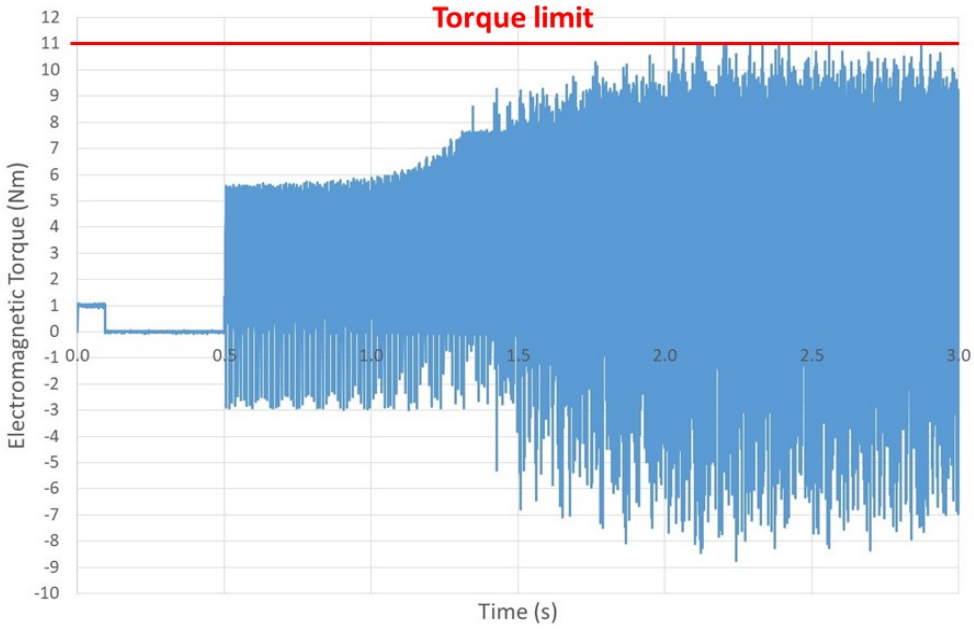

Figure 90 Predicted electromagnetic torque variation during simulation for a cutting depth of 14 mm at a nominal speed set-point of 3000 rpm with a high bandwidth speed controller (50,000 rad/s) - tool and cutting parameters as Table 1

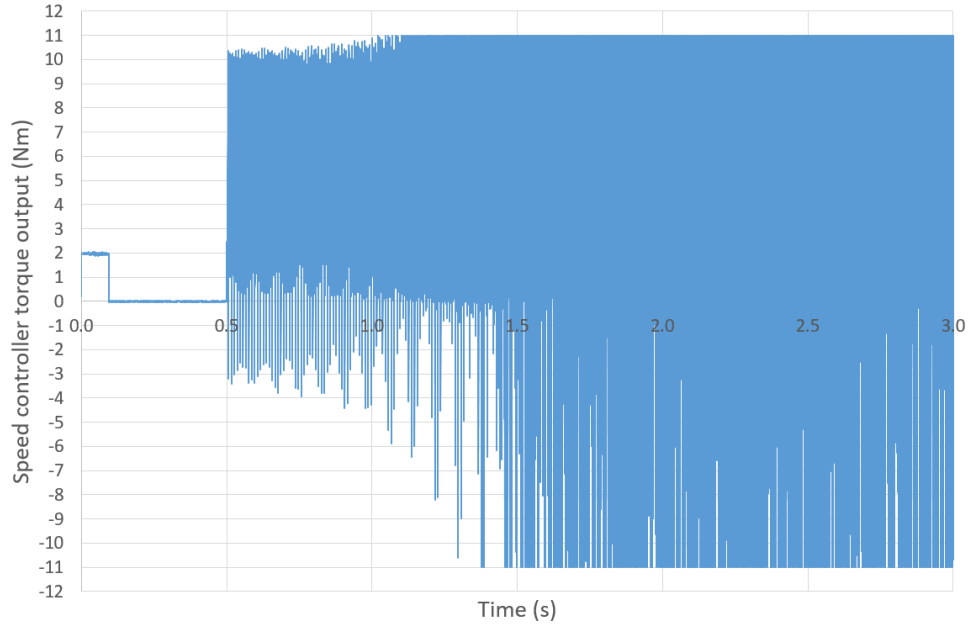

Figure 91 Predicted speed controller output torque (hard torque limited to 11 Nm) during simulation for a cutting depth of 14 mm at a nominal speed set-point of 3000 rpm with a high bandwidth speed controller (50,000 rad/s) - tool and cutting parameters as Table 1

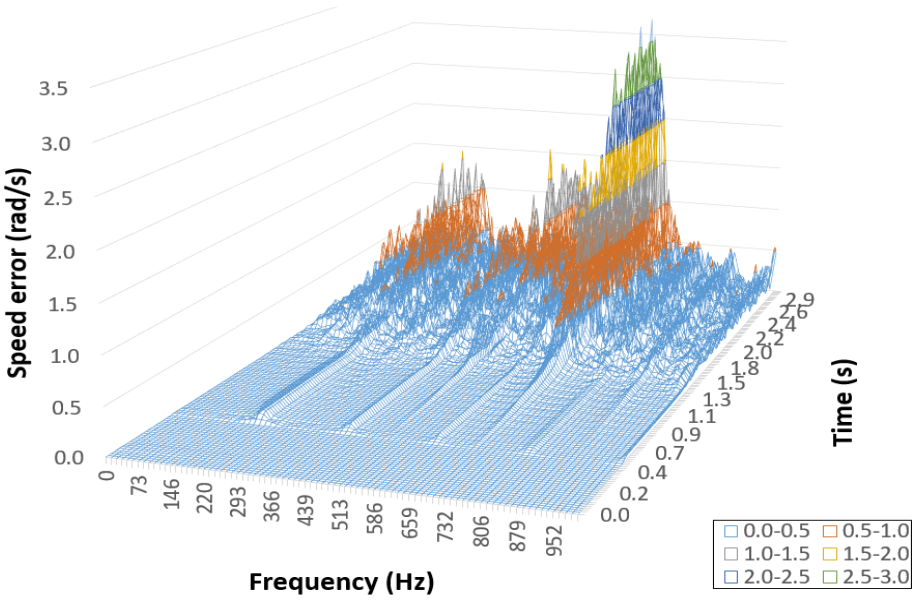

Figure 92 STFT of the speed error signal for a cutting depth of 14 mm at a nominal speed set-point of 3000 rpm with a high bandwidth speed controller (50,000 rad/s) - tool and cutting parameters as Table 1 (Note: Plotted on the same vertical scale as the corresponding STFT for the low bandwidth speed controller)

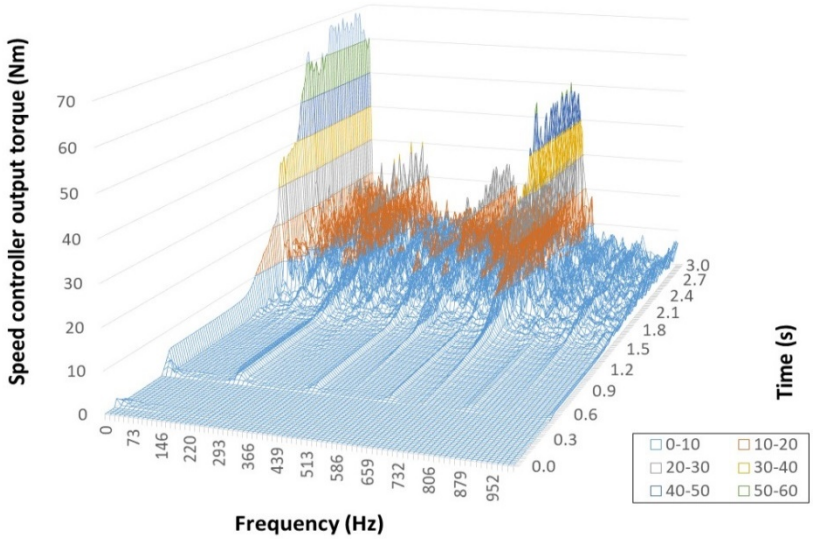

Figure 93 Predicted variation in time of the STFT of the speed controller output torque demand for the current controller for a cutting depth of 14 mm at a nominal speed set-point of 3000 rpm with a high bandwidth speed controller (50,000 rad/s) - tool and cutting parameters as Table 1

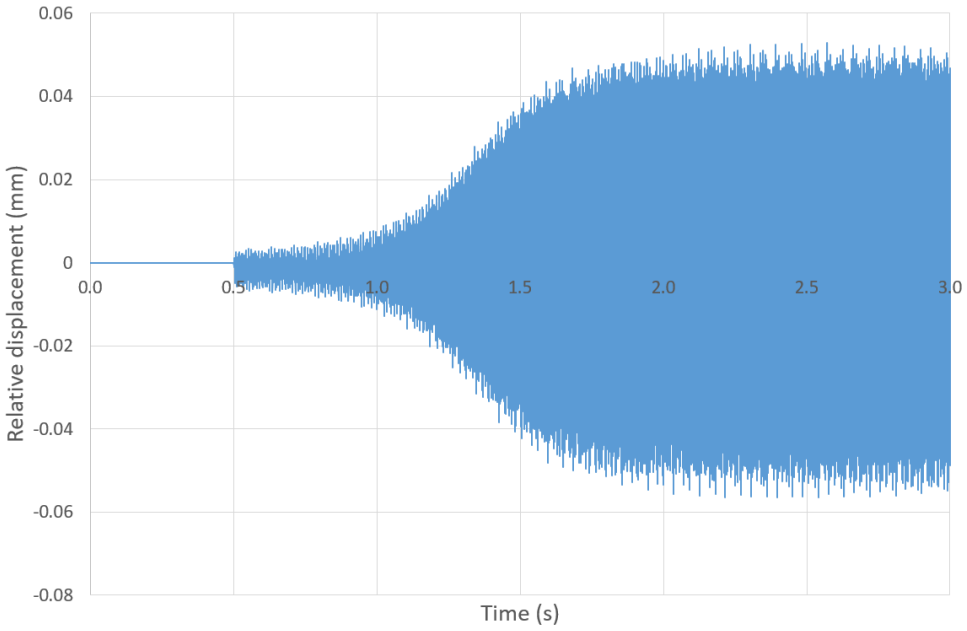

Figure 94 Predicted displacement in the direction of feed for a cutting depth of 14 mm at a nominal speed set-point of 3000 rpm with a high bandwidth speed controller (50,000 rad/s) - tool and cutting parameters as Table 1

4.5. Implementation of chatter detection with practical encoders

As demonstrated previously in this chapter, a precise measurement of speed offers the potential to detect chatter from speed fluctuations. However, the simulations presented up to this point have been based on access to a continuous and 'perfect' speed variable within the SIMULINK model. In any practical implementation, the speed signal from which chatter would be detected would need to be provided by a speed sensor. In principle, so-called 'sensor-less' position / speed estimation strategies could be used, but the accuracy and uncertainty in such methods are unlikely to meet the exacting requirements for chatter detection, e.g. the speed variations are typically of the order of 0.1% of the overall speed. The following sections consider the feasibility of detecting chatter from practically realisable speed measurements. The performance requirements for a speed sensor and the associated signal processing requirements are

established and a model is developed and deployed to establish the performance that is likely to be achieved.

Many high performance electrical machines, including many of those used for high speed CNC machines are equipped with digital rotatory encoders or analogue resolvers to provide a measure of rotational speed/or and position. These measurements are used in closed loop speed and/or position control systems.

4.5.1. Analogue resolver

Resolvers are rotary electrical device that can be used to measure the speed of rotation. Resolvers are electromagnetic devices that outputs analogue signal to indicate rotation and are capable of absolute positions measurement. The most widely used analogue resolver are to so-called brushless transmitter resolvers. The major difference in configurations of the wires is that the brushless transmitter resolver two sets of windings: an exciter winding and two sets of two phase windings. The exciting winding also referred as X winding, acts as a rotary transformer. Since there is no direct electrical connection, brushes are not required. This exciting winding is laid on the top. The other two sets of two phase winding also called Y windings laid on the bottom with 90^0 degrees phase difference. As the shaft rotates the two sets of winding, generates sine signal and a cosine signal.

The advantage of resolver is that it can provides very high resolution and accurate analogue signal. One of the most important specifications for a resolver is number of sinusoidal cycles in one revolution. Due to the nature of the structure of the resolvers, the number of cycles is limited by the sizes of the device. Due to the simple structure, robustness and reliability, resolvers are popular for harsh environments. However, the analogue nature of the output signal tends to limit their application in servo control area. Despite some useful features, resolvers were not selected as the speed measurement device in this thesis.

4.5.2. Digital angular position and speed encoders

There two major types of digital rotatory encoders, absolute and incremental. Absolute encoders, which can be magnetic or optical devices, employ multiple tracks and sensor arrays to provide position information immediately on powering up the device. They are complex and high cost devices which measure position directly to a resolution which is set by the number of tracks on the encoder.

Incremental encoders only measure changes in positions, but when equipped with a once per revolution reset pulse, position can be inferred from counting pulses from the reset reference position. Incremental encoders are lower cost devices with more straightforward conditioning electronics and hence as by far the most common type of encoder used in drive systems. Incremental angular position encoders which produce a stream of digital pulses with rotation can be used to indirectly measure speed. In principle, the accuracy of the speed measurement is reliant only on the precision with which the encoder disk and sensing element is manufactured, i.e. the repeatability of the pulse intervals, and the precision to which the pulse edges can be detected.

The mechanical error, also referred as pulse width error, is one factor that can influence of the accuracy of position measurement. An error of $\pm\varepsilon$ in angular degrees between successive pulses will set a limit on the accuracy by which speed can be measured, unless some elaborate calibration is performed.

The vast majority of general purpose incremental encoders have two output channels in addition to a once per revolution reset signal. The two channels, which are often referred to as channel A and B, are configured to be in quadrature with respect to each other as shown in Figure 95. This provides a mechanism to detect rotation. Since each pulse represents a defined angle of rotation (subject to a tolerance) an estimate of the shaft speed can be obtained by either counting the

number of pulses within a defined interval or by measuring the time between successive rising or falling edges.

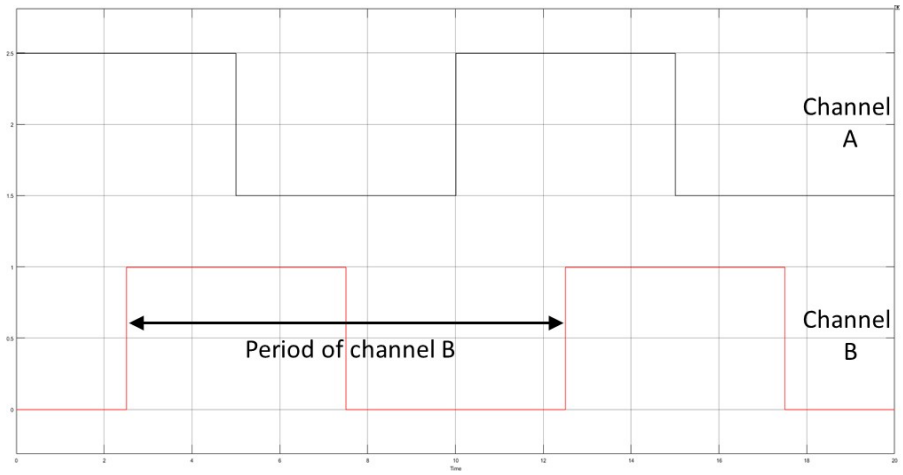

Figure 95 Typical incremental encoder channel outputs

The pulse stream generated by an incremental encoder is often processed by dedicated hardware within in microcontrollers or DSPs. Many modern or Digital Signal Processors (DSPs) which are tailored for motion control applications incorporate dedicated circuitry for encoder inputs, which is usually referred to as a Quadrature Encoder Interface (QEI). The QEI has dedicated high speed electronics for reading and decoding the signal from incremental encoder. The key element of the QEI for this chapter is its capability for precise time-stamping of the rising and falling edges of the encoder signal. This process runs independently from the main control loop in the DSP (which may only be running on a cycle in tens of microseconds). By way of example, the QEI on a DSPTI320f28335 samples the input channel at 100 MHz. Whereas the rising and falling edges can be time-stamped to a high resolution and hence provide a precise estimate of average rotational speed between successive edges, this method does limit the rate at which speed can be updated.

For a two-channel encoder with N_p pulses per channel per mechanical revolution, a new estimate of speed can be derived four times within one period, e.g. from the time difference between the

rising edge of channel B and the falling edge of channel A as shown previously in Figure 95. The rate at which speed estimates can therefore be updated (f_u) is limited by the number of pulses per revolution and the rotation angular frequency ω_r according to:

$$f_u = \frac{4N_p\omega_r}{2\pi} \qquad (4\text{-}7)$$

By way of an example, for a 1000 pulse per revolution encoder, rotating at 4000 rpm (equivalent to 418.9 rad/s) estimates of speed are available at a rate of 266 kHz, which corresponds to an update every 3.75 µs.

This section will focus on what are the requirements of QEI and encoder to detect the often very small speed fluctuation caused by chatter in high speed milling process. The challenge can be illustrated by considering the cases considered earlier in chapter. In these cases, the speed errors were of interest were of the order of 0.5 rad/s extracted from a speed of 942 rad/s at 9,000 rpm.

Encoders are often specified in terms of lines (per revolution). In terms of the waveforms shown previously in Figure 95, this can also be expressed in terms of pulses per revolution. The input frequency on any given channel is given by 1/period of pulse as defined in Figure 95.

The frequency of the square wave output signals on channels A and B are proportional to the rotational speed of the shaft. For an encoder with N_{ep} pulses per revolution on a motor rotating at S_{rpm} revolutions per minute (rpm), the input frequency on each encoder channels is given by:

$$f_{ech} = \frac{S_{rpm}}{60} \times N_{ep} \qquad (4\text{-}8)$$

There are two possible sources of error in deriving rotational velocity from a time-stamped encoder pulse train:

- Any intrinsic mechanical errors in the manufacture of the encoder disk or sensor position, which will result in variations in the angular distance between successive rising edges of the detector. If rotational velocity is to be derived from rising edges only, then there is no requirement for an exact 50:50 pulse train. In the following analysis the maximum deviation in rising edge to rising edge angular displacement is δ.
- Resolution of the time stamping capability of the QEI. If the pulse train is sampled (time-stamped) at a sampling frequency, then the error introduced by time stamping resolution lies in the range:

$$\epsilon = [0, \frac{f_{ech}}{f_{QEI}}] \qquad (4\text{-}9)$$

Since the incremental encoder is a position sensor, estimating velocity can be achieved by following two first order approximations:

The average angular velocity between two timed events (e.g between successive rising edges on a channel or between some integer multiple of rising edges) is given simple by:

$$\dot{\theta}(\tau) \approx (\theta(\tau) - \theta(\tau - 1))f_{ech}$$

The error in the inferred angular velocity due to mechanical tolerance in the encoder disk is:

$$Error\ in\ \dot{\theta}(\tau) \approx \pm\delta f_{ech}$$

The uncertainty in the inferred angular velocity is:

$$Uncertainty\ in\ \dot{\theta}(\tau) \approx \pm\frac{f_{ech}\,\dot{\theta}(\tau)}{f_{QEI}} \qquad (4\text{-}10)$$

For the studies considered in this chapter, a 100 MHz QEI interface was selected. This is representative of a mainstream motion control DSP. The various trade-offs in the performance at 3,000 rpm of encoders with different number of pulses per revolution are summarised in Table

11. The encoder pulsed output frequency gives an indication of the rate at which speed estimates are available. The uncertainty in the speed with no encoder pulse tolerance (i.e. $\delta=0$) and with a 0.01% error are shown. As will be apparent, increasing the number of encoder pulses per revolution increases the rate at which estimates of speed are available, but the uncertainty in the speed estimate increases with encoder pulse number.

Table 11 Variation in speed update rate and speed uncertainty with the number of encoder pulses per revolution (QEI sampling frequency 100 MHz in all cases)

Encoder Pulses per rev	Encoder pulsed output frequency @3000 rpm	speed uncertainty assuming $\delta=0$ and 4 kHz updating rate
20	1000	0.00400%
40	2000	0.00200%
60	3000	0.00133%
80	4000	0.00100%
100	5000	0.00080%
200	10000	0.00040%
300	15000	0.00027%
400	20000	0.00020%
500	25000	0.00016%
600	30000	0.00013%
700	35000	0.00011%
800	40000	0.00010%
900	45000	0.00009%
1000	50000	0.00008%

The results in Table 11 provide an indication of the achievable performance in speed measurement from a series of different encoders. The significance of the update frequency depends on the sampling frequency of the overall controller, i.e. the rate at which updated

measurements of speed can be usefully used. If the speed is sampled once every cycle of time of the main control loop, then any intermediate values of speed are of no value, particularly as they are obtained at the expense of greater uncertainty in the speed measurement.

4.6. Encoder model

The SIMULINK model shown in Figure 96 was developed in order to represent the behaviour of a practical encoder for measuring rotational speed. The main elements in the encoder model are:

- A zero-order hold block which is set to have a sampling time which corresponds to the update frequency, f_u, calculated previously. Strictly, this update frequency varies with the rotational speed of the machine, but for the purposes of this study, the update frequency was fixed at a value which corresponds to the nominal steady-state operating speed.
- A random generator block with a maximum output of ±1 that is clocked at f_u, which is then scaled by the fractional uncertainty calculated in Table 11 for the combination of QEI sampling frequency, encoder pulse number and rotational speed. This fractional uncertainty is then added to the continuous input signal to provide a representation of the effect of uncertainty. It is recognised that this uncertainty is not a random process, but the very high QEI sampling rate precludes it being implemented in the model in a rigorous manner. This random approach to add in uncertainty into the model is based on an even distribution of uncertainties.

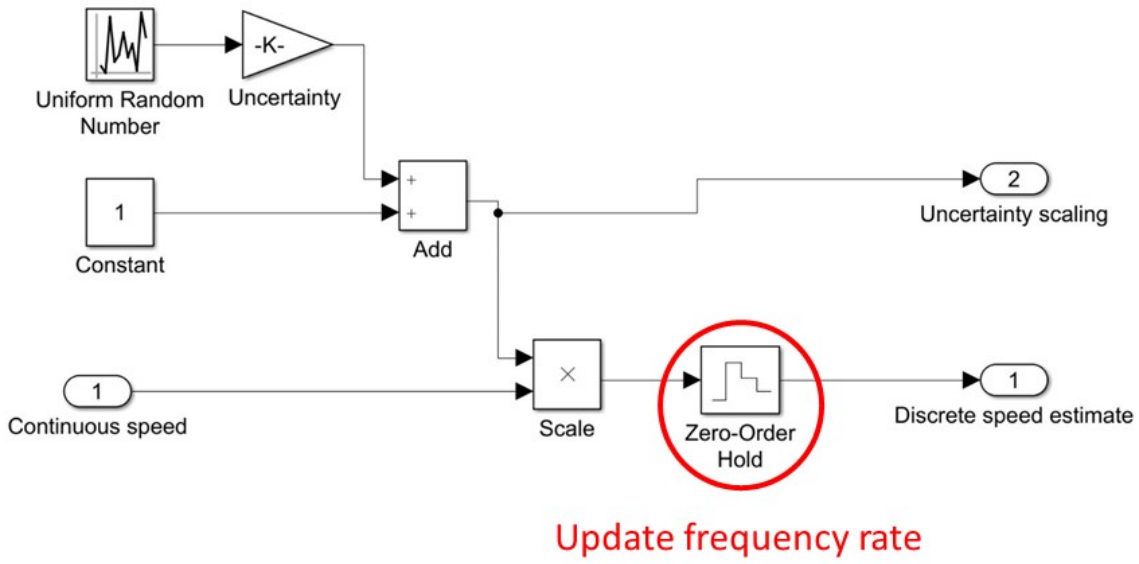

Figure 96 Encoder block diagram

It is important to note that there will be an additional zero-order hold present at the input of the controller to represent the rate at which the controller samples the speed signal and that this sampling frequency may be the limiting factor on the ability of the system to measure precisely small fluctuations in speed.

The basic operation of this model can be illustrated by considering the case of a rotational speed of 3,000 rpm with a depth of cut of 14 mm in which the main system controller is operating at 5 kHz (i.e. a cycle time of 200 μs). Figure 97 and Figure 98 show 5 kHz sampled speed signals for the same cutting conditions for 100 and 1000 pulse per revolution encoders respectively. As will be apparent, the 5 kHz sampling frequency is by the far the dominant factor and in this case, and the reduced uncertainty associated with a 100 pulse per revolution encoder is likely to yield the better performance at this combination of rotational speed and sampling frequency.

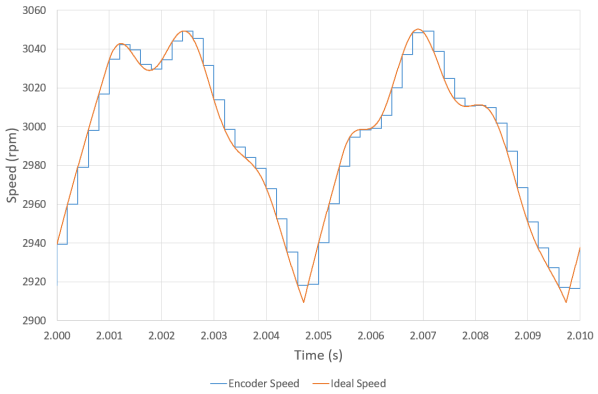

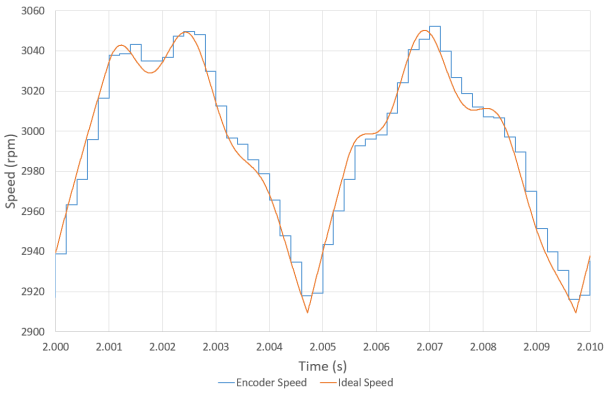

100 pulse per revolution 1000 pulse per revolution

Figure 97 Comparison between ideal speed signal and the signal generated for 100 and 1000 pulse per revolution encoders with a speed uncertainty of 0.02% and sampled at 5 kHz (3,000 rpm nominal demand set-point and 14 mm cut depth).

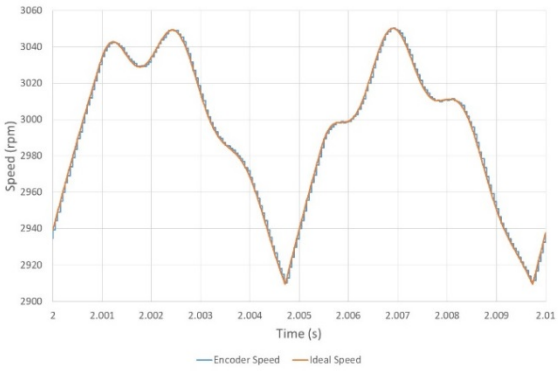

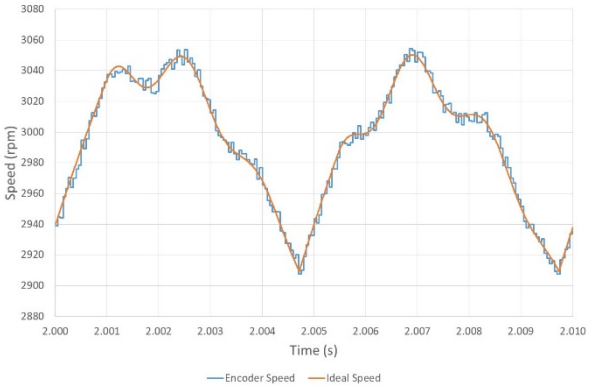

100 pulse per revolution 1000 pulse per revolution

Figure 98 Comparison between ideal speed signal and the signal generated by a 1000 pulse per revolution encoder with a speed uncertainty of 0.2% and sampled at 20 kHz (3,000 rpm nominal demand set-point and 14 mm cut depth).

4.7.Simulation and validation

In order to establish whether a representative incremental encoder can provide sufficiently precise speed information to detect the onset of chatter, a series of simulations were performed using the system model shown in Figure 99

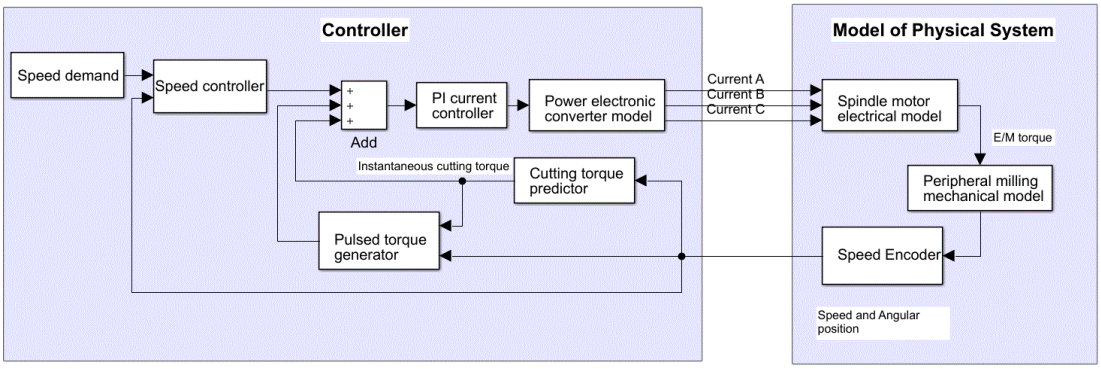

Figure 99 Block diagram of system model incorporating the encoder model

The cutting model was based on the parameters shown previously in Table 1. The specific operating point considered was a cutting depth of 14 mm, a rotational speed of 3,000 rpm and a feed rate of 0.05 mm/tooth which is equivalent to 10 mm/s at this rotational speed. Simulations were initially performed for a 1000 pulse per revolution encoder sampled for the generation of the STFT at frequencies of 5 kHz and 10 kHz. In all cases, the QEI was assumed to have a sampling rate of 100 MHz and the angular uncertainty in the spacing of the encoder pulses (δ) was set to 0.0036° (i.e. 0.001%). In every simulation, a low bandwidth (314 rad/s) speed controller was used. Figure 100 shows the resulting STFTs throughout the simulation for a controller sampling frequency of 5 kHz. Even this modest sampling frequency captures many of the features of the corresponding STFT for an ideal speed signal (shown previously in

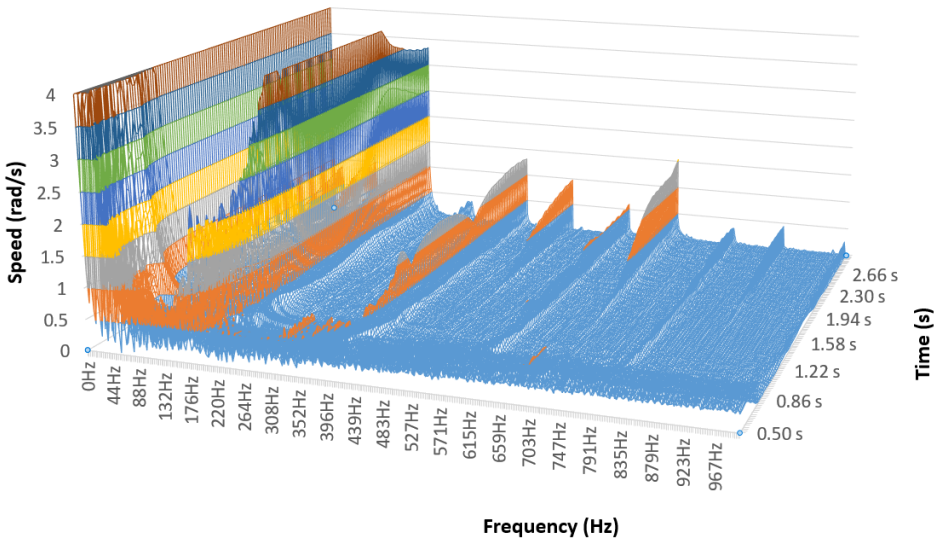

Figure 100 Evolution in the STFT from the point of tool engagement at 0.5 sec for a speed demand set-point of 3000 rpm and a depth of cut of 14 mm (1000 pulse per revolution encoder sampled at 5 kHz)

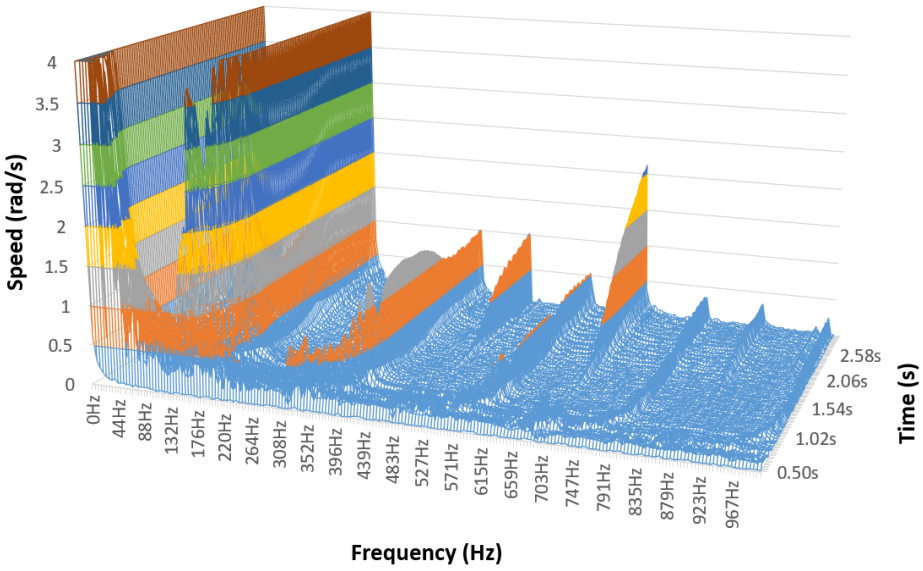

Figure 101 Evolution in the STFT from the point of tool engagement at 0.5 sec for a speed demand set-point of 3000 rpm and a depth of cut of 14 mm (1000 pulse per revolution encoder sampled at 10 kHz)

A useful summary of these results, which illustrates the influence of the main controller sampling rate is shown in Figure 102. This shows the magnitude of the different frequency components around the chatter frequency for both 100 and 1000 pulse per revolution encoders at different sampling frequencies. The magnitude quoted is for the STFT taken at 2 sec, which is near the beginning of the emergence of significant chatter. As will be apparent, the magnitude of the component which corresponds to chatter seems to increase with increased sampling frequency. Thjs is however in part due to the change in the frequency resolution of the STFT.

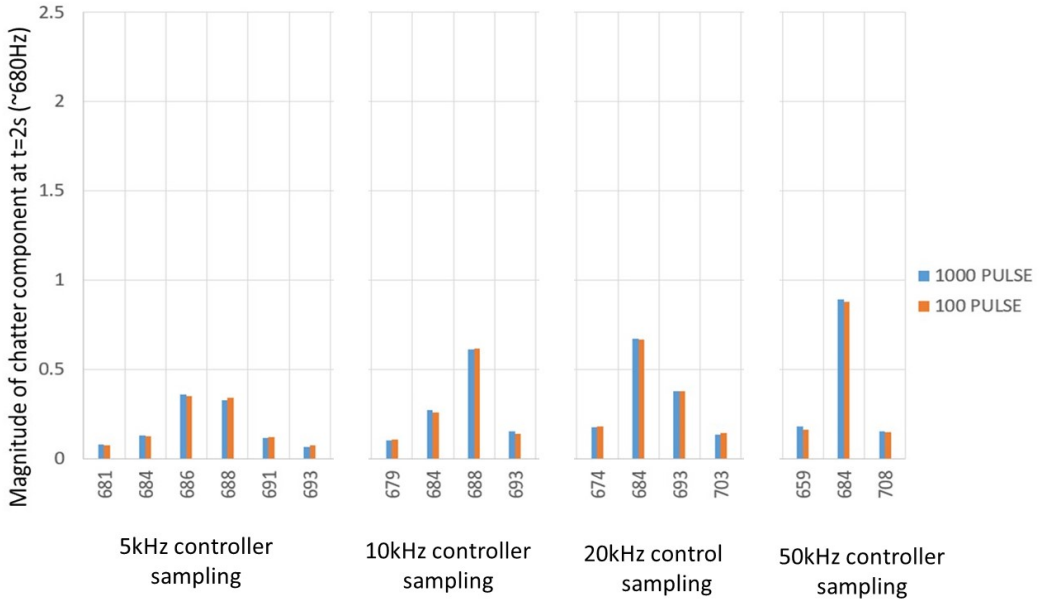

Figure 102 Series of spectra around 680 Hz for different controller sampling frequencies

4.8. Chatter identification algorithm

Although the results shown in demonstrate a well-defined and consistent chatter signature at the same frequency for a range of rotational speeds, the frequency of ~700 Hz is specific to the combination of cutting tool properties and other parameters listed in Table 1. Under different feed-rates of with a different tool and/or work-piece, this natural chatter frequency will vary and hence it is necessary to have a general method for identifying the chatter frequency.

The approach adopted and implemented in the simulations which will be reported in chapter 5 is based on a straightforward method of identifying component in the spectrum that exceed some threshold and then discarding these according some straightforward rules.

The algorithm used takes the following approach to identifying chatter, recognising that in practice, its frequency is not known on an a-priori basis:

- Set a threshold for the magnitude of a harmonic which makes it ‘significant’
- Identify all harmonics greater than the threshold
- Eliminate the tooth passing frequency and the associated direct multiples of the tooth passing frequency
- Use the remaining frequency components in combination with the tooth passing and multiples of tooth passing to identify a common frequency that fits the pattern identified in Figure 9 and check that this component is present and growing in magnitude.

The next chapter considers the use of this chatter detection algorithm in a sequence of machining operations.

Chapter 5 - Dynamic operation

5.1. Introduction

The preceding chapters have considered a series of monitoring and control strategies that can detect chatter and allow stable cutting to be maintained with combinations of rotational speed, depth of cut and feed rate that would cause chatter otherwise. This chapter considers the performance of the system controller that combines both monitoring and control functions that is capable of adapting the cutting conditions to main stability.

The system controller combines the speed error chatter detection method developed in chapter 4 with the rapid torque modulation method developed in chapter 3. This system configuration is suited to a low bandwidth speed controller in which the onset of chatter at ~700 Hz leads to speed variations that cannot be corrected to any significant degree by a low bandwidth speed controller. It is recognised that for a higher bandwidth speed controller, it may be necessary to make use of the speed controller torque demand signal to monitor chatter.

5.2. Simulation specification

Simulations were performed for rotational speeds of 3,000 rpm and 9,000 rpm. The 3,000 rpm case provides consistency with several of the cases considered in previous chapters. The SLD shown previously in Figure 31 indicates that there are stable operating regions on either side of this operating point, e.g. the full tool height of 20 mm can be used for speeds below ~2,700 rpm and above ~3,500 rpm. This in part suggests that this operating point is well suited to chatter correction using variable-speed milling or rapid torque modulation. Moreover, if the stability lobe diagram, which is established for one set of cutting parameters provides a reliable means of selecting the speed demand set-point then a small increase in the set-point to 3,500 rpm would result in much more stable cutting conditions.

The 7,500 rpm operating point provides a more challenging case since there is no speed above 7,500 rpm (at least within the maximum operating range of the motor) in which stable cutting can be achieved with the full cutting tool depth. Hence, speed fluctuations above 7,500 rpm will not enter regions of greatly improved stability as is the case for 3,000 rpm, although there is some increase in the critical cutting depth beyond ~9,500 rpm.

From a practical point of view, the 7,500 rpm case provides a more interesting case since the SLD of Figure 31 indicates that the inability to operate with stable cutting beyond 7,500 rpm with the full depth of the tool (20 mm) imposes a limit on material removal rate.

The system modelled for both speeds has a low bandwidth speed controller (314 rad/s) and a hard torque limit of 11 Nm. The various cutting parameters where set to the values shown previously in Table 1. The feed rate was fixed at 0.05m / tooth which corresponds to 10 mm/s and 30 mm/s for speeds of 3,000 rpm and 7,500 rpm respectively. The operation cycle for each speed involved the following sequence:

- Accelerate from standstill following a ramped speed demand up to the nominal speed.
- Maintain the demand speed with no cutting force up to 0.5 sec.
- At 0.5 sec the tool engages the work-piece at a cutting depth which is less than the critical cutting depth (10 mm for 3,000 rpm and 3 mm for 7,500 rpm).
- Continue cutting at this stable cutting up to 2 sec.
- Step change in the cutting depth to a value which exceeds the critical cutting depth (14 mm for 3,000 rpm and 10 mm for 7,500 rpm).
- Continued normal cutting until the chatter detection function identifies the onset of chatter
- Application of rapid torque modulation in order to restore stable cutting.

5.3.Simulation results at 3,000 rpm

Figure 103 shows the variation in rotational speed predicted when the machine is following the operating schedule defined in section 5.2 with a speed set-point of 3,000 rpm. Since speed control is provided by a low bandwidth speed controller, there are significant dips in speed at 0.5 sec when the tool engages the workpiece and at 2 sec when the depth of cut is increased from 10 mm to 14 mm. As the chatter starts to build up it is detected by the controller at ~3.4 sec and a series of 5 Nm pulses with a repetition rate of 12 tooth passing intervals is applied. This causes the significant increase in the speed fluctuations beyond 3.4 sec as shown in the close up of Figure 104. There is an initial transient associated with the introduction of the torque modulating pulses, but this is gradually corrected by the speed controller, bringing the speed back down so that the fluctuations are centered on 3000 rpm.

The variation in the electromagentic torque and the cutting tool reaction torque are shown in Figure 105 and rapid torque modulation signal shown in Figure 106, while the corresponding variation in the chip-thickness is shown in Figure 107. The displacement of the tool in the feed direction (i.e. the tool vibration) is shown in Figure 108

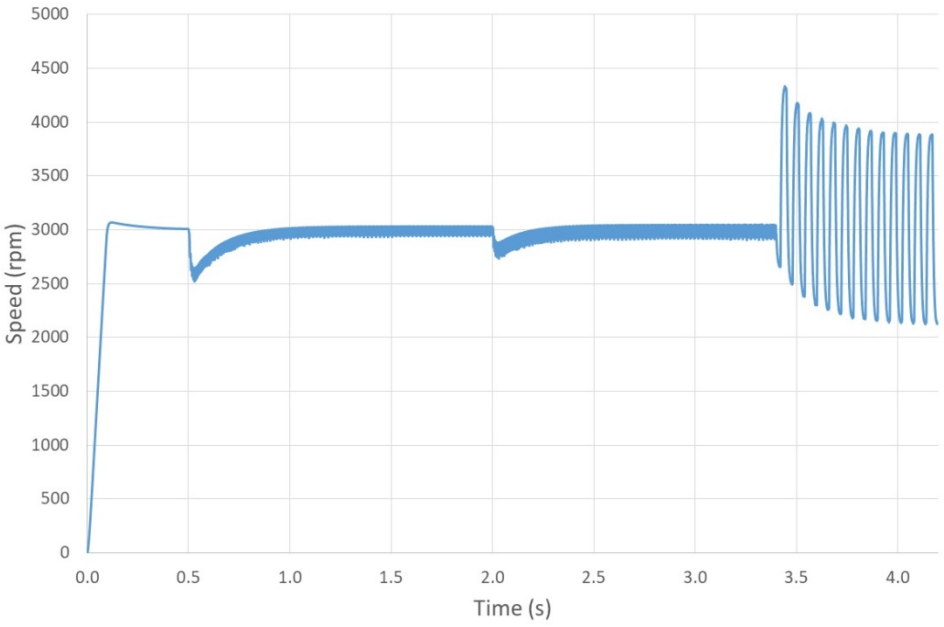

Figure 103 Simulated speed variation for a nominal speed of 3,000 rpm

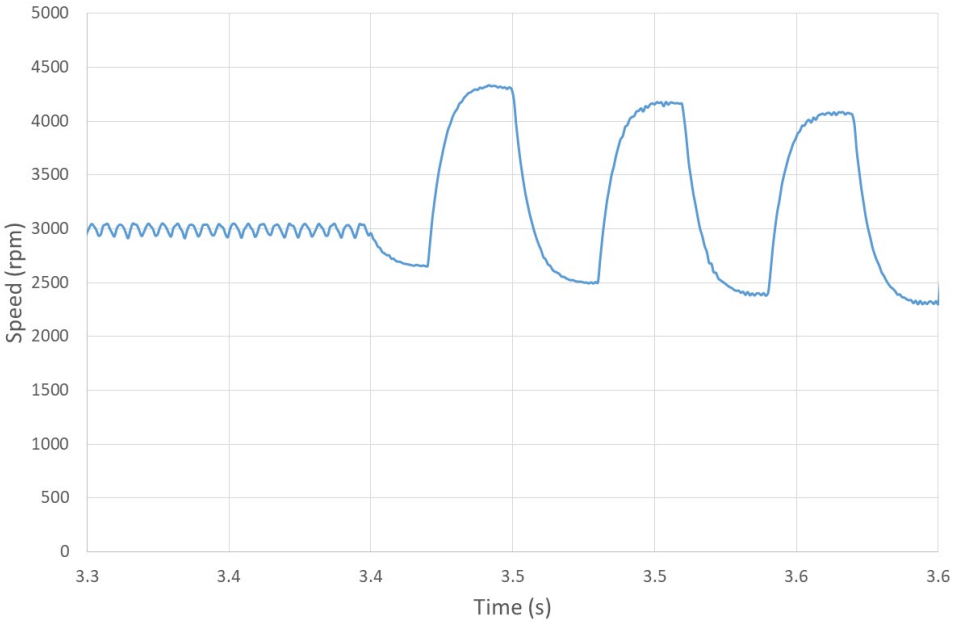

Figure 104 Close-up of the speed variation between 3.3 sec and 3.6 sec

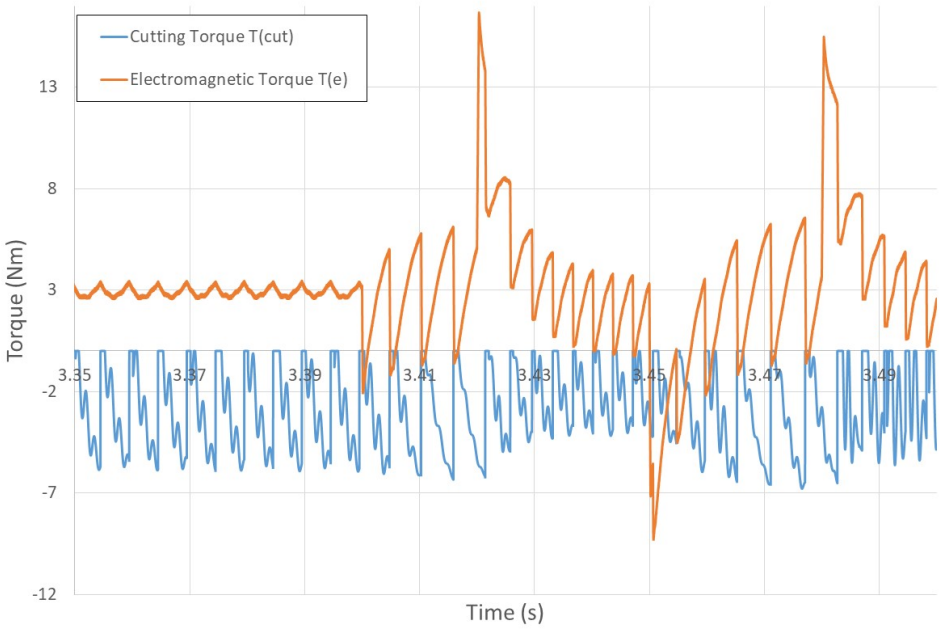

Figure 105 Simulated cutting tool torque and electromagnetic torque over the interval 3.35 sec to 3.50 sec

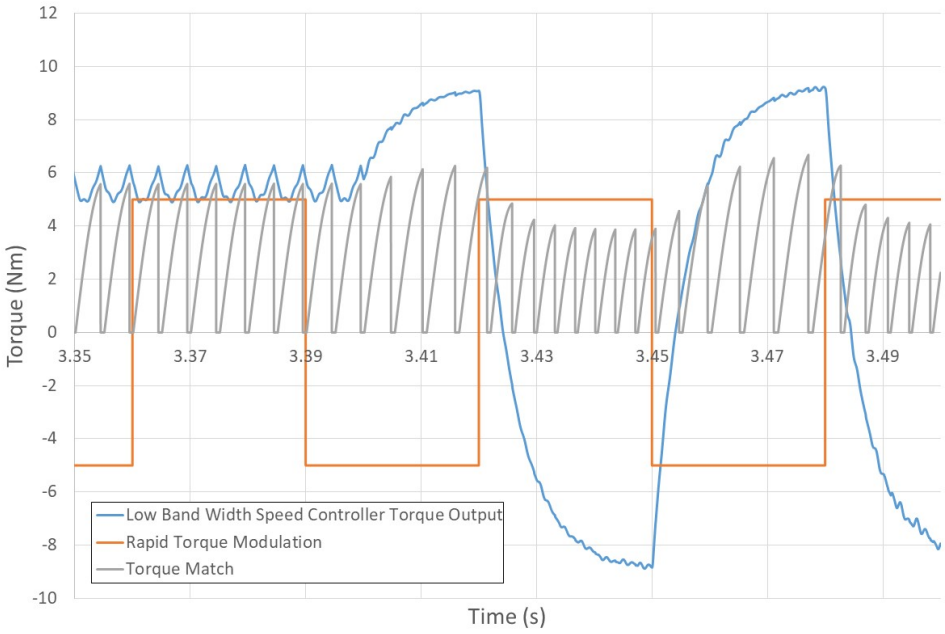

Figure 106 Rapid torque modulation and speed controller torque output

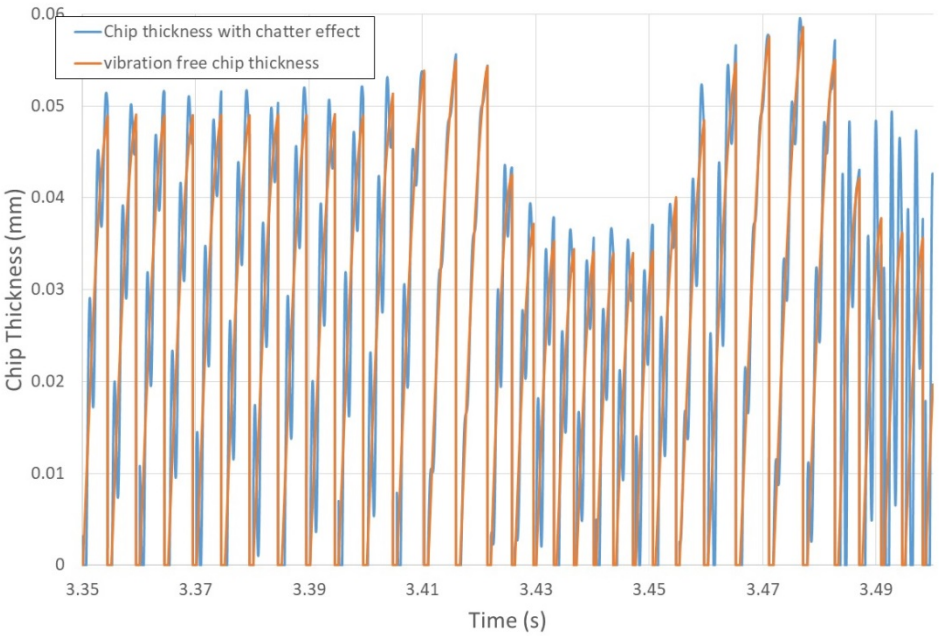

Figure 107 Variation in chip thickness over the interval 3.35 sec to 3.50 sec

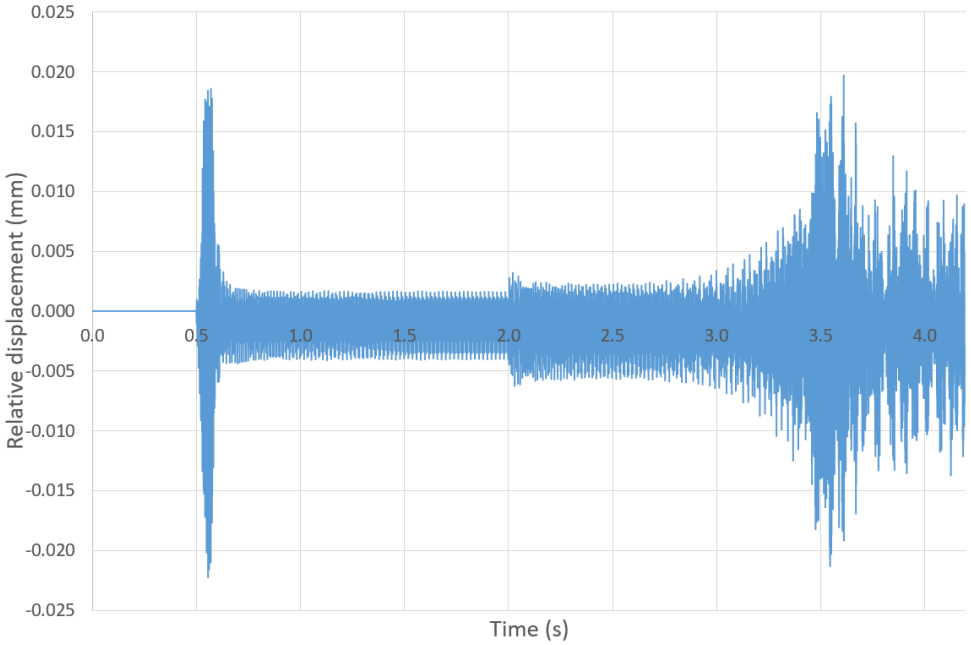

Figure 108 Variation in displacement in the direction of feed across the full simulation

The evolution of the STFT is shown in Figure 109. There is a growing component of speed error at 695 Hz which is identified as the chatter frequency using the methodology described in Chapter 4 - . The magnitude of the speed error frequency component at 695 Hz increases beyond the threshold of 0.5 at 3.40 sec triggering the application of torque modulation action. When the

open-loop torque modulation is applied the speed error inevitably increases across the full range of the spectrum since the motor speed now includes an additional 5 Nm torque modulation which in effect acts as a disturbance to the speed controller.

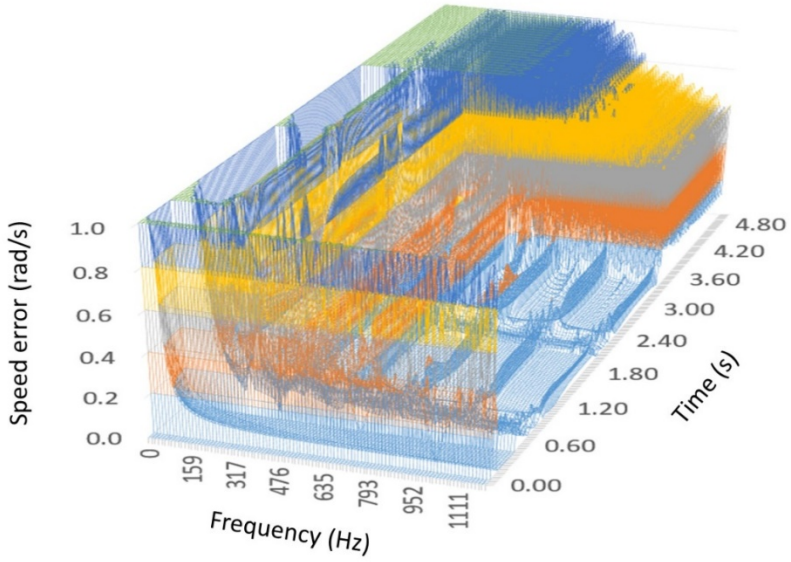

Figure 109 Evolution of STFT of speed error (chatter detected at 3.40 sec)

It is important to recognise that once torque modulation is applied, there is no prospect of establishing whether it is effective in terms of eliminating regenerative chatter since the speed error STFT becomes dominated by the speed errors introduced by the modulation. Hence, the effectiveness of a combination of magnitude and duration of the pulses cannot be assessed through the speed signal nor from the speed controller torque action

5.4.Simulation results at 7,500 rpm

The variation in rotational speed is shown in Figure 110. As was the case for the simulations at 3,000 rpm, there are two speed dips, the first dip is at 0.5 sec when the tool engages, and the second dip is at 2.0 sec when the depth of cut increases. In this case, the chatter detection triggers the use of rapid torque modulation at ~ 2.1 sec. Following the detection of chatter, a sequence of square waves of torque modulation with magnitude 8 Nm and a duration of 32 tooth

passes were set as the demand for the PI current controller. The variation in electromagnetic torque over the full simulation duration is shown in Figure 112 along with the cutting tool torque and the net accelerating torque, i.e. the difference between the electromagnetic and cutting tool torques. A close up of the force variations over the interval 2.0 sec to 2.14 sec, an interval that spans the point at which the torque modulation starts up is shown in Figure 113. As shown, the 32 tooth passes correspond to a period of 64ms for this rotational speed. The net force demand supplied to the current controller in the block diagram of Figure 59 comprises three components which are shown separately in Figure 114. The speed controller, even though it only has a modest bandwidth of 314 rad/s gradually corrects the speed error which is generated by the open-loop torque pulsations. The tooth passing frequency variation in the net torque is generated by the open-loop torque matching facility which is incorporated into the overall controller to aid the speed regulation.

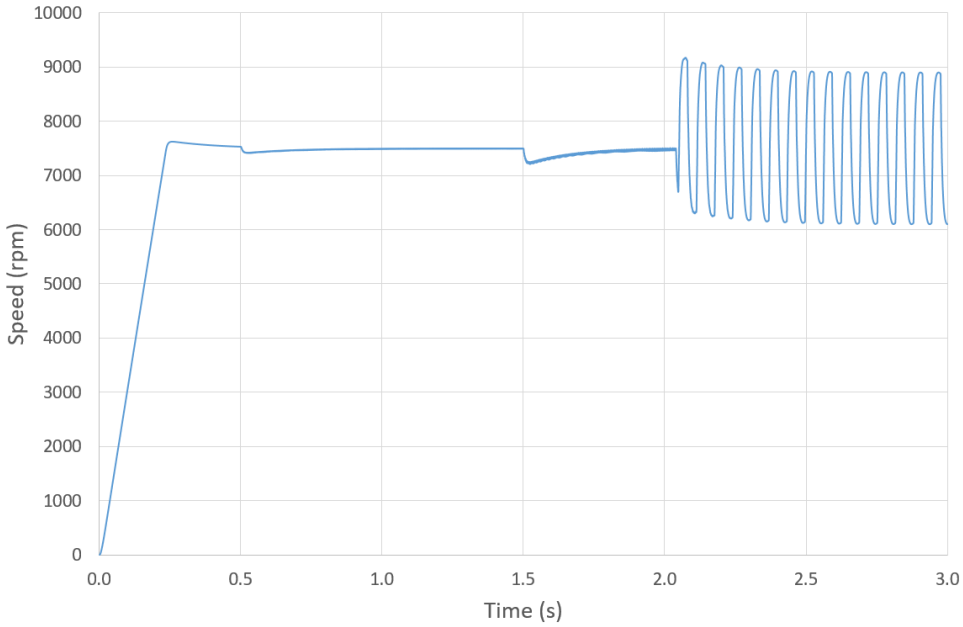

Figure 110 Simulated speed variation for a nominal speed of 7,500 rpm

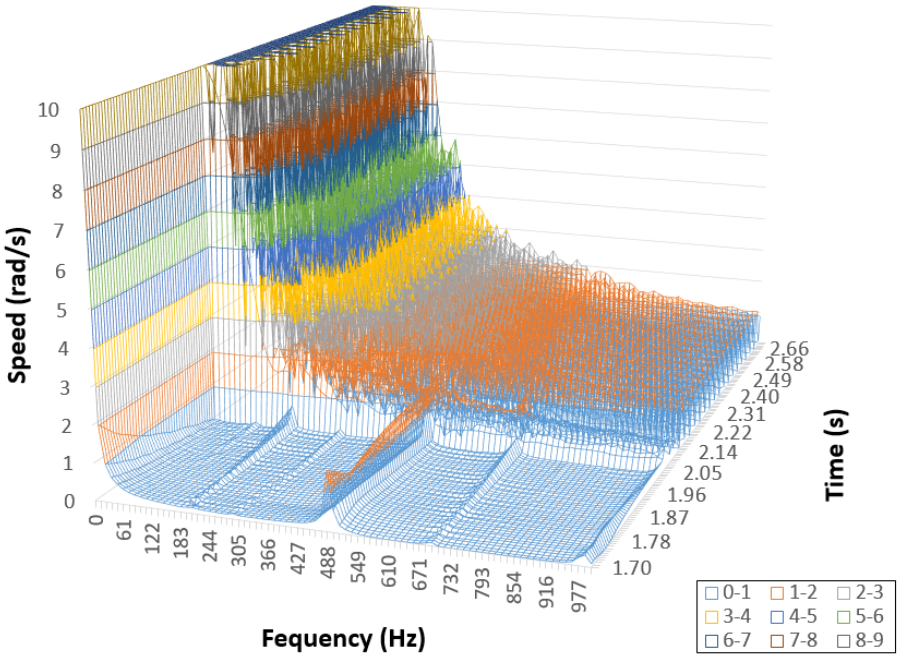

Figure 111 STFT of speed error for nominal speed of 7,500 rpm

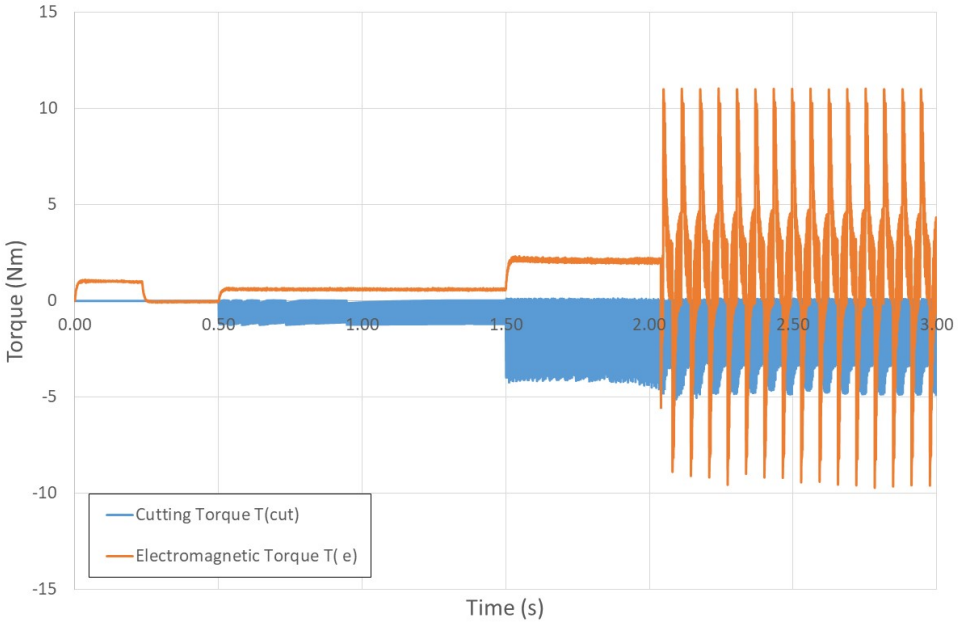

Figure 112 Simulated cutting tool torque and electromagnetic torque for a nominal speed of 7,500 rpm

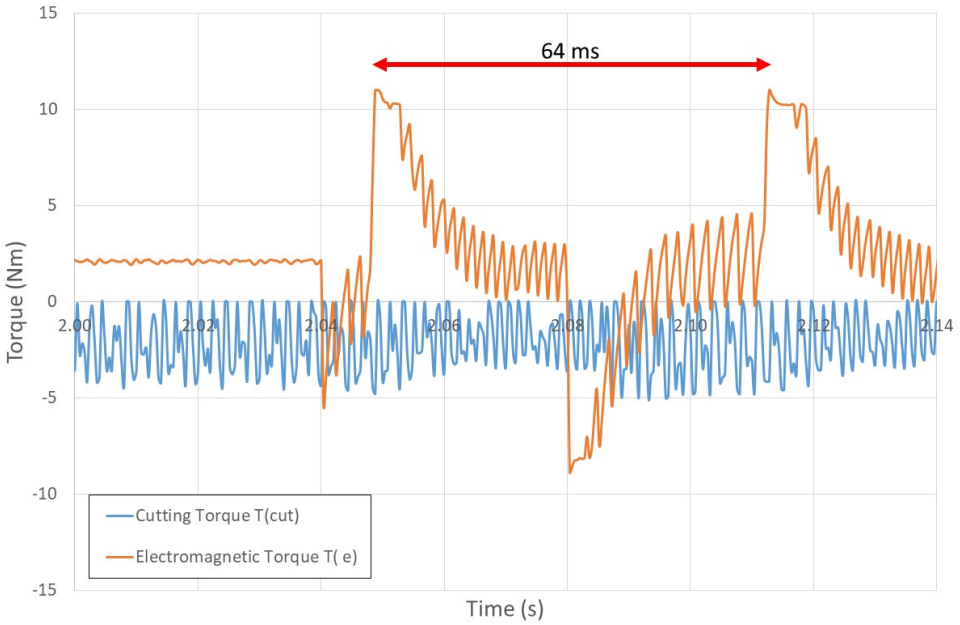

Figure 113 Close up of cutting tool torque and electromagnetic torque waveform

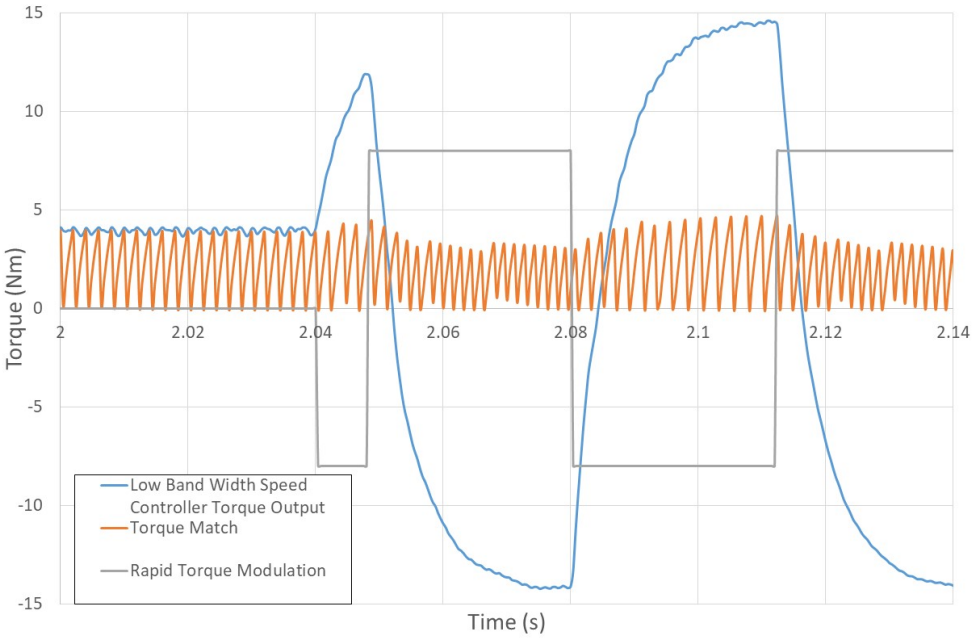

Figure 114 Speed control torque demand and open-loop torque modulation (includes torque match)

The variation in the displacement in the direction of the feed is shown in Figure 115. This shows the build-up in vibration from 1.5 sec when the depth of cut is increased to the 2.04 sec when the

open-loop torque modulation is applied. As shown, this is effective in restoring stable cutting, although the steady-state vibration is considerably greater than was the case with the 3 mm depth of cut up to 1.5 sec. This vibration may be regarded as excessive in terms of a high-quality surface finish depending on the application. The simulated variation in chip thickness in shown in Figure 116 along with the corresponding chip thickness predicted with an ideal vibration-free cutting model which is fed with the same speed variation. Much of the variation in chip thickness, in particular the chip to chip variation, is present in both models and results from the speed variation rather than from vibration. This coupling between rotational speed and chip thickness is a consequence of the fact that the feed rate is set to 0.05 mm/tooth at the nominal speed of 7,500 rpm and remains fixed at 25 mm/s. Hence the speed variation shown previously in Figure 110 in which the speed varies between ~6,000 rpm to ~9,000 rpm which corresponds to a variation in feed rate between 20 mm/s to 30 mm/s. The differences between the chip thicknesses predicted by the vibration-free and vibration models in Figure 116 is due to the vibration.

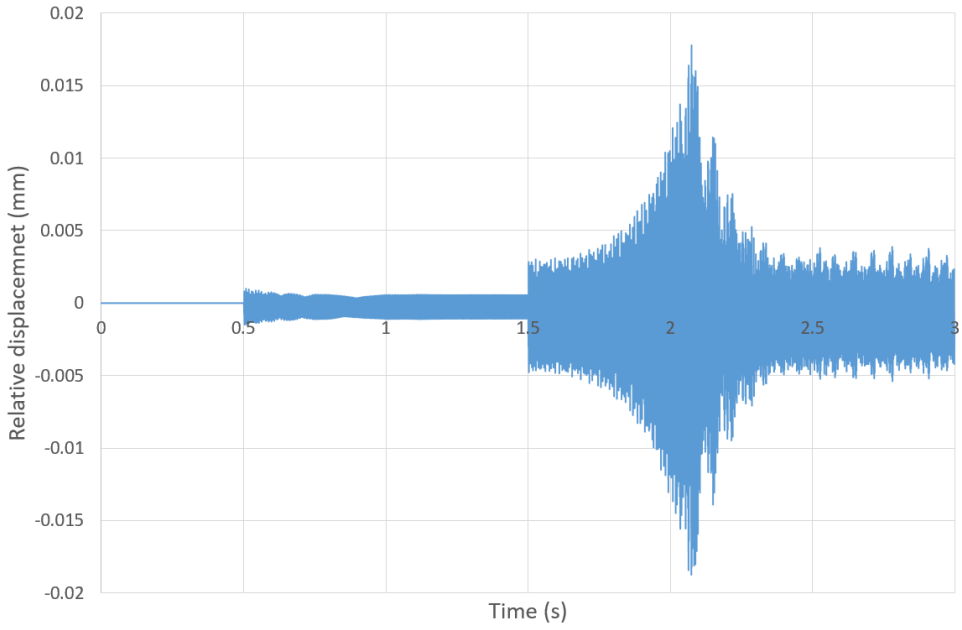

Figure 115 Simulated displacement in feed direction at 7,500 rpm

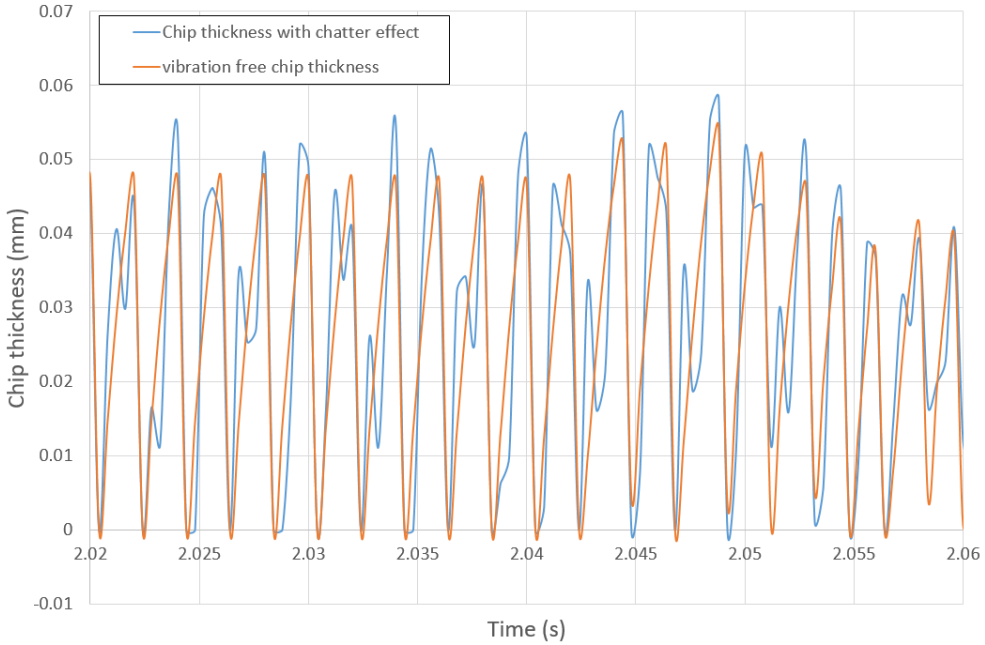

Figure 116 Close up of chip thickness variation over the interval 2.02 sec and 2.06 sec along with the corresponding vibration-free chip thickness.

Chapter 6 - Conclusions and Further Work

This research reported in this thesis has investigated several aspects of high speed milling with a focus on the interaction between the drive control system, the power converter and the cutting process on short-time scales of the order of individual passes of the teeth. This coupling between controller and power converter behaviour and the dynamic cutting conditions is the key novelty in this research as all previous reported models of milling have been based on idealised speed-stiff input. The research has demonstrated several interesting and novel features of milling performance:

- Rapid torque modulation provides a route to significantly increasing the critical cutting depth at key pinch-points in the stability lobe diagram. The method developed detailed in section 3.4 significantly out-performed more established variable speed milling operations.
- The addition of open-loop torque matching in which torque profiles are derived from dynamic models has the potential to increase the dynamic response of milling process.
- There are complex interactions between speed control settings and cutting performance, and in many cases a speed controller with modest bandwidth offers the best solution.
- A method has been developed for identifying the onset of chatter using speed measurements. Although there remains some further work on increasing the robustness of the approach, e.g. adaptively setting the threshold used to identify key frequencies, the method is very attractive as it may well involve no additional hardware or modifications in many machines.

However, there are still limitations and boundaries to apply the proposed technique. Rapid torque modulation and high frequency variable speed milling require both high current control bandwidth to accomplish the control effort and special designed drive train system with reduced

moment of inertia. Chatter identification with spindle speed requires the encoder with high accuracy and speed update rate.

6.1. Future work

6.1.1. Experimental measurements

A shortcoming in the programme of research reported in this thesis is the absence of direct experimental validation of the detailed modelling, although simulations was compared to both published simulation and experimental results with good agreement. However, this is a very significant task as it would involve access to an instrumented milling machine. The arrangement shown previously in Figure 23 in which the work-piece was attached to a bed with some degree of flexure is useful for measuring vibration, but does not have the sensing capability to measure instantaneous speed and torque. The latter is particularly challenging. The design and construction of a fully instrumented milling machine capable of measuring dynamic torques and speed would be a useful test-bed in terms of experimental validation and process optimisation.

6.1.2. Electromechanical optimisation of the spindle drive

This thesis has considered the case of a commercial spindle motor with parameters that are representative of a high specification machine. In many respects, existing machines which are driven at a series of fixed set-points, could be optimised to have adequate moment of inertia. Indeed, other than during rapid acceleration or deceleration, it is likely to be desirable to increase the moment of inertia of the spindle motor. This thesis has demonstrated the merits of being able to rapidly change speed. This would be better achieved by a re-design of the motor to improve the torque to inertia ratio, e.g. by changing the aspect ratio of the machine to a longer and thinner rotor.

6.1.3. Chatter detection algorithm

Although a chatter detection algorithm was developed and deployed in a full system model of a machining sequence to good effect, there are several aspects of detection that could be improved with further work, e.g. remover the limit on the upper frequency sampled and an adaptive means of setting the threshold for harmonics to be considered significant.

References

[ABU 06] Abukhshim, N.A., Mativenga, P.T. and Sheikh, M.A., 2006. Heat generation and temperature prediction in metal cutting: A review and implications for high speed machining. *International Journal of Machine Tools and Manufacture*, *46*(7), pp.782-800.

[ALT 00] Altintas, Yusuf. 2000. Manufacturing automation: metal cutting mechanics, machine tool vibrations, and CNC design. *Cambridge university press*.

[ALT 92] Altintas, Y. and Chan, P.K., 1992. In-process detection and suppression of chatter in milling. *International Journal of Machine Tools and Manufacture*, *32*(3), pp.329-347.

[BOW 75] Bowes, S.R., 1975, November. New sinusoidal pulsewidth-modulated invertor. In *Proceedings of the Institution of Electrical Engineers* (Vol. 122, No. 11, pp. 1279-1285.

[BRE 10] Brecher, C., Manoharan, D., Ladra, U. and Köpken, H.G., 2010. Chatter suppression with an active workpiece holder. *production engineering*, *4*(2-3), pp.239-245.

[BRO 97] Browning, D.R., Golioto, I. and Thompson, N.B., 1997, May. Active chatter control system for long-overhang boring bars. In *Proceedings of Smart Structures and Materials Conference* pp. 3044-26.

[BUD 03A] Budak, E., 2003. An analytical design method for milling cutters with nonconstant pitch to increase stability, part I: theory. *TRANSACTIONS-AMERICAN SOCIETY OF MECHANICAL ENGINEERS JOURNAL OF MANUFACTURING SCIENCE AND ENGINEERING*, *125*(1), pp.29-34.

[BUD 03B] Budak, E., 2003. An analytical design method for milling cutters with nonconstant pitch to increase stability, part 2: application. *TRANSACTIONS-AMERICAN SOCIETY OF*

MECHANICAL ENGINEERS JOURNAL OF MANUFACTURING SCIENCE AND ENGINEERING, *125*(1), pp.35-38.

[CHO 03] Choi, T. and Shin, Y.C., 2003. On-line chatter detection using wavelet-based parameter estimation. *TRANSACTIONS-AMERICAN SOCIETY OF MECHANICAL ENGINEERS JOURNAL OF MANUFACTURING SCIENCE AND ENGINEERING*, *125*(1), pp.21-28.

[DEL 92] Delio, T., Tlusty, J. and Smith, S., 1992. Use of audio signals for chatter detection and control. *ASME J. Eng. Ind*, *114*(2), pp.146-157.

[DEV 07] Devillez, A. and Dudzinski, D., 2007. Tool vibration detection with eddy current sensors in machining process and computation of stability lobes using fuzzy classifiers. *Mechanical systems and signal processing*, *21*(1), pp.441-456.

[DIM 00] Dimla, D.E. and Lister, P.M., 2000. On-line metal cutting tool condition monitoring.: I: force and vibration analyses. *International Journal of Machine Tools and Manufacture*, *40*(5), pp.739-768.

[DOH 04] Dohner, J.L., Lauffer, J.P., Hinnerichs, T.D., Shankar, N., Regelbrugge, M., Kwan, C.M., Xu, R., Winterbauer, B. and Bridger, K., 2004. Mitigation of chatter instabilities in milling by active structural control. *Journal of sound and vibration*, *269*(1), pp.197-211.

[DUN 05] Duncan, G.S., Tummond, M.F. and Schmitz, T.L., 2005. An investigation of the dynamic absorber effect in high-speed machining. *International Journal of Machine Tools and Manufacture*, *45*(4), pp.497-507.

[FAA 03] Faassen, R.P.H., Van de Wouw, N., Oosterling, J.A.J. and Nijmeijer, H., 2003. Prediction of regenerative chatter by modelling and analysis of high-speed milling. *International Journal of Machine Tools and Manufacture*, *43*(14), pp.1437-1446.

[FAZ 09] Fazelinia, H. and Olgac, N., 2009. New perspective in process optimisation of variable pitch milling. *International Journal of Materials and Product Technology*, *35*(1-2), pp.47-63.

[GRA 05] Gradišek, J., Kalveram, M., Insperger, T., Weinert, K., Stépán, G., Govekar, E. and Grabec, I., 2005. On stability prediction for milling. *International Journal of Machine Tools and Manufacture*, *45*(7), pp.769-781.

[HAS 96] Hashimoto, M., Marui, E. and Kato, S., 1996. Experimental research on cutting force variation during regenerative chatter vibration in a plain milling operation. *International Journal of Machine Tools and Manufacture*, *36*(10), pp.1073-1092.

[HOL 92] Holtz, J., 1992. Pulsewidth modulation-a survey. *IEEE transactions on Industrial Electronics*, *39*(5), pp.410-420.

[HTC 17] Product Catalogs. 2017. HTC tooling manufactor. [ONLINE] Available at: http://www.htcmfg.com/index.php?route=common/home. [Accessed 31 October 2017].

[INS 03] Insperger, T., Stépán, G., Bayly, P.V. and Mann, B.P., 2003. Multiple chatter frequencies in milling processes. *Journal of sound and vibration*, *262*(2), pp.333-345.

[ISM 97] Ismail, F. and Soliman, E., 1997. A new method for the identification of stability lobes in machining. *International Journal of Machine Tools and Manufacture*, *37*(6), pp.763-774.

[JAY 00] Jayaram, S., Kapoor, S.G. and DeVor, R.E., 2000. Analytical stability analysis of variable spindle speed machining. *Journal of Manufacturing Science and Engineering*, *122*(3), pp.391-397.

[KHA 13] Saleh, K., 2013. *Modelling and Analysis of Chatter Mitigation Strategies in Milling* (Doctoral dissertation, University of Sheffield).

[KUL 08] Kuljanic, E., Sortino, M. and Totis, G., 2008. Multisensor approaches for chatter detection in milling. *Journal of Sound and Vibration*, *312*(4), pp.672-693.

[KUL 09] Kuljanic, E., Totis, G. and Sortino, M., 2009. Development of an intelligent multisensor chatter detection system in milling. *Mechanical Systems and Signal Processing*, *23*(5), pp.1704-1718.

[LEE 91] Lee, A.C. and Liu, C.S., 1991. Analysis of chatter vibration in the end milling process. *International Journal of Machine Tools and Manufacture*, *31*(4), pp.471-479.

[LIA 96] Liao, Y.S. and Young, Y.C., 1996. A new on-line spindle speed regulation strategy for chatter control. *International Journal of Machine Tools and Manufacture*, *36*(5), pp.651-660.

[LIN 90] Lin, S.C., DeVor, R.E. and Kapoor, S.G., 1990. The effects of variable speed cutting on vibration control in face milling. *Journal of Engineering for Industry*, *112*(1), pp.1-11.

[LIU 02] Liu, X.W., Cheng, K., Webb, D. and Luo, X.C., 2002. Prediction of cutting force distribution and its influence on dimensional accuracy in peripheral milling. *International Journal of Machine Tools and Manufacture*, *42*(7), pp.791-800.

[LIU 05] Liu, Y., Zhu, Z.Q. and Howe, D., 2005. Direct torque control of brushless DC drives with reduced torque ripple. *IEEE Transactions on Industry Applications*, *41*(2), pp.599-608.

[MA 13] Ma, L., Melkote, S.N. and Castle, J.B., 2013. A model-based computationally efficient method for on-line detection of chatter in milling. *Journal of Manufacturing Science and Engineering*, *135*(3), p.031007.

[MEB 16] Mebrahitom, A., Rizuan, D., Azmir, M. and Nassif, M., 2016, February. Effect of High-speed Milling tool path strategies on the surface roughness of Stavax ESR mold insert

machining. In *IOP Conference Series: Materials Science and Engineering*(Vol. 114, No. 1, p. 012006). IOP Publishing.

[MEI 09] Mei, D., Kong, T., Shih, A.J. and Chen, Z., 2009. Magnetorheological fluid-controlled boring bar for chatter suppression. *Journal of materials processing technology*, *209*(4), pp.1861-1870.

[MEI 10] Mei, D., Yao, Z., Kong, T. and Chen, Z., 2010. Parameter optimization of time-varying stiffness method for chatter suppression based on magnetorheological fluid-controlled boring bar. *The International Journal of Advanced Manufacturing Technology*, *46*(9), pp.1071-1083.

[OLG 98] Olgac, N. and Hosek, M., 1998. A new perspective and analysis for regenerative machine tool chatter. *International Journal of Machine Tools and Manufacture*, *38*(7), pp.783-798.

[PRA 01] Pratt, J.R. and Nayfeh, A.H., 2001. Chatter control and stability analysis of a cantilever boring bar under regenerative cutting conditions. *Philosophical Transactions of the Royal Society of London A: Mathematical, Physical and Engineering Sciences*, *359*(1781), pp.759-792.

[QUI 11] Quintana, G. and Ciurana, J., 2011. Chatter in machining processes: a review. *International Journal of Machine Tools and Manufacture*, *51*(5), pp.363-376.

[RAH 86] Rahman, M. and Ito, Y., 1986. Detection of the onset of chatter vibration. *Journal of Sound and Vibration*, *109*(2), pp.193-205.

[REG 03] Al-Regib, E., Ni, J. and Lee, S.H., 2003. Programming spindle speed variation for machine tool chatter suppression. *International Journal of Machine Tools and Manufacture*, *43*(12), pp.1229-1240.

[RIV 206] Riviére, E., Stalon, V., Van den Abeele, O., Filippi, E. and Dehombreux, P., 2006, March. Chatter detection techniques using microphone. In *Seventh national congress on theoretical and applied mechanics 2006*.

[RVA 98] Ryabov, O., Mori, K. and Kasashima, N., 1998. Laser displacement meter application for milling diagnostics. *Optics and lasers in engineering*, *30*(3-4), pp.251-263.

[SAS 02] Sastry, S., Kapoor, S.G. and DeVor, R.E., 2002. Floquet theory based approach for stability analysis of the variable speed face-milling process. *Journal of manufacturing science and engineering*, *124*(1), pp.10-17.

[SAT 08] Sathianarayanan, D., Karunamoorthy, L., Srinivasan, J., Kandasami, G.S. and Palanikumar, K., 2008. Chatter suppression in boring operation using magnetorheological fluid damper. *Materials and Manufacturing Processes*, *23*(4), pp.329-335.

[SCH 01] Schmitz, T.L., Davies, M.A., Medicus, K. and Snyder, J., 2001. Improving high-speed machining material removal rates by rapid dynamic analysis. *CIRP Annals-Manufacturing Technology*, *50*(1), pp.263-268.

[SCH 02] Schmitz, T.L., Medicus, K. and Dutterer, B., 2002. Exploring once-per-revolution audio signal variance as a chatter indicator. *Machining Science and Technology*, *6*(2), pp.215-233.

[SCH 03] Schmitz, T.L., 2003. Chatter recognition by a statistical evaluation of the synchronously sampled audio signal. *Journal of Sound and Vibration*, *262*(3), pp.721-730.

[SEG 09] Seguy, S., Insperger, T., Arnaud, L., Dessein, G. and Peigné, G., 2009. Chatter suppression in milling processes using periodic spindle speed variation. In *12th Cirp Conference on Modelling of Machining Operations. Donostia-San Sebastián, Spain* (pp. 887-894).

[SEG 10] Seguy, S., Insperger, T., Arnaud, L., Dessein, G. and Peigné, G., 2010. On the stability of high-speed milling with spindle speed variation. *The International Journal of Advanced Manufacturing Technology*, *48*(9-12), pp.883-895.

[SEJ 09] Sejdić, E., Djurović, I. and Jiang, J., 2009. Time–frequency feature representation using energy concentration: An overview of recent advances. *Digital Signal Processing*, *19*(1), pp.153-183.

[SHA 05] Shaw, M.C., 2005. Metal cutting principles–Oxford series on advanced manufacturing. *Publ. Oxford University Press, New York (USA)*.

[SHI 96] Shirase, K. and Altintaş, Y., 1996. Cutting force and dimensional surface error generation in peripheral milling with variable pitch helical end mills. *International Journal of Machine Tools and Manufacture*, *36*(5), pp.567-584.

[SIM 05] Sims, N.D., 2005. The self-excitation damping ratio: a chatter criterion for time-domain milling simulations. *Journal of Manufacturing Science and Engineering*, *127*(3), pp.433-445.

[SIM 08] Sims, N.D., Mann, B. and Huyanan, S., 2008. Analytical prediction of chatter stability for variable pitch and variable helix milling tools. *Journal of Sound and Vibration*, *317*(3), pp.664-686.

[SS 08] SIEMENS, 2008. SIMODRIVE 611 universal Control Components for Closed-Loop Speed Control and Positioning Function Manual, *S. documentation, Editor 02*.

[STO 72] Stoferle, T. and Grab, H., 1972. Vermeiden von Ratterschwingungen durch periodische Drehzahlanderung. *Werkstatt und Betrieb*, *105*(10), pp.727-730.

[TAK 74] Takemura, T., Kitamura, T. and Hoshi, T., 1974. Active Suppression of Chatter by Programed Variation of Spindle Speed. *Journal of the Japan Society of Precision Engineering*, *41*(484), pp.489-494.

[TAN 12] Tansel, I.N., Li, M., Demetgul, M., Bickraj, K., Kaya, B. and Ozcelik, B., 2012. Detecting chatter and estimating wear from the torque of end milling signals by using Index Based Reasoner (IBR). *The International Journal of Advanced Manufacturing Technology*, *58*(1), pp.109-118.

[TEK 05] Tekeli, A. and Budak, E., 2005. Maximization of chatter-free material removal rate in end milling using analytical methods. *Machining science and technology*, *9*(2), pp.147-167.

[TES 05] Testa, A. and Langella, R., 2005, June. Power system subharmonics. In *Power Engineering Society General Meeting, 2005. IEEE*, pp. 2237-2242.

[TLU 00] Tlusty, J., 2000. *Manufacturing processes and equipment*. Prentice Hall.

[TSA 93] Tsao, T.C., McCarthy, M.W. and Kapoor, S.G., 1993. A new approach to stability analysis of variable speed machining systems. *International Journal of Machine Tools and Manufacture*, *33*(6), pp.791-808.

[TUR 06] Turner, S., Merdol, D., Altintas, Y. and Ridgway, K., 2007. Modelling of the stability of variable helix end mills. *International Journal of Machine Tools and Manufacture*, *47*(9), pp.1410-1416.

[TUR 07] Turner, S., Merdol, D., Altintas, Y. and Ridgway, K., 2007. Modelling of the stability of variable helix end mills. *International Journal of Machine Tools and Manufacture*, *47*(9), pp.1410-1416.

[WAN 09] Wang, L. and Liang, M., 2009. Chatter detection based on probability distribution of wavelet modulus maxima. *Robotics and Computer-Integrated Manufacturing*, *25*(6), pp.989-998.

[WAN 2011] Jibing Wang., 2011. Motion Control and Servo Drive Systems: Axis transformations [Lecture Notes] *EEE department University of Sheffield*.

[WEC 75] Weck, M., Verhaag, E. and Gather, M., 1975. Adaptive control for face-milling operations with strategies for avoiding chatter vibrations and for automatic cut distribution. *Annals of the CIRP*, *24*(1), pp.405-409.

[WEI 06] Weingaertner, W.L., Schroeter, R.B., Polli, M.L. and de Oliveira Gomes, J., 2006. Evaluation of high-speed end-milling dynamic stability through audio signal measurements. *Journal of Materials Processing Technology*, *179*(1), pp.133-138.

[WU 88] Wu, D.W., 1988. Application of a comprehensive dynamic cutting force model to orthogonal wave-generating processes. *International journal of mechanical sciences*, *30*(8), pp.581-600.

[YAN 03] Yang, F., Zhang, B. and Yu, J., 2003. Chatter suppression with multiple time-varying parameters in turning. *Journal of Materials Processing Technology*, *141*(3), pp.431-438.

[YAO 10] Yao, Z., Mei, D. and Chen, Z., 2010. On-line chatter detection and identification based on wavelet and support vector machine. *Journal of Materials Processing Technology*, *210*(5), pp.713-719.

[YUS 10A] Yusoff, A.R., Turner, S., Taylor, C.M. and Sims, N.D., 2010. The role of tool geometry in process damped milling. *The International Journal of Advanced Manufacturing Technology*, *50*(9), pp.883-895.

[ZAT 08] Zatarain, M., Bediaga, I., Munoa, J. and Lizarralde, R., 2008. Stability of milling processes with continuous spindle speed variation: analysis in the frequency and time domains, and experimental correlation. *CIRP Annals-Manufacturing Technology*, *57*(1), pp.379-384.

[ZHA 05] Zhang, Y. and Sims, N.D., 2005. Milling workpiece chatter avoidance using piezoelectric active damping: a feasibility study. *Smart materials and structures*, *14*(6), pp.65.

[ZHO 02] Zhou, K. and Wang, D., 2002. Relationship between space-vector modulation and three-phase carrier-based PWM: a comprehensive analysis [three-phase inverters]. *IEEE transactions on industrial electronics*, *49*(1), pp.186-196.

Appendices

Appendix A - Motor Parameters

Motor data for 1FE series SIEMENS permanent magnet high speed synchronous motor

App			
Rated motor speed			10000 [1/min]
Motor stand still torque (T0)			11 [Nm]
Control drive	611D/U		
P1102	2758		motor code number
P1100	5333	[Hz]	frequency pulse-width modulation
P1103	19	[A]	rated motor current
P1104	38	[A]	Max. motor current
P1112	3		motor pole pair number
P1113	0.57	[Nm/A]	torque constant
P1114	41	[V/(1000 1/min)]	voltage constant
P1115	0.68	[Ohm]	armature resistance
P1116	2.2	[mH]	armature inductance
P1117	0.0003	[kgm²]	moment of inertia
P1118	19	[A]	motor standstill current
P1122	38	[A]	motor limiting current
P1128	90	[°]	optimum load angle
P1136	32	[A]	short-circuit current

P1142	10300	[1/min]	field weakening speed
P1145	70	[%]	stall torque reduction factor
P1146	15000	[1/min]	Max. motor speed

Appendix B – PI Tuning

For the current control loop. As showed in Figure 9, the q- axis current control loop contains a back emf produced by the motor. However, since the current response is much faster than the speed response, the effect of back emf on the q- axis current can be neglected in the controller design. Hence, the transfer functions for both d- and q- axis current control loops are as follows:

$$\begin{cases} G_1(s) = \dfrac{i_d}{i_d^*} = \left(k_{pc} + \dfrac{k_{ic}}{s}\right)\left(\dfrac{1}{sL_d + R}\right) \\ G_2(s) = \dfrac{i_q}{i_q^*} = \left(k_{pc} + \dfrac{k_{ic}}{s}\right)\left(\dfrac{1}{sL_q + R}\right) \end{cases}$$

where i_d, i_q are output d- and q- axis currents, and $i_d^* i_q^*$ are input d- and q- axis currents.

Bode plot is a classical way to define the frequency response (i.e. cut off frequency or bandwidth) and phase margin of this system. The cut off frequency is the frequency where the amplitude of output signal is at 70.7% of the amplitude of input signal. Figure 117 shows the a typical bode plot for bandwidth at 100,000 rad/s (i.e. cut off frequency at 7,975 Hz) and phase margin at 90 degrees with the motor parameters from **Appendix A**. The calculated value for k_{pc} is 220 and for k_{ic} is 385000.

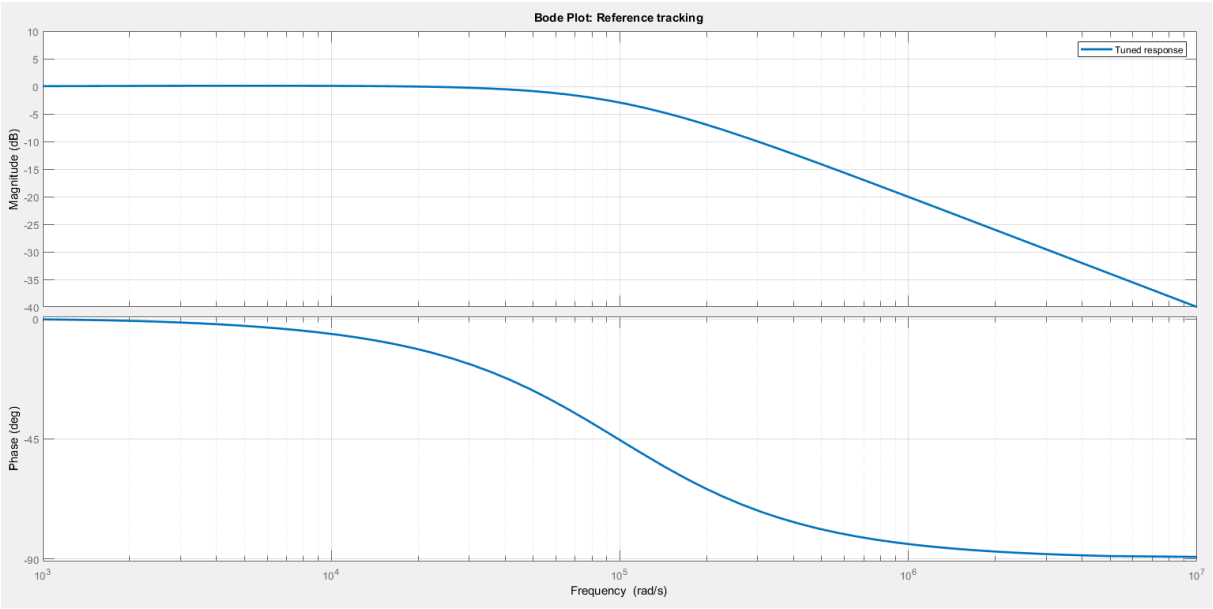

Figure 117 Bode plot for current loop controller

For the speed control loop, the transfer function is as follows:

$$H(s) = \left(k_{ps} + \frac{k_{is}}{s}\right)\left(\frac{G_2(s)}{1 + G_2(s)}\right)\left(\frac{K_t}{Js + B}\right)$$

Table 12 PI tuning for speed control loop with different bandwidth

Bandwidth (rad/s)	Speed control loop proportional gain k_{sp}	Speed control loop integral gain k_{si}
314	0.1652	0.9077
2500	1.303	57.02
5000	2.6	227.5
7500	3.903	512.3
10000	5.214	912.6
15000	7.869	2066
25000	13.37	5852
50000	29.07	25440

Appendix C- Space-vector PWM calculation

The vector $\vec{U}$ is composed of the two nearest voltage vectors and two zero vectors$\vec{U}_0, \vec{U}_7$. For instance, the vector $\vec{U}$ shown in figure 3.4 is in sector 1, then this vector can also have expressed as:

$\vec{U} = \frac{T_1}{T_S}\vec{U}_1 + \frac{T_2}{T_S}\vec{U}_2 + \frac{T_0}{T_S}\vec{U}_0 + \frac{T_7}{T_S}\vec{U}_7$ and T_S is the sampling time, T_1, T_2, T_0, T_7 are the time acting on corresponding vectors.

Resolving the vector $\vec{U}$ into $\alpha\beta$ reference system, we have:

$$U_\alpha = \vec{U}\cos\varphi_{\omega t} = \vec{U}_1\frac{T_1}{T_s} + \vec{U}_2\frac{T_2}{T_s}\cos\frac{\pi}{3}\ in\ alpha\ aixs$$

$$U_\beta = \vec{U}\sin\varphi_{\omega t} = \vec{U}_2\frac{T_2}{T_s}\sin\frac{\pi}{3}\ \ in\ beta\ axis$$

Hence, the acting time T_1, T_2 are:

$$T_1 = \frac{2}{\sqrt{3}}mT_s\sin\left(\frac{\pi}{3} - \varphi_{\omega t}\right), T_2 = \frac{2}{\sqrt{3}}mT_s\sin\varphi_{\omega t}$$

Where m is the modulation ratio $m = \sin\frac{2\pi}{3}\frac{T_1}{T_S}\frac{1}{\sin\left(\frac{\pi}{3}-\varphi_{\omega t}\right)} = \sin\frac{2\pi}{3}\frac{T_2}{T_S}\frac{1}{\sin\varphi_{\omega t}}$

And $T_0 + T_7 = T_s - T_1 - T_2$

For other sectors, the results are showed in the Table 13 Switching time on each sector below:

Table 13 Switching time on each sector

Sector 1	Sector 2	Sector 3
$T_1 = \frac{\sqrt{3}}{2} m T_s \sin\left(\omega t + \frac{\pi}{6}\right)$ $T_2 = \frac{\sqrt{3}}{2} m T_s \sin(\omega t + \frac{3\pi}{2})$	$T_2 = \frac{\sqrt{3}}{2} m T_s \sin\left(\omega t + \frac{11\pi}{6}\right)$ $T_3 = \frac{\sqrt{3}}{2} m T_s \sin(\omega t + \frac{7\pi}{6})$	$T_3 = \frac{\sqrt{3}}{2} m T_s \sin\left(\omega t + \frac{3\pi}{2}\right)$ $T_4 = \frac{\sqrt{3}}{2} m T_s \sin(\omega t + \frac{5\pi}{6})$
$T_0 + T_7 = T_s - T_1 - T_2$	$T_0 + T_7 = T_s - T_2 - T_3$	$T_0 + T_7 = T_s - T_3 - T_4$
Sector 4	Sector 5	Sector 6
$T_4 = \frac{\sqrt{3}}{2} m T_s \sin\left(\omega t + \frac{7\pi}{6}\right)$ $T_5 = \frac{\sqrt{3}}{2} m T_s \sin(\omega t + \frac{\pi}{2})$	$T_5 = \frac{\sqrt{3}}{2} m T_s \sin\left(\omega t + \frac{5\pi}{6}\right)$ $T_6 = \frac{\sqrt{3}}{2} m T_s \sin(\omega t + \frac{\pi}{6})$	$T_6 = \frac{\sqrt{3}}{2} m T_s \sin\left(\omega t + \frac{\pi}{2}\right)$ $T_1 = \frac{\sqrt{3}}{2} m T_s \sin(\omega t + \frac{11\pi}{6})$
$T_0 + T_7 = T_s - T_4 - T_5$	$T_0 + T_7 = T_s - T_5 - T_6$	$T_0 + T_7 = T_s - T_1 - T_6$

Appendix D - Block diagram for cutting model

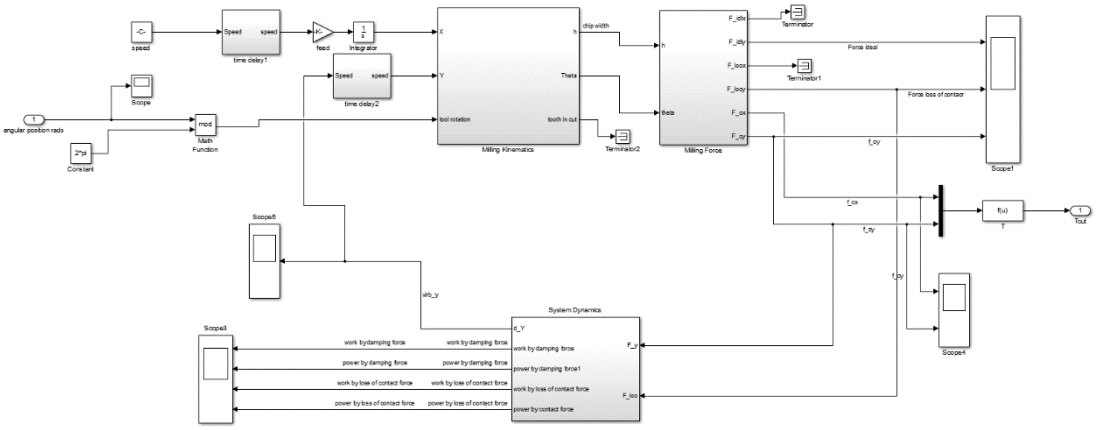

Appendix E - Code for cutting surface and chip thickness formation:

```
function Chipwidth = fcn(simtime,toolcx,toolcy,cutx,cuty,toothnumber)
%#codegen
persistent  data_mem;
persistent  prev_cut;
persistent  step;
persistent  prev_toothno;        %difne cutter number
persistent  stepcount;           %for find previous cutting data sizes
persistent  cutcount;            %define cutting cycle


sample_time = simtime;           %globe sampling time (s)
sizes = 5000;
toolr = 0.01;                   %tool radius in m
angle_st = -90;                 %start angle (degree)
angle_ex = -11.54;              %exit angle (degree)

% Initialise all Variables that are persistent
if (isempty(data_mem))
      data_mem = zeros(sizes,2);end
if (isempty(prev_cut))
      angle_sp = (angle_ex-angle_st)/sizes;
      data_ma = [0:sizes-1];
      data_max = rot90(rot90(rot90(data_ma)));                          %deifne
initial matrix size
      data_angle = angle_st+(angle_sp)*data_max;
      prev_cut = toolr*[cosd(data_angle) sind(data_angle)];
      end
if (isempty(step))
      step = 1; end
if (isempty(prev_toothno))
      prev_toothno = 1; end
if (isempty(stepcount))
      stepcount = sizes; end
if (isempty(cutcount))
      cutcount = 1; end

%Save Data
```

```
if (toothnumber ~=0)
    if (toothnumber ~= prev_toothno)   % this means a new cut has started
    prev_cut = data_mem;
    cutcount=cutcount+1;              %for finding cutting cycle
    data_mem = zeros(sizes,2);         %clear the memory
    stepcount = step-1;               %this is the number of datapoints in prevous cut
    step = 1;
    end


%Store x,y values for this timestep
data_mem(step,:) = [cutx cuty];
%increment step and store tooth number for next cur
step = step+1;
prev_toothno = toothnumber;

%calcuate Angle from current tool position to each of the previous cuts
%X,Y location also changed to degreess
theta_pre =
atan2d((prev_cut(1:stepcount,2)-toolcy),(prev_cut(1:stepcount,1)-toolcx)); %Make
sure theta is only calculated for valid data %changed to degreess

%calculate theta for current cut (current step)
theta =  atan2d((cuty-toolcy),(cutx-toolcx));

%find Point above and below current theta and test for bounds
%only one of these is required as you know other point is +1 or -1
index_equ = find(theta==theta_pre,1,'first');
index_above = find(theta<theta_pre,1,'first');
index_below = find(theta>theta_pre,1,'last');

  %test and mitigation for end conditions...
  if (isempty(index_equ))
    if (isempty(index_above))
      index_above=index_below;
    end
    if (isempty(index_below))
      index_below=index_above;
    end
```

```
  else
      index_above=index_equ;
      index_below=index_equ;
  end

  %global X Y of point above theata
  x_above = prev_cut(index_above,1);
  y_above = prev_cut(index_above,2);
  x_below = prev_cut(index_below,1);
  y_below = prev_cut(index_below,2);

    r_0 = sqrt((x_above-toolcx)^2+(y_above-toolcy)^2) ;     %length above
    r_1 = sqrt((x_below-toolcx)^2+(y_below-toolcy)^2) ;     %length below
between two pre points degree
    L_01 = (r_0+r_1)/2;
    h = toolr-L_01;


else
  x_above =0;
  y_above = 0;
  x_below = 0;
  y_below = 0;
  h = 0;
end
```

Appendix F- Published paper

- Q. Pan and G. W. Jewell, "Modelling of dynamic machine behavior in peripheral milling operations," 2017 IEEE International Electric Machines and Drives Conference (IEMDC), Miami, FL, 2017, pp. 1-8. doi: 10.1109/IEMDC.2017.8002347

Modelling of Dynamic Machine Behaviour in Peripheral Milling Operations

Mr *Qinwei Pan*
Department of Electronic and Electrical Engineering,
The University of Sheffield
Sheffield, UK

Professor Geraint Jewell
Department of Electronic and Electrical Engineering,
The University of Sheffield
Sheffield, UK

***Abstract*— This digest describes the modelling of the dynamic behavior of a permanent magnet synchronous machine when used as the spindle drive in peripheral milling. The system model, which includes a detailed model of the cutting process, is described and its utility demonstrated in assessing the merits of control strategies which seek to exploit the high dynamic torque response which can be achieved. Simulation results are presented for cases of torque matching and the injection of large torque pulsations.**

Topic*— *Motor control, variable speed milling

I. INTRODUCTION

Machining operations, particularly milling, remain a central feature of many high value manufacturing processes with a continued drive for reduced machining time and enhanced quality. The efficiency and quality of milling operations are influenced by a combination of metal removal rate, tool wear, cycle time and surface finish. A key limiting factor in many operations is the need to avoid the onset of so-called chatter in which excessive vibrations lead to poor surface finish and diminished tool life and can ultimately seriously damage to the work-piece and/or tool. The need to avoid the onset of chatter with a given tool and workpiece is usually achieved by avoiding particular combinations of cutting depth, tool rotational speed and feed rate. A common means of characterizing chatter behavior in a given set-up is by means of a so-called stability lobe diagram, in which a contour